Optimising Fuel Cell Hybrid Train Operation

A Convex Optimisation Approach

by

RABEE RAED SARI JIBRIN

A thesis submitted to the University of Birmingham for the degree of

DOCTOR OF PHILOSOPHY

Birmingham Centre for Railway Research and Education

School of Engineering

College of Engineering and Physical Sciences

University of Birmingham

April 2024

UNIVERSITY OF
BIRMINGHAM

University of Birmingham Research Archive

e-theses repository

This unpublished thesis/dissertation is copyright of the author and/or third parties. The intellectual property rights of the author or third parties in respect of this work are as defined by The Copyright Designs and Patents Act 1988 or as modified by any successor legislation.

Any use made of information contained in this thesis/dissertation must be in accordance with that legislation and must be properly acknowledged. Further distribution or reproduction in any format is prohibited without the permission of the copyright holder.

Abstract

This work focuses on optimising the operation of fuel cell hybrid trains with the primary objective of reducing fuel consumption to improve financial viability. It builds on the basic premise that conventional practices are suboptimal for fuel cell hybrid trains due to the novelty of this class of trains. Given the hybrid nature of this powertrain, it is hypothesised that it is necessary to jointly optimise the energy management system along the driving style and timetable to achieve true optimal operation. Furthermore, it is hypothesised that implementing measures against fuel cell degradation to extend lifetime would come at the expense of additional fuel consumption.

Jointly optimising multiple variables that are dynamically coupled increases computational complexity, especially when they are coupled non-linearly. Therefore, this work sets out to use convex optimisation, as it comes with practical guarantees on global optimality and computational complexity. Formulating a convex problem that models the system adequately is non-trivial which is why it is hypothesised whether it is possible.

A series of optimisation problems with increasing levels of fidelity are built and convexified with various techniques, such as replacing non-linear variables, introducing surrogate variables, approximating discrete data by convex polynomials, and relaxing non-linear equality constraints. Moreover, a hybrid modelling approach that relies on both spatial and temporal domains is proposed. All of this enables building a joint convex optimisation formulation for speed, energy management and timetable.

Simulation results prove that jointly optimising speed and energy management is considerably more fuel efficient than coasting, as the latter fails to effectively leverage regenerative braking to recover kinetic energy. Adding measures against fuel cell degradation was found to come at the expense of additional fuel consumption, though the percentage reduction in degradation was found to be substantially greater than the additional fuel use. Lastly, jointly optimising speed, energy management and timetable was found to yield better fuel economy by distributing running time between stations more efficiently.

Acknowledgements

I would first like to acknowledge the invaluable role of my supervisors, Prof. Stuart Hillmansen and Prof. Clive Roberts. Thanks Stuart for the regular feedback, support and encouragement, all of which was instrumental in shaping this work. Thanks Clive for inspiring me to pursue opportunities beyond my thesis, especially teaching at NCATI and organising the summer school. These have enriched my doctorate experience and prepared me for what's next in every sense of the word.

I am particularly proud of delivering the 2023 Decarbonisation Summer School, a feat that would not have been possible without the help and input of many individuals. I extend my sincerest gratitude to Dr. Lennie Foster, who skilfully guided me in organising the event from inception to execution. I also wish to thank Dr. Daniel Donaldson, Dr. Nan Chen, and the UoB IEEE Student Branch for their invaluable support throughout planning and execution. Moreover, thanks to all seminar speakers, whom are acknowledged in Appendix C.2. I am very grateful to Jake Cartmell, representing Ricardo plc, for being the best industrial partner the summer school could have asked for. Thanks to BCRRE professional services for ensuring a smooth event, particularly Katherine Roberts, Clare Walsh, and Dr. Jenny Illingsworth.

My heartfelt thanks go to the rest of the BCRRE for the wonderful experience, with special gratitude to Dr. Paul Weston for proofreading this thesis. I would also like to express my deep appreciation to my dear friend, Dr. Issa Hammoud. Embarking on a PhD journey alongside one's best friend is truly an unforgettable experience.

Finally, my sincerest appreciation goes to my family and wife. Your belief in me and unwavering support have been vital throughout this journey. Thank you Yara, my love, for not teasing me about finishing your PhD two years ahead of me!

Contents

Nomenclature

Sets

Variables

Parameters

Functions

List of Optimisation Problems

List of Figures

List of Tables

1 INTRODUCTION

This chapter firstly motivates research on fuel cell hybrid trains and justifies the interest to tackle operational costs. Section 1.2 introduces two basic aims of this work, which is optimising operation to reduce fuel consumption and efficiently computing this operational pattern. Section 1.3 briefly explores which operational aspects could be optimised for fuel cell hybrid trains and contrasts them with conventional practice. Section 1.4 briefly introduces convex optimisation and motivates its use. Lastly, Section 1.5 states the research hypotheses.

1.1 Background on Hydrogen in Rail

1.1.1 Phasing Out Diesel Traction

In 2018, the UK Rail Minister proposed to ban diesel-only trains by the year 2040 to decarbonise rail traction [1]. This proposal came despite rail's low-carbon status, e.g. rail emitted only 1.4% of the UK's CO_2e transport emissions in 2019 while accounting for 9.5% of passenger kilometres [2]. Nonetheless, fleet-wide statistics mask the real environmental cost of diesel trains. As a matter of fact, passenger diesel trains collectively emit more CO_2e than their electric counterparts in Great Britain while only constituting 29% of the network's fleet.

Diesel engine emissions are also a threat to public health. In 2012, the World Health Organization (WHO) classified diesel engine exhaust emissions as a Group 1 carcinogen (proven to cause cancer in humans) [3]. Indeed, an elevated cancer risk has been found amongst rail workers who are continuously exposed to diesel train emissions [4]. This is alarming in light of the high diesel engine emissions measured at several train stations in the UK [5] and even inside diesel train cabins [6].

Another reason for forgoing diesel trains is to provide a quieter travel experience to passengers. On average, diesel trains are 16dB louder than their electric counterparts during dwell time [7]. A quieter travel experience will become increasingly important as silent electromobility becomes the norm across various modes of transport. Passengers of electric buses already view the lower levels of noise and vibration as a hallmark of electrified public transport [8].

Lastly, there are national security concerns about the use of imported fossil fuels to power public transport [9], a concern that is repeatedly exacerbated during periods of political instability.

1.1.2 Decarbonisation Pathways

In response to the proposed diesel ban, the Rail Industry Decarbonisation Taskforce was commissioned to assess the technical feasibility of decarbonising the nation's fleet of diesel trains [10]. Electrification was recommended for routes with high traffic volumes that present a strong business case for costly infrastructure upgrades. Battery and hydrogen trains were recommended for routes with lower traffic volumes, as the cost of ownership of these alternative technologies was found to be lower than the costs of electrification for the given volume of traffic. The report strongly discouraged the adoption of bi-mode diesel-electric trains because they were deemed overly complex while only offering an incremental reduction in emissions. In response to this report, Network Rail (the rail infrastructure manager in Great Britain) published its Traction Decarbonisation Network Strategy (TDNS) [11].

The TDNS assessed the alternatives to diesel for the entire network using a top-down analysis of costs and benefits. It outlined ambitious plans to electrify 11,700 single track kilometres (STK) out of the currently unelectrified 15,400 STK. Battery and hydrogen trains were recommended for branch lines that experience low volumes of traffic, 400 STK and 900 STK, respectively. Battery trains would be used for short branch lines

due to their lower cost of ownership compared to hydrogen trains. On the other hand, hydrogen trains would be used for longer branch lines whose long distance could not be accommodated by the lower energy density of batteries.

In 2021, the Treasury rejected funding the TDNS electrification proposals, citing concerns about costs and delivering the best value for the taxpayer [12]. This is by no means the first time a rail electrification scheme has been scaled back or cancelled due to the lack of "political will". For instance, the electrification of the Great Western Mainline was cut short after its costs ballooned to twice the planned budget [13] and this phenomena is hardly unique to the UK [14].

The demonstrated vulnerability of rail electrification to "political will" suggests that it is an unreliable pathway to phasing out diesel trains. It seems very reasonable to expect that battery and hydrogen trains will play a bigger role than initially proposed in the TDNS. This calls for further research and development to improve the technical standing of these alternative technologies. This thesis focuses on the development of hydrogen trains.

1.1.3 The Economic Challenge for Hydrogen

The management consultancy Ronald Berger concluded in 2019 that there are "no fundamental show stoppers" for the use of hydrogen as a traction energy source, though cited the lack of precedence as a major barrier [15]. Indeed, the successful trial of the Alstom Coradia iLint in Germany [16] triggered interest from the USA [17], Germany [18, 19, 20, 21], France [18], Italy [18] and the UK [22].

More recently, the environmental and engineering consultancy Ricardo surveyed the attendees of the World Congress on Railway Research 2022 about barriers to adopting hydrogen traction in rail. Figure 1.1 shows the distribution of votes among the 117 respondents. It reveals that rail researchers and industry professionals believe economics to be the leading barrier, followed by hydrogen storage technology, safety, and sourcing

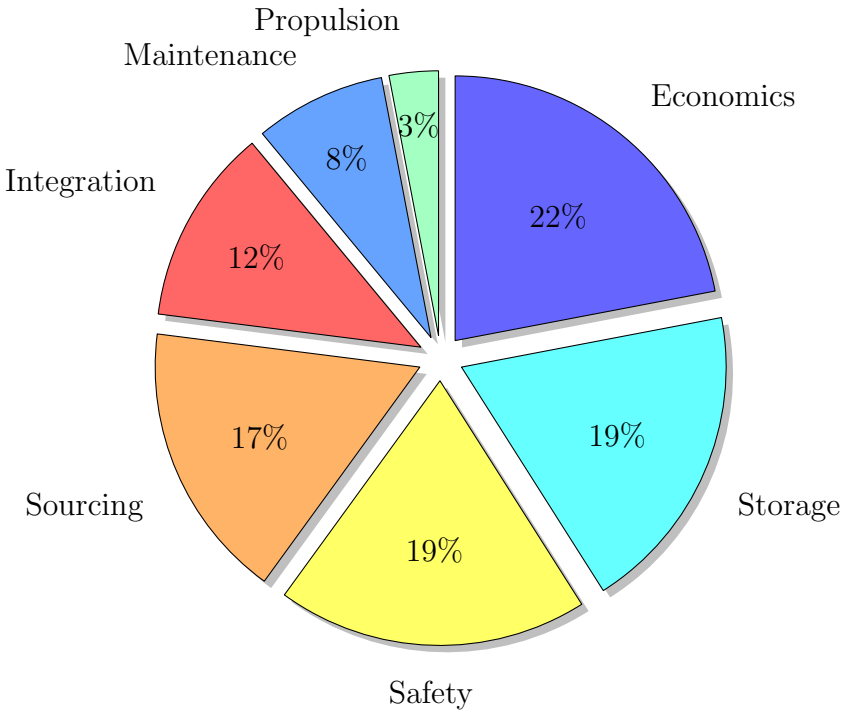

Figure 1.1: Distribution of 117 responses to the multiple choice question *"What is the biggest challenge to put hydrogen on-track?"*. Question asked by Ricardo at the World Congress on Railway Research 2022.

hydrogen fuel.

Inline with Ricardo's finding about the economic barrier, the Hydrogen Council predicts that early adopters of hydrogen trains will pay a premium due to the high cost of green hydrogen and a high capital cost due to novelty [23]. While technological improvements and mass production will reduce capital costs [11], fuel costs are still expected to dominate the cost of ownership well into the future. Figure 1.2 shows a breakdown of cost of ownership for hydrogen and diesel trains. It confirms that the cost of fuel will remain the leading cost for hydrogen trains as is already the case for diesel trains. This is followed by maintenance and replacement costs upon powertrain end-of-lifetime.

1.1.4 The Fuel Cell Hybrid Powertrain

The fuel cell hybrid powertrain shown in Fig. 1.3 is the most commonly proposed hydrogen vehicle architecture [25]. Alternative concepts using combustion engines exist, but these

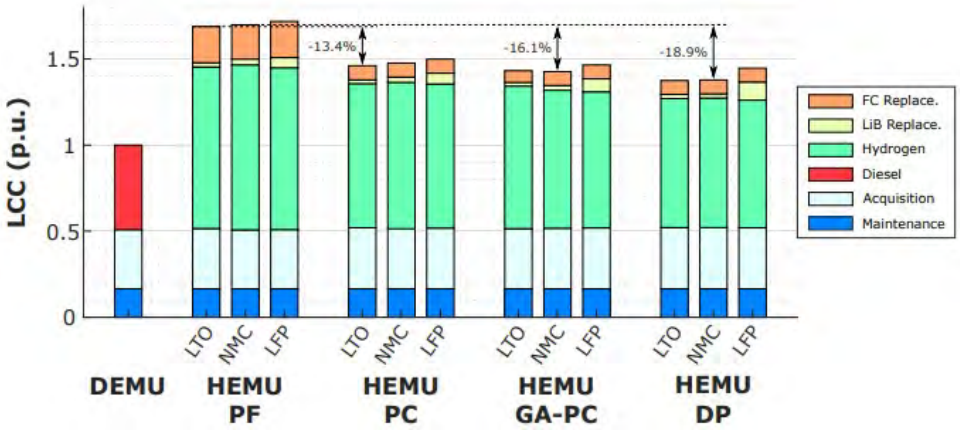

Figure 1.2: TCO of diesel electric multiple unit (DEMU) and hydrogen electric multiple unit (HEMU). Reprinted from [24]. © 2021 IEEE.

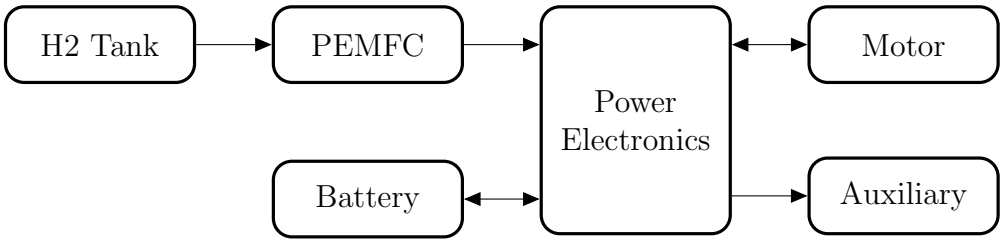

Figure 1.3: The fuel cell hybrid architecture studied in this thesis.

are less efficient and harmful NOx emissions [26]. Moreover, the cost of ownership of fuel cells are expected be lower than combustion engines by 2030 [27].

The fuel cell hybrid powertrain consists of a polymer electrolyte membrane fuel cell (PEMFC) and a traction battery. The battery is typically specified as a high-power battery to assist the fuel cell in supplying peak power. The fuel cell is specified as the prime mover thereby leveraging the higher energy density of hydrogen. The vehicle is propelled by an electric motor that draws power during motoring and returns power to the battery during regenerative braking. This powertrain only emits water vapour, which warrants its green status if the hydrogen fuel was obtained from low-carbon sources.

The power split between the fuel cell and the battery is decided by an energy management system (EMS). Given that the fuel cell and battery posses unique characteristics, the EMS plays a highly consequential role in determining powertrain efficiency and degradation.

1.2 Aims

This thesis pursues two main aims:

1. Optimising the operation of fuel cell hybrid trains with the objective of minimising fuel consumption. This would help alleviate the economic barrier described in Section 1.1.3.

2. Formulate an algorithm to solve the first aim that:

   (a) guarantees finding the optimal solution. This increases the confidence of the professional user (e.g. powertrain designer, fleet engineer, timetable planner).

   (b) is computationally efficient. This enables quick computation time for future real-time applications and streamlines use by professionals.

1.3 Operational Aspects to Optimise

Traction is the leading consumer of energy for trains [28], therefore reducing traction demand is an effective means towards achieving the first aim outlined in Section 1.2. Figure 1.4 lists a range of measures to reduce traction consumption in conventional trains (diesel and electric). This thesis builds on the premise that while these measures are likely to remain relevant to fuel cell hybrid trains, further research is required to maximise returns due to the novelty of this variant of trains.

The fuel cell hybrid powertrain already implements the measure with the highest energy-saving potential from Fig. 1.4, which is installing an on-board energy storage system (battery in this case). This measure saves energy by recovering kinetic energy through regenerative braking for later use. Nonetheless, the energy savings returned by the battery are dependent on the amount of kinetic energy recovered which is dependent on the driving style and timetable. To this end, it is worthwhile asking whether conventional ecodriving practice and conventional timetables are able to fully leverage the energy-saving potential

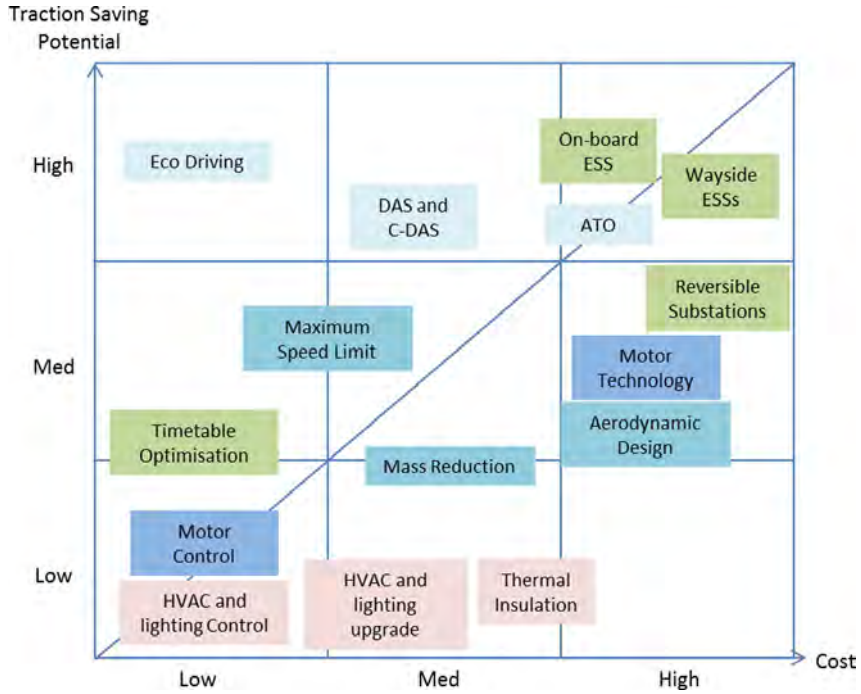

Figure 1.4: Energy saving potential and implementation cost of various rolling stock measures. Reprinted from [28]. © 2015 Elsevier.

of the fuel cell hybrid powertrain.

Ecodriving Figure 1.5 depicts conventional ecodriving practice: maximum acceleration rate, cruising (maintain speed), coasting (cut off traction) and maximum braking. This ecodriving style is being practised by various railways around the world [29, 30, 31]. The basic premise of this driving style is to save energy by maximising the span of coasting. This requires delaying and minimising the braking span as much as possible, hence maximum braking towards the end. Nonetheless, doing such deters from maximising energy recovery returns, because regenerative braking will need to be heavily supplemented by mechanical braking to achieve the short braking span. This lost opportunity at recovering kinetic energy is often ignored in the context of conventional trains due to the lack of an energy storage solution. However, hybrid trains are able to store recovered energy for later use which implies a wasted energy-saving opportunity. All of the above suggests that there could be a more efficient driving style for fuel cell hybrid trains.

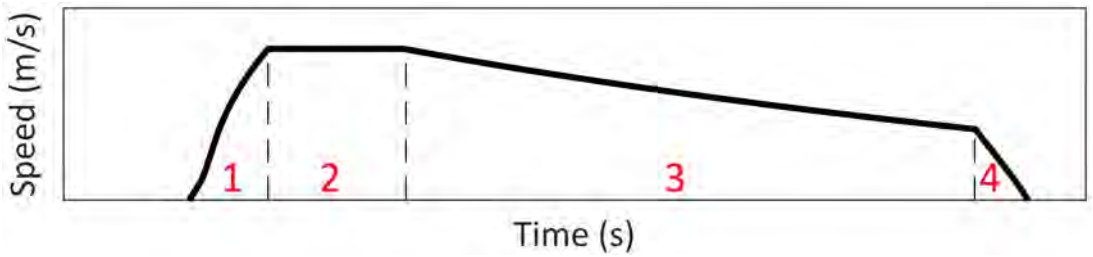

Figure 1.5: Current ecodriving practice: 1) maximum acceleration, 2) cruising, 3) coasting, 4) maximum braking.

Driving Style and EMS The energy management system (EMS) plays a pivotal role in storing the recovered energy into the battery and reusing it later to offset fuel consumption. Therefore, one needs to be aware of the EMS to drive the train efficiently. The most direct means of achieving this is to influence both driving style and EMS simultaneously. This suggests that jointly optimising speed and EMS is more fuel efficient than otherwise.

Connection to Degradation Relevant evidence from automotive literature suggests that tuning the EMS for maximum fuel economy can harm hybrid cars [32, 33]. This implies a compromise between fuel consumption and maintenance costs. Given the high capital cost of fuel cell hybrid trains, it becomes important to understand the impact of fuel economy on maintenance costs and thus cost of ownership on the long run.

Timetable Similarly to the conventional ecodriving style, it is to be expected that existing timetables are suboptimal for fuel cell hybrid trains. This is because existing timetables would have been designed to suit the characteristics of incumbent trains and thus fail to leverage kinetic energy recovery for a hybrid train. While some timetabling algorithms address kinetic energy recovery, this has primarily been done for urban rail transit (metros and trams) which possess different powertrain characteristics to fuel cell hybrids and are subject to a different duty cycle [34].

In light of the above, it is reasonable to hypothesise that train operating companies ought to rethink the adopted driving style and timetable for fuel cell hybrid trains to minimise costs. Moreover, these factors need to be optimised jointly with the EMS to

fully leverage the powertrain's characteristics. Jointly optimising this many factors at once is computationally challenging which motivates the next section.

1.4 Convex Optimisation

Convex optimisation problems posses a convex objective function and a convex feasible set [35]. The global optimal solution for this class of problems can be guaranteed to be found, because the convexity conditions themselves imply that any local minimum coincides with the global minimum. This also enables numeric algorithms to solve this class of problems efficiently and quickly. Therefore, convex optimisation meets the second aim outlined in Section 1.2 making it worthwhile pursuing in this work.

One challenge against using convex optimisation is that convexity conditions can limit model complexity and fidelity. This becomes restrictive when one attempts to model complex non-linear dynamics, which is often the case for real-world systems. Nonetheless, there is a growing body of research that attempts to optimise real-world systems using convex optimisation. This requires the modeller to balance between model convexity and model fidelity. Based on the author's previous research on automotive cruise control, such work already takes place in the automotive sector and is potentially very relevant to rail [36, 37]; both share the problem setting of optimising vehicle motion in the longitudinal plane.

This thesis builds on the premise that the computational properties of convex optimisation could become of utility to big optimisation problems in rail. This is particularly true in light of the joint optimisation problem previously motivated in Section 1.3 that is expected to be computationally complex, because it would jointly optimise many variables.

1.5 Research Hypotheses

Based on the motivation to optimise operation as described in Section 1.3 and use convex optimisation as described in Section 1.4, this thesis poses two categories of hypotheses. The first category of hypotheses concerns the optimal operation of fuel cell hybrid trains and is called operational hypotheses (HO). The second category concerns the algorithm used to deduce this optimal operation and is called algorithmic hypotheses (HA).

1.5.1 Operational Hypotheses

The following set of hypotheses are based on the initial findings of Section 1.3. For fuel cell hybrid trains:

HO1. Jointly optimising driving style and energy management system is more fuel efficient than conventional ecodriving that emphasises coasting.

HO2. Pursuing degradation-aware measures costs more fuel than otherwise.

HO3. Jointly optimising the driving style, energy management system and timetable saves fuel compared to following a given timetable.

1.5.2 Algorithmic Hypotheses

Given the benefits of using convex optimisation outlined in Section 1.4, it is highly desirable to asses whether the following hypotheses are true:

HA1. The joint optimisation of driving style and energy management system of a fuel cell hybrid train can be done using convex optimisation without overly simplifying system dynamics.

HA2. The joint optimisation of driving style, energy management system and timetable of a single fuel cell hybrid train can be done using convex optimisation without overly simplifying system dynamics.

2 LITERATURE REVIEW

This literature review firstly covers lithium battery degradation and PEMFC degradation in Sections 2.1 and 2.2, respectively. This knowledge is required to design and assess degradation-aware operating strategies.

Sections 2.3 and 2.4 review hybrid vehicle literature from rail and automotive domains, respectively. Automotive literature is added to this review due to the larger number of publications in the automotive domain, evidenced by the Scopus search results in Figure 2.1. This difference in publications is due to the longer prominence of hybrid cars on the market in comparison to hybrid trains.

Lastly, Section 2.5 identifies the gap between the current state of literature and the hypotheses presented in Section 1.5.

2.1 Lithium-Ion Battery Degradation

Subsection 2.1.1 first presents the composition of a lithium-ion battery and degradation basics that apply to most lithium battery chemistries. Subsections 2.1.2 and 2.1.3 then dive into the degradation specifics of lithium iron phosphate (LFP) and lithium titanate oxide (LTO) batteries, respectively. It was chosen to investigate these battery chemistries because they were among the safest high-power variants at time of writing, making them more suitable for hybrid rail vehicles [38]. Lastly, Section 2.1.4 summarises the reviewed knowledge into a group of insights that would directly influence the operating strategies derived in this thesis.

2.1.1 Basics

Figure 2.2 shows a 3D drawing of a single lithium-ion battery. It consists of two sides, namely a cathode side and anode side, kept apart by a separator layer that only permits

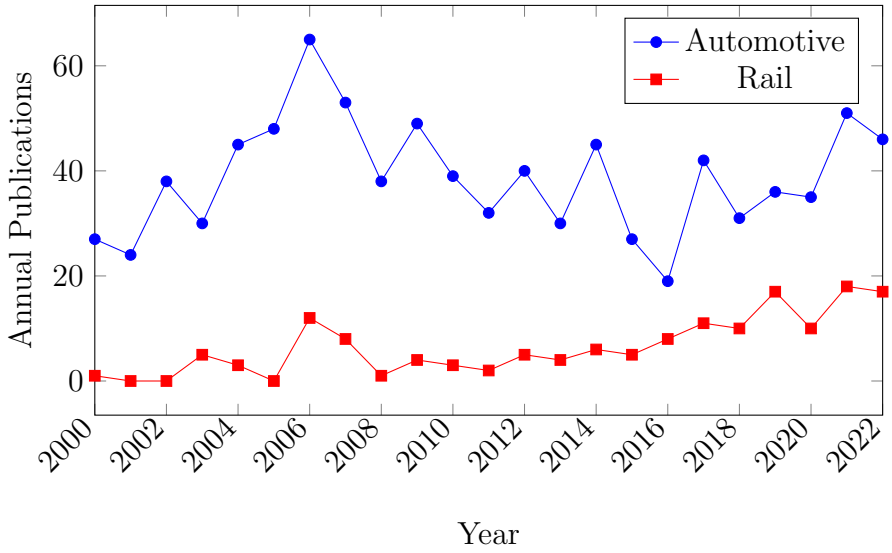

Figure 2.1: Scopus search of articles with automotive and rail keywords. Automotive represents the keywords "fuel cell hybrid" and "automotive", whereas rail represents the keywords "fuel cell hybrid" and "rail". Search performed on 13/09/2023.

the passage of positive lithium ions and prohibits the passage of electrons. This separator plays a crucial role in creating current by directing electrons towards the current collectors when connected to an external circuit. The electrolyte, often a liquid-based solution, acts as a charge carrier for lithium ions. During charging, lithium ions pass through the separator and intercalate into the anode material, whereas during discharging, they deintercalate from the anode to return to the cathode.

The anode and cathode are made of "active materials" that contribute to the battery's functionality. The cathode is made of a lithium-metal oxide that acts as an "active lithium" donor to the battery. The anode is made of a material of which lithium ions can easily intercalate into and out of. The choice of these active materials greatly influences battery characteristics, such as energy density, peak power, and lifetime.

Depending on the exact chemistry of the battery, degradation is caused by side reactions that deplete the active materials and active lithium, deteriorate the electrolyte, puncture the separator, and damage the current collectors. The accumulation of these side reactions over the lifetime of a battery will diminish its ability to store energy and deliver peak power, which will negatively affect vehicle fuel economy and performance.

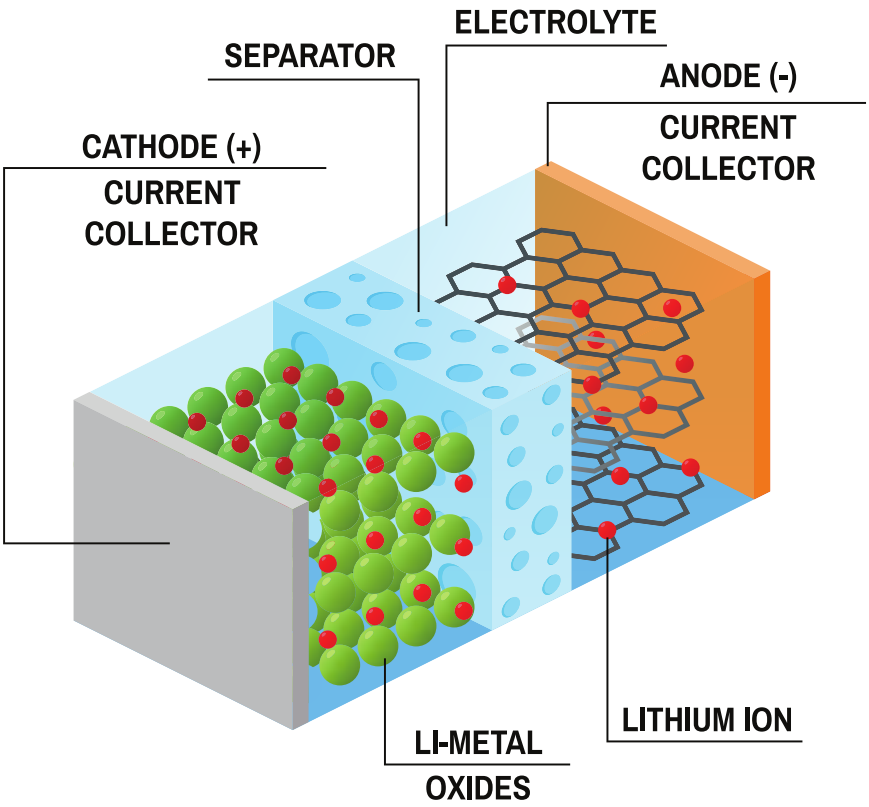

Figure 2.2: 3D drawing of a battery cell. Reprinted from iStock.com, artist ser_igor.

Degradation side reactions occur continuously regardless of whether the battery is being used or not. This has led to the terms "calendar ageing" and "cyclic ageing". Calendar ageing is degradation that is merely caused by the passage of time. Cyclic ageing is degradation caused by charge-throughput (exchange of charge) during active use. The rate of ageing at any given instance is dependent on stress factors. A test campaign of 124 lithium-ion batteries revealed that elevated cell temperature is a leading stress factor, followed by rate of charging, average SoC and rate of discharging [39]. These stress factors will be explored in more detail in Subsections 2.1.2 and 2.1.3.

The rate of battery ageing also depends on the current state-of-health; batteries with poorer state-of-health are expected to degrade at a faster rate than healthier batteries. Figure 2.3 shows how a lithium battery ages non-linearly with cyclic testing. The first subplot shows the storage capacity fading linearly after which it fades exponentially. The onset of exponential fade is often reported after the battery storage capacity has reached

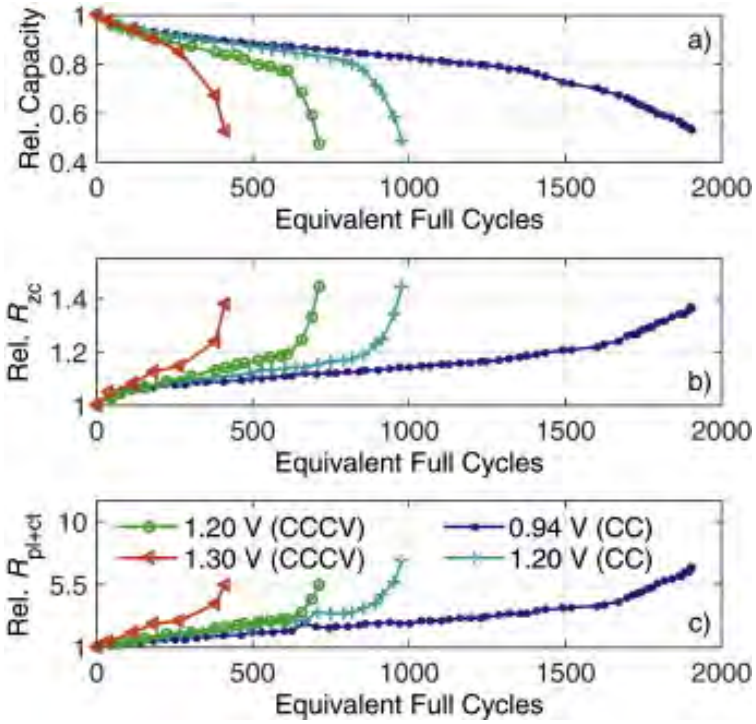

Figure 2.3: (a) Change in battery's energy capacity versus number of full cycles; (b) and (c) change in battery's impedance versus number of full cycles; a higher impedance causes larger power fade. Reprinted from [41]. © 2015 Elsevier.

80% of the original. The second and third subplots show a similar trend for impedance, which negatively affects battery power delivery. This trend has been documented for various lithium-ion chemistries [40, 41, 42].

2.1.2 LFP Batteries

LFP batteries are named after their use of lithium iron phosphate $LiFePO_4$ as the cathode's active material. The anode is made of a carbon-based material which is the most common anode material for lithium batteries. The state-of-health of the carbon-based anode is the limiting factor towards LFP's lifetime. This is because the carbon anode is electrochemically unstable and therefore vulnerable to side reactions with the surrounding electrolyte solution [42, 43, 44].

The most prominent side reaction affecting the carbon anode is the formation of the solid electrolyte interphase (SEI) layer. This is a layer of deposited electrolyte solvents

and lithium ions [45]. The materials forming the SEI layer become inactive, and thus, the lithium ions forming the SEI are no longer active, which leads to a loss in storage capacity. Nonetheless, an evenly formed SEI layer is beneficial because it protects the anode from further reacting with the surrounding electrolyte. This is why SEI formation is a vital step during the manufacture of lithium batteries [46]. The SEI layer also protects the battery from the formation of "lithium dendrites", which are needle-like structures of deposited lithium that grow unevenly and could short-circuit the battery by puncturing the separator. Therefore, any conditions that disrupt the SEI layer are undesirable.

The influence of calendar ageing on the SEI layer is primarily determined by the average temperature and average state-of-charge (SoC). Leaving the battery at high temperature and high SoC increases the risk of cracking the SEI layer [47, 48, 49, 50].

It is recommended to operate LFP batteries within the temperature range of $25 - 40\text{C}^\circ$ [51, 52]. Higher temperatures negatively affect SEI stability [53], while lower temperatures cause a power fade due to slower ionic kinetics. Furthermore, operating at lower temperatures induces irreversible lithium plating instead of reversible lithium intercalation [45]. Plated lithium also increases the risk of fire because it is known to reduce the onset temperature of thermal runaway [54].

The magnitude of current (C-rate) also affects SEI stability due to local ohmic heating [55], although some high-power LFP batteries are better at handling high currents [56]. Charging a battery above its rating invariably causes lithium plating [57].

Carbon-based anodes experience a considerable change in volume when cycled. The anode expands as lithium ions are intercalated during charging, whereas it anode shrinks when lithium ions are deintercalated during discharging [58]. Repeating these physical changes weakens the existing SEI layer and causes it to crack [59]. The magnitude of these volumetric variations increases with a deeper DoD, leading to faster ageing when operating in a wider SoC range [55, 60, 61]. In addition to its impact on the SEI layer, periodic changes in the anode's volume weakens the interface between the current collector

and the anode, which causes a rise in electric impedance.

The degradation of an LFP battery over its lifetime follows the same non-linear trend previously shown in Fig. 2.3. This is directly coupled to the state-of-health of the SEI layer. The battery initially experiences slow degradation as the original SEI layer is still intact, but then accelerates later as damage to the SEI layer accumulates. This accelerated degradation occurs because an unevenly worn SEI layer will be disproportionately stressed at its weakest points which will ultimately restrict the useful life of the battery [62].

2.1.3 LTO Batteries

LTO batteries are named after their use of lithium titanate oxides as the anode's active material. Unlike the carbon-based anode used in LFP batteries, titanate oxide anodes are electrochemically stable and thus do not grow an SEI layer. Furthermore, they are not susceptible to growing lithium dendrites or lithium plating, which improves electric safety and thermal stability [63]. Titanium oxide anodes also exhibit very little volumetric changes during cycling, which circumvents physical cracking of the current collector. These favourable characteristics lead the LTO battery to last significantly longer than LFP batteries [44]. Indeed, LTO batteries are known to surpass 20,000 cycles of use, whereas LFP batteries can only achieve up to 5,000 cycles.

Unlike LFP batteries, LTO batteries can operate safely over a wider temperature range, including freezing temperatures. This is possible due to the lack of lithium plating [64], which also allows LTO batteries to achieve much higher C-rates.

It is discouraged to store LTO batteries at low SoCs because titanate oxide anodes are not chemically stable at low SoCs. LTO batteries are also prone to high self-discharge rates when stored at low SoCs [46, 47, 65].

Lastly, LTO batteries exhibit the same non-linear degradation trend shown in Fig. 2.3 [66, 67, 68], though timescales are much longer than LFP batteries.

2.1.4 Concluding Remarks on Battery Degradation

The following has been concluded from the preceding battery review:

- Charge-throughput is the main driver behind cyclic ageing for lithium chemistries.
- Battery temperature is to be regulated to slow down harmful side reactions.
- Battery current is to be limited to avoid excessive ohmic heating.
- Avoid high state-of-charge levels for LFP batteries to circumvent harming the SEI layer.
- Avoid low state-of-charge levels for LTO batteries to prevent self-discharge.

Given that LTO batteries are more durable, last longer, and can achieve higher power than LFP, they are becoming an increasingly popular choice for heavy-duty transport applications. As a matter of fact, the *Siemens Mireo Plus B* (battery train) is already being offered with a 700 kWh LTO battery [69].

While LTO exhibits a lower energy density than LFP (in some cases less than half the energy density), this is not anticipated to be a limiting factor to hybrid applications that have another prime mover (fuel cell in the case of this thesis). Moreover, the cost of LTO batteries is expected to be cheaper than LFP batteries per unit power [70].

Therefore, for the purposes of this thesis, it is reasonable to assume that the LTO chemistry will be used for upcoming fuel cell hybrid trains.

2.2 PEMFC Degradation

This section firstly introduces the composition of a PEMFC and degradation-related facts in Subsection 2.2.1. It then reports on PEMFC ageing studies found in literature, namely lab-based in Subsection 2.2.2 and vehicle-based in Subsection 2.2.3. Lastly, Section 2.2.4 summarises the reviewed knowledge into a group of insights that would directly influence

the operating strategies derived in this thesis.

2.2.1 Basics

The durability of PEMFCs is becoming increasingly more compatible with rail's requirements. The Clean Hydrogen Joint Undertaking estimates that heavy duty PEMFCs currently achieve 15,000 hours of operational life, where this figure is expected to increase to 30,000 hours by 2030 [71]. The latter figure seems increasingly realistic to achieve given that hydrogen bus trials have already surpassed the 20,000-hour mark [72] and Ballard claims that its heavy-duty offering is capable of more than 25,000 hours [73]. Nevertheless, simply meeting these durability targets does not guarantee economic operation because consumption increases as efficiency drops with ageing. This motivates developing a thorough understanding of the mechanisms and conditions that induce PEMFC degradation to best counteract it.

The degradation of a PEMFC can be characterised by a decrease in power output at a given current density [74]. Figure 2.4 shows how the voltage-current curve drops with ageing which leads to a drop in nominal and peak power. A $10 \sim 15\%$ drop in power output is widely cited in literature as the end-of-life criterion for fuel cells. The decline in power output is initially linear but later accelerates toward the end of a fuel cell's lifetime [75].

Figure 2.5 shows a 3D drawing of a single PEMFC cell, where multiple similar cells are joined in series to achieve a stack's required voltage. Multiple stacks are connected in parallel to achieve the required power output. The external bipolar plates double as current conductors on the outside and provide a flow pathway for gas species on the inside. A layer inwards of that, the gas diffusion layer (GDL), is a hydrophobic carbon-based material that flushes excess water to prevent water blockages [77]. Catalyst particles (usually platinum held in place by carbon supports) are embedded into the anode and cathode to sustain the cell's redox reaction at its low operating temperature; hydrogen

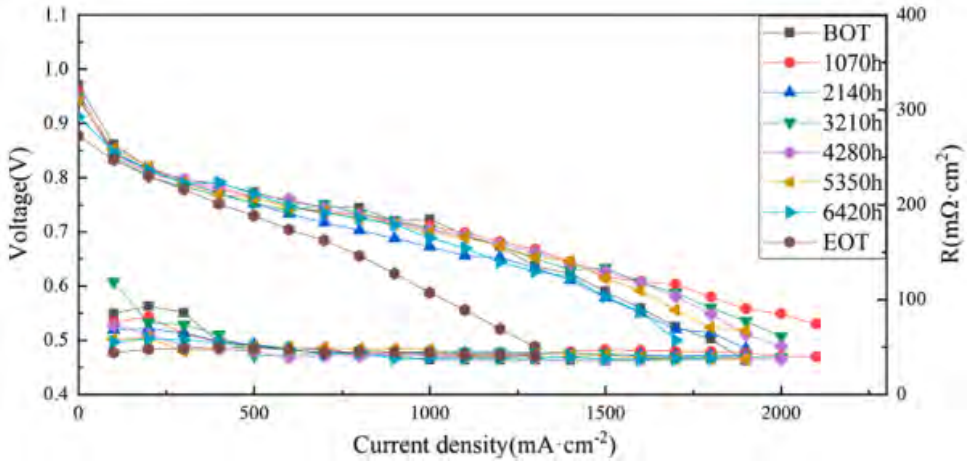

Figure 2.4: Fuel cell voltage (left axis) and resistance (right axis) at Beginning of Testing (BoT), several testing snapshots and End of Testing (EOT). Reprinted from [76]. © 2022 Elsevier.

oxidation occurs on the anode side and oxygen reduction on the cathode side. Lastly, the polymer electrolyte membrane in the middle plays the crucial role of conducting hydrogen ions from the anode to the cathode while redirecting electrons to the external circuit. The membrane is made of a polymer material that conducts hydrogen ions at high relative humidity; therefore, its water content needs to be regulated to maintain ionic conductivity while not causing water blockages. Water is inherently introduced into a fuel cell as a byproduct of the redox reaction, and more water can be introduced by humidifying the cell's air supply. Conversely, water can be expelled by the supply of high flowrates of dry air.

2.2.2 Lab-based Ageing Studies

A substantial number of studies suggest that membrane and catalyst deterioration are the leading causes of PEMFC performance degradation [78, 79, 80, 81, 82]. These findings are also confirmed by fault tree analysis [83] and prognostic models [84, 85].

Among the primary issues affecting the membrane is cracking and thinning. These cause ohmic shorting and reactant crossover between the cathode and anode, which reduce the amount of current produced. In some cases of severe reactant crossover, a cell can become

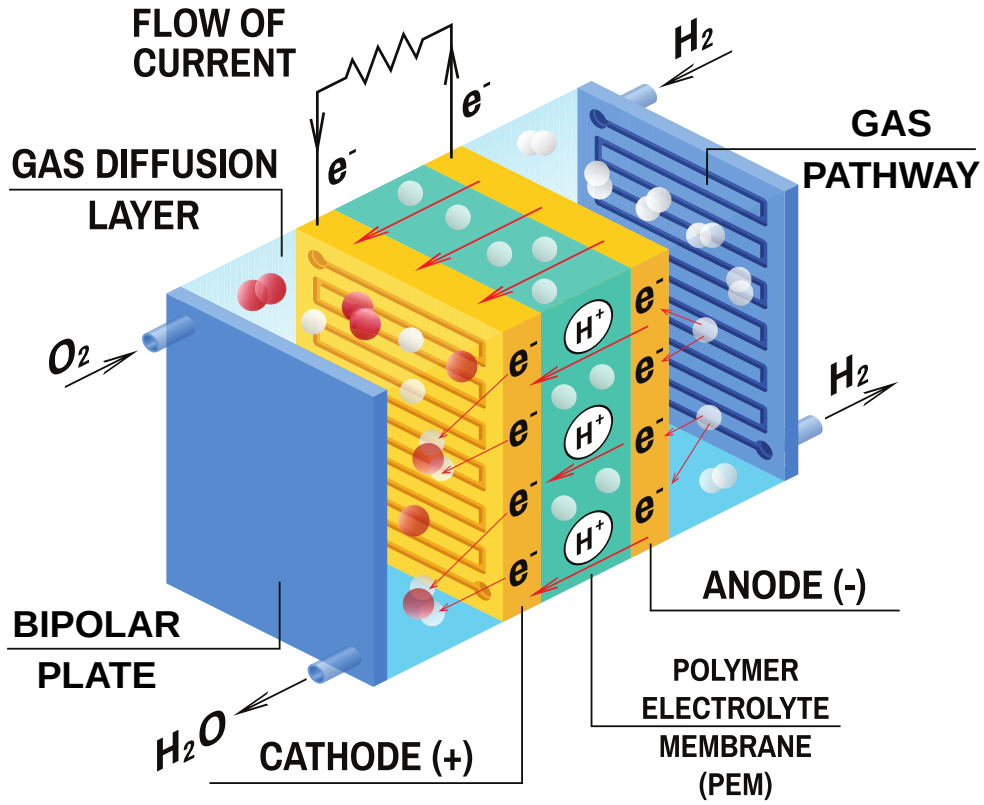

Figure 2.5: 3D drawing of a PEMFC cell. Reprinted from iStock.com, artist ser_igor.

completely inoperable, adversely affecting all surrounding cells connected in series [86]. Furthermore, reactant crossover has been identified as the most prevalent cause of sudden catastrophic failure. An example of this can be seen in Fig. 2.6, which shows a pronounced drop in stack voltage at the onset of severe crossover.

Membrane cracks arise primarily due to fluctuations in humidity. These fluctuations occur because of the change in water byproduct formation as the cell's power output is varied. As the membrane expands and contracts with varying humidity levels, fatigue-induced microtears form [88]. Larger and faster changes in hydration induce greater stresses, which increases the probability of tearing [89]. Over time, the accumulation of these microtears can evolve into larger cracks. On the other hand, membrane thinning is triggered by side reactions that occur due to the unexpected presence of crossover reactants [90]. This sets off a detrimental feedback loop where crossover reactants further weaken the membrane, leading to increased thinning and cracking.

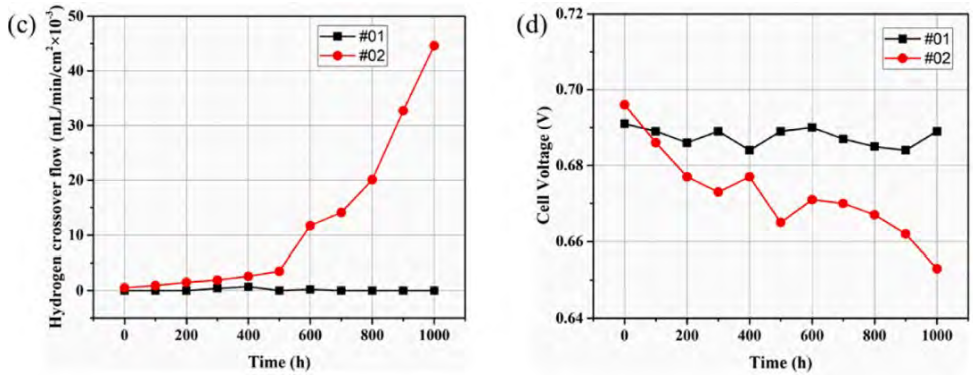

Figure 2.6: Fuel cell ageing testing on two stacks #01 and #02. Plot c) shows that #02 suffered from catastrophic reactant crossover starting from about hour 600. Plot d) shows the accompanying collapse in cell voltage after onset of reactant crossover [87]. © 2023 Elsevier.

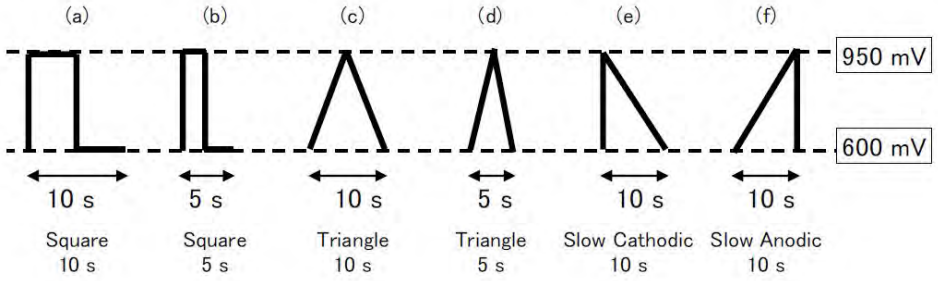

Figure 2.7: Voltage cycle profiles. Profile a) is the most damaging while profile f) is the least. Reprinted from [96]. © 2007 ECS - The Electrochemical Society.

The health of the catalyst layer is determined by its remaining active area. It faces degradation from several mechanisms, each slowing the cell's redox reaction. The most significant of these mechanisms involves the oxidation and agglomeration of catalyst particles, particularly during changes in cell potential and sustained open-circuit voltage [91]. Research indicates that larger and more frequent swings in potential towards the open-circuit voltage are particularly detrimental to the active area of the catalyst [92, 93, 94]. The specific shape of the cycled voltage profile also influences degradation [95, 96]. Fig. 2.7 illustrates various voltage profiles, with profile a) being the most damaging and profile f) the least.

The catalyst's active area can also be diminished if catalyst particles were displaced. This can occur when their carbon supports corrode due to reactant starvation [97]. Similarly, reactant starvation can erode the carbon in the GDL, thereby compromising its

hydrophobic structure that is crucial for water flushing [98]. Notably, these carbon corrosion instances also increase the cell's impedance.

It is worth noting that the aforementioned degradation mechanisms accelerate at higher operating temperatures and pressures because of the acceleration of harmful side reactions. While elevated conditions as such can also enhance the fuel cell's redox reaction, thus boosting performance [99], it is vital to strike a balance between performance and degradation.

2.2.3 Vehicle-based Ageing Studies

Figures 2.8a and 2.8b depict the degradation attributed to various phases of the duty cycle of a hydrogen bus and car, respectively. Specifically:

- load-cycling refers to periods of varying power output,
- start-stop refers to the starting-up and shutting-down stages,
- idling refers to near zero power output,
- high-power refers to operating near peak power rating.

The discrepancy observed between both figures is probably attributed to differences in duty cycle and system design. Nonetheless, the load-cycling and start-stop phases consistently emerged as the most detrimental.

Load-cycling is a recurring event during a duty cycle, primarily because power demand fluctuates in tandem with traction needs. This phase affects the fuel cell in multiple ways: i) it affects the catalyst particles as a result of potential cycling and ii) it leads to membrane tearing and cracking as a result of humidity fluctuations that accompany varying levels of water byproduct formation.

On the other hand, the damage associated with the start-stop phase can be traced back to a pronounced occurrence of reactant starvation as the system transitions between its

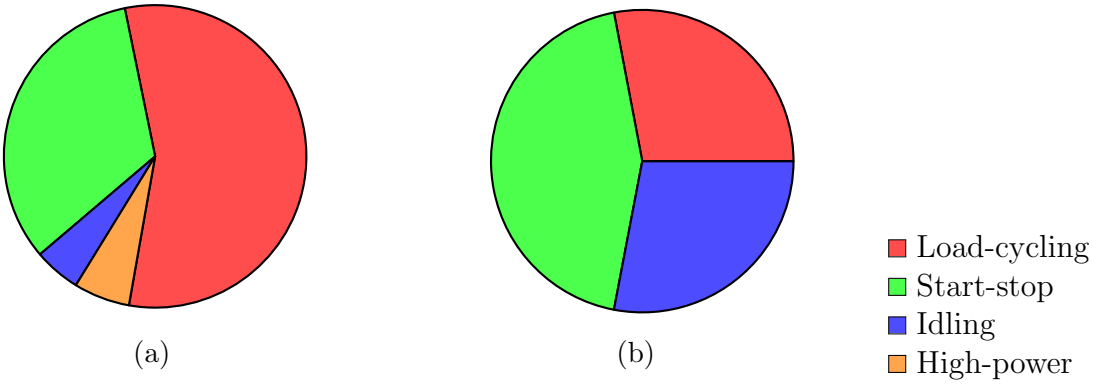

Figure 2.8: Fuel cell degradation contribution by phases of road duty cycles; (a) hydrogen bus data adapted from [103]; (b) hydrogen car data adapted from [104]. High-power data for (b) was not found.

off and on states [100].

Lastly, the idling phase poses risks to the catalyst, mainly because it maintains the cell potential at open-circuit levels. The likelihood of reactant crossover also increases as static pressure builds up during idle [101, 102].

2.2.4 Concluding Remarks on Fuel Cell Degradation

The following has been concluded from the preceding PEMFC review:

- Avoid idle power to reduce reactant crossover and damaging the catalyst through open-circuit voltage.
- Avoid high-power power outputs to maintain uniform and steady reactant distribution within the fuel cell.
- Avoid frequent power swings to minimise membrane damage.

2.3 Railway Literature

This review covers speed optimisation, EMS and timetabling practices from rail literature. The body of literature that specifically addresses fuel cell hybrid trains is relatively small; therefore, this review is not exclusive to fuel cell hybrid publications and covers other

relevant powertrains as well, such as diesel-hybrid trains [105], battery-powered trains [106] and supercapacitor-powered trains [107]. A recent review exclusive to fuel cell hybrid trains was covered by [108].

Subsection 2.3.1 covers publications that exclusively address one of the following: speed, EMS, and timetabling. On the other hand, Subsection 2.3.2 covers publications that address multiple of these objectives. These publications are reviewed separately to better showcase the potential benefits of jointly optimising multiple objectives together. Lastly, Subsection 2.3.3 summarises relevant insights from the rail review and identifies potential deficiencies in literature.

2.3.1 Single Objectives

Dynamic System Optimisation The most prominent methods to optimise the trajectory of dynamic systems are: direct methods, indirect methods, dynamic programming (DP), metaheuristic optimisation methods.

Direct and indirect methods optimise by searching for a trajectory that satisfies conditions of optimality derived using the system's model. The difference between these methods is the means of deriving the conditions of optimality. Direct methods directly form a finite optimisation problem to search for a finite-step trajectory. The optimality conditions are decided by the numeric algorithm used. Indirect methods firstly derive conditions of optimality in the continuous domain using calculus of variations or what is commonly known as Pontryagin's Maximum Principle (PMP). This involves forming and solving a boundary-value problem (setting equality constraints at problem boundaries).

One benefit of using indirect methods is that the derived optimality conditions provide physical insight into the system's optimal behaviour which can be generalised. These conditions can also sometimes be solved analytically instead of numerically. However, adding inequality and complex constraints makes these optimality conditions more difficult to

compute. On the other hand, direct methods natively support a wide range of constraints by leveraging recent advances in numeric methods.

Dynamic programming relies on "Bellman's Principle of Optimality" to construct the optimal trajectory by optimising constituent sub-problems. This makes DP a very capable optimisation tool that possesses guarantees towards finding the optimal solution. Nonetheless, DP requires discretising the search space (system states and intputs) which causes computational complexity to grow exponentially with problem size, known as "Bellman's Curse of Dimensionality". Therefore, DP is often reserved for offline analysis instead of real-time control and often requires simplifying assumptions to maintain computational tractability.

Stochastic Dynamic Programming (SDP) is a further variation of DP that assumes stochastic system dynamics instead of deterministic dynamics. One use of this extension is modelling uncertainties to obtain a more resilient trajectory.

Metaheuristic methods often use nature-inspired algorithms to solve complex optimisation problems where traditional methods, like direct, indirect, or dynamic programming, struggle due to large search spaces and non-linearity. Metaheuristic methods seek near-optimal solutions by intelligently exploring the search space through iterative, stochastic processes. Examples include genetic algorithms (GA) which depends on evolution of solution populations, and ant colony optimisation (ACO) which mimics the way ants find optimal paths by laying and following pheromones. Both are more flexible and scalable compared to dynamic programming (DP), which ensures optimality but suffers from exponential computation time as problem size increases. Metaheuristics offer a powerful alternative by trading off guaranteed optimality for practical efficiency.

Speed Optimisation The majority of speed optimisation literature focuses on reducing traction consumption to reduce energy consumption. This domain was extensively reviewed by [109].

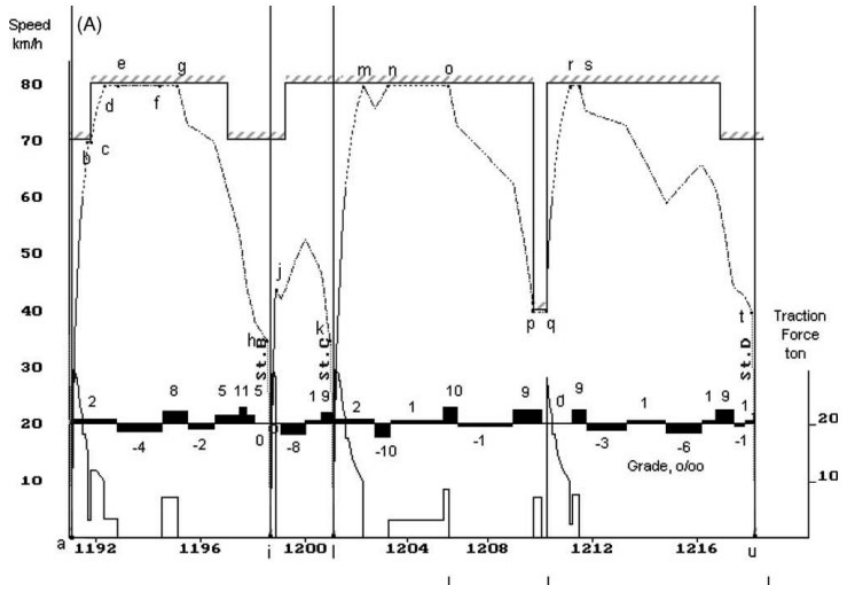

Figure 2.9: Train speed on left axis, traction force on right axis, speed limit illustrated as hatched line on top, gradient shown as solid bars. The figure shows the use of five phases (partial power, partial braking, full power, full braking and coasting) to suit the optimised route. Reprinted from [111]. © 2003 Elsevier.

The simplest use of the indirect method (Pontryagin's Principle) assumes level track and no speed limits which yields the ordered four phases of Fig. 1.5 [110]. Upon adding gradient and speed limits, the solution deviates from the aforementioned four phases and applies the following five phases: partial power, partial braking, full power, full braking and coasting [111]. On the contrary to the former four phases, the latter five phases are deployed in an order that is specific to the route optimised and can even be repeated and interleaved. This is to meet varying speed limits and steep gradients. Figure 2.9 shows an example of this.

A recent development of using the indirect method is the ability to include further dynamics such as non-linear regenerative braking which was achieved by solving the optimality conditions using the pseudospectral method [112]. This derives a more complicated operation regime of seven phases: 1) maximum acceleration, 2) holding speed by partial traction, 3) coasting, 4) holding speed by partial regenerative braking, 5) maximum regenerative braking, 6) cruising by maximum regenerative braking and partial mechanical braking, and 7) maximum braking.

The implementation of direct methods depends on the numeric method used to formulate the optimisation problem. This most often includes nonlinear programming and integer programming. The resulting fidelity is highly dependent on the formulation built. Integer programming is often used due to its superior expressiveness though this comes at a high computational cost due to its use of boolean optimisation variables. For instance, the speed of a hydrogen train was optimised using integer programming in [113]. They used special ordered set (SOS2) constraints to simplify the boolean search thus controlling computational complexity. Nonetheless, they did not include EMS optimisation, possibly to avoid excessive computational complexity.

Ant colony optimisation (ACO), genetic algorithm (GA) and dynamic programming (DP) were compared for single-train speed optimisation [114]. In terms of solution optimality, DP was best followed by GA then ACO, which however came at a higher computational cost. Both ACO and GA rely on solution convergence until the termination criteria is reached. Although ACO reached a lesser optimal solution than GA, it converged to a solution in a more stable manner.

EMS Railway EMS algorithms can be classified into: rule-based, optimisation-based and data-based algorithms. They vary in objective and computational complexity.

Rule-based methods fall into the subcategories: crisp logic, fuzzy logic and frequency decoupling. Crisp logic is synonymous with boolean logic, where a decision is dependent on whether a statement is true or false. These algorithms can be implemented using computationally light if-then statements or state machines.

The earliest examples of crisp logic EMS were primarily concerned with maintaining battery state-of-charge within bounds [115, 116, 117]. Later work sought to improve dynamic performance and kinetic energy recovery around steep slopes [118]. Fuel cell efficiency parameters has also been integrated into algorithm design to focus operation around the most efficient points [119]. A rule-based algorithm was also designed to mimic the optimal behaviour of offline DP on a specific route [120].

Designing and testing crisp logic can become laborious task. An alternative is fuzzy logic: using intermediate input and output values that are intuitive to describe linguistically rather than crisp values. Kinetic energy recovery can be improved using fuzzy logic [121]. Fuel cell efficiency parameters can be integrated into fuzzy logic [122]. Moreover, fuzzy logic parameters can be tuned offline using computer simulations [123].

To reduce load-cycling on the fuel cell, it could be operated with a soft-run strategy, where fuel cell power is kept steady and demand transients are delegated to the battery. This has the added benefit of reducing fuel cell degradation, though comes at the expense of additional fuel consumption because power could be held unnecessarily high. An attempt to achieve soft-run using heuristics is to divide the journey into a finite number of sections during which fuel cell power is held steady [124].

Despite the positive impact of a soft-run strategy on fuel cell health, it could have adverse effects by excessively charging or discharging the battery [125]. To this end, fuzzy logic has been used to design EMS to limit battery degradation [126]. The parameters were tuned using a Genetic Algorithm to minimise energy consumption and battery degradation. The latter was modelled using the Rainbow Flow algorithm, which counts the number of full charge-discharge cycles.

In order to encourage more research around hydrogen trains, the IEEE Vehicular Technology Society held a design competition for the EMS of a dual-mode hydrogen locomotive [127]. The locomotive can be powered by overhead catenary as well as its on-board fuel cell, battery, and supercapacitor. Contestant submissions were evaluated according to the running cost of overhead electricity, hydrogen fuel, and component degradation. Both the winner [128] and the runner-up [129] submitted rule-based algorithms that prioritise fully charging on-board storage by the overhead catenary when available. This provides an energy buffer to be used on non-electrified segments prior to relying on more expensive hydrogen fuel to power the fuel cell. A similar scheme was proposed for dual-mode hydrogen trains by [130] though is not related to the aforementioned IEEE competition.

All of the aforementioned uses rule-based algorithms and heuristics which were proven sub-par compared to optimisation-based methods [131]. The equivalent consumption minimisation strategy (ECMS) is an indirect optimisation method based on PMP. It can be solved analytically under certain simplifying assumptions which explains its popularity [132, 133, 134, 135].

Optimisation methods were not limited to minimising fuel consumption but also included constraints to limit degradation, e.g. a constraint on fuel cell slew rate [136]. Optimisation methods have also been reported to outperform reinforcement learning in terms of solution optimality [137].

Timetabling Timetables are designed to provide good performance for passenger and freight traffic [138]. The following performance indicators are often considered during timetable design:

- Travel time efficiency, which considers running time, dwell time and transfer.
- Energy efficiency of the running rail traffic.
- Utilisation rate of existing rail infrastructure.
- Timetable robustness to service deviations.
- Timetable resilience, which is its ability to recover from major disruptions.
- Timetable flexibility, which is the ability to adjust, e.g., to meet unexpected demand.

The design of a timetable goes through four planning stages:

1. Strategic planning: addresses aspects that require long-term planning, e.g., infrastructure investments to meet capacity targets. Therefore, it takes place years in advance. It primarily relies on macro-level simulation which only covers main stations, main junctions and traffic flow.
2. Tactical planning: addresses schedule design, train routing, arrival and departure

times from stations as well as platform assignments. This takes place up to one year in advance. A mixture of macro and micro level simulations are used.

3. Operational mid-term adjustment takes place up to 6 months to 1 week in advance. This is to account for maintenance issues, rolling stock availability, and variable traffic demand.

4. Operational short-term adjustment take place up to 48 hours in advance and is mainly concerned with near real-time re-planning to meet unexpected changes.

Of these stages, tactical and operational planning are the most relevant to this thesis. Tactical planning operates at both macro and micro levels. The macro level focuses on high-level aspects, such as traffic flow, routing, and planned stops, whereas the micro level delves into detailed aspects like train speed profiles, traction power profiles, and track occupancy. The difference in modelling detail allows the macro level to address broader network-wide considerations, while the micro level provides greater precision for specific areas that require detailed analysis.

Macro-level optimisation, such as in [139], is particularly effective for addressing large-scale railway networks. In this study, a mixed-integer programming approach is applied to optimise schedules for passenger and freight trains. The model does not take into account detailed speed profiles but rather high-level traffic flow. The model estimates emissions using train weight, the number of planned stops, delays, and waiting times. This high-level approach enables planners to assess the schedule of a wide geographic area.

As the focus shifts to smaller, more localised sections of the rail network, micro-level optimisation plays a crucial role in fine-tuning train operations. One study explores micro-level speed optimisation for multiple trains, aiming to minimise energy consumption and delay through three techniques: enhanced brute force (EBF), ant colony optimisation (ACO), and genetic algorithms (GA) [140]. While EBF consistently finds a more optimal solution, it requires significantly more computational power than ACO and GA, which

converge faster but provide slightly less optimal results. This illustrates the trade-offs in computational load and optimisation quality at the micro level, particularly relevant for short-term operational planning where near real-time adjustments are necessary.

Further enhancing micro-level optimisation, another study focuses on the integrated optimisation of both train speeds and timetables, aiming to improve metro operations by synchronising departures and arrivals to better utilise regenerative braking energy [141]. By employing genetic algorithms, this joint optimisation approach not only maximises energy efficiency but also enhances timetable precision, which is especially critical in dense urban environments. The topic of speed and timetable optimisation has been reviewed by [109], though primarily covers conventional traction (electric and diesel).

2.3.2 Multiple Objectives

Some rail research has attempted to optimise more than one operational variable. This could take a sequential form where variables are optimised separately in a specific sequence with decisions flowing forward only. For instance, a timetable could be optimised offline by network planners after which a separate entity optimises the speed profile of individual trains [142]. Another example is sequential optimisation of a hybrid train where speed is optimised first which dictates power demand that the EMS attempts to cater to [143]. Sequential optimisation also includes hierarchical control, e.g., top layer plans journey trajectory, intermediate level optimises speed until next stop, and lowest layer optimises EMS in real-time for current horizon [144].

While there is lack of published data, sequential optimisation is believed to be the most used in practice. This is because the majority of literature addresses individual objectives as shown in Section 2.3.1. It is also more natural for organisations to adopt, because it is compatible with the idea of "separation of concerns". Moreover, it is easier to implement from a computational perspective because it naturally breaks down a big optimisation problem into smaller more manageable ones.

Nonetheless, sequential optimisation cannot guarantee finding the global optimal solution because it fails to leverage the dynamic interaction between variables. This is because decisions that are passed as optimal from a previous step cannot be changed/optimised in light of the currently optimised variable. An example of such dynamic interaction is the interaction between electric trains running simultaneously on an overhead section. Overhead power peaks could be reduced and recovered kinetic energy (regenerative braking energy) could be more efficiently reused if the timetable were adjusted with prior knowledge of these aspects [145, 146].

An alternative approach that mitigates the aforementioned limitation of sequential optimisation is joint optimisation, where all variables are optimised simultaneously. This empowers the optimisation problem to fully leverage the dynamic interaction between optimised variables. However, this comes with computational concerns as complexity increases by encapsulating all smaller problems into a single bigger one. Various means of dealing with this complexity was found in hybrid rail literature.

Examples include the use of the gradient method to jointly optimise speed and EMS for electric trains with way-side storage [147]. The problem is simplified by only optimising operation between a single pair of stations instead of the entire journey. The authors do not mention specifics about compute time but acknowledge that it is lengthy.

Non-linear programming was used to jointly optimise speed and EMS of a battery electric multiple unit for an entire journey [106]. A large discretisation step of 100 metres was used to obtain acceptable compute time on the order of tens of seconds. The error from using this big discretisation step was reported to be around 5%.

Dynamic programming was used for jointly optimising speed and EMS for urban trains with on-board storage [148]. They do not report compute time but discretise their DP search space very coarsely to maintain computational tractability. A comparable example of an urban train with on-board storage required 1 hour to optimise operation between a single pair of stations using DP [149]. It showed a very promising reduction in energy con-

sumption of 13 % for joint optimisation when compared to sequential optimisation.

In another study about urban trains with on-board storage, integer programming was used to optimise operation between a single pair of stations [150, 151]. The computational time was under 1 second for 1.8 km distance though for a relatively large discretisation grid of 100 metres per step. This work was then extended to a complete line with multiple stops by "stitching up" the optimised segments between each pair of consecutive stations [152]. A drawback of this "stitching" approach is causing state discontinuity between neighbouring segments. Moreover, it fails to account for the impact of dwell time on the state. Indeed, the state-of-charge of the energy storage device was found not to be matching between neighbouring segments. This a potential source of sub-optimality as it fails to effectively optimise the operation of the energy storage device. Worse still, it could harm the energy storage device by excessive charging and discharging.

Integer programming was also used for jointly optimising speed and EMS for fuel cell hybrid trains [153]. The benefit of using the joint method was around 6 % in comparison to the sequential method. Compute time was on the order of seconds for a consecutive pair of stations 10 km apart.

One of the only examples in literature that considers speed, EMS and timetable of fuel hybrid trains was found in [154]. They use dynamic programming sequentially to first optimise timetable, then speed and lastly apply a rule-based method for EMS. Despite them using sequential optimisation, the computation time lasts 13 hours for optimising an entire regional line that is 80 km long.

2.3.3 Concluding Remarks on Railway Literature

The following keys insights were concluded from the rail review:

- The energy savings from joint optimisation was in the range of 5%–20% when compared to sequential optimisation.

- There is lack of understanding of whether conventional ecodriving that emphasises coasting is efficient or optimal for hybrid trains. Joint optimisation of speed and EMS could offer insights that answer this.
- There is lack of understanding about the impact of measures against degradation on fuel economy.
- There is need for an alternative approach for joint optimisation that is computationally efficient. This is because existing publications, especially joint speed-EMS in Section 2.3.2, make simplifying assumptions to mitigate computational complexity. These assumptions come at the expense of solution optimality. Convex optimisation has not been considered by any of these publications which suggests it is worth investigating further.
- There is no research on the joint optimisation of speed-EMS-timetable for hybrid trains. The only relevant example found uses sequential optimisation [154].

2.4 Automotive Literature

The energy management system (EMS) of automotive hybrid vehicles has received substantial research interest due to their prominence. There are several review papers concerning the EMS of fuel cell hybrid vehicles in particular [155, 156, 157, 158]. Much of this knowledge could be utilised in the rail problem setting and is thus reviewed in this section.

Subsection 2.4.1 focuses on the most common objective of the EMS which is improving operational efficiency. Subsections 2.4.2 and 2.4.3 present EMS designs that mitigate battery and fuel cell degradation, respectively. Subsection 2.4.4 outlines a new paradigm of combining EMS optimisation with wider system-level optimisation. Lastly, Subsection 2.4.5 distils insights from the automotive review that could be relevant to this research.

2.4.1 EMS

EMS algorithms broadly fall into three categories: (i) rule-based, (ii) optimisation-based, and (iii) learning-based. This classification is based on the methodology underpinning the EMS power-split decision. Rule-based methods are computer expert systems that embed human intuition and expert knowledge about powertrain energy management into a set of rules. Optimisation-based methods use powertrain models to mathematically optimise an objective, such as minimising fuel costs, within given constraints. Learning-based methods deploy machine learning to make decisions based on historic duty cycle data.

Table 2.1 lists the EMS algorithms from automotive publications that focus primarily on fuel economy. This table first segregates the literature based on the three categories mentioned above and then further divides them based on the specific algorithm used.

Rule-based Methods

Rule-based methods fall into the subcategories: crisp logic, fuzzy logic, frequency decoupling and time series. An example of crisp logic is thermostat and hysteresis algorithms.

With a thermostat-based algorithm, the fuel cell is switched on and off to maintain the battery's SoC within a predefined range. When switched on, the fuel cell is operated only at a predefined power level, most favourably its peak efficiency power level, regardless of the vehicle's power demand. Following this heuristic, however, does not always lead to efficient operation: (i) excessively charging the battery up to the upper SoC limit would impede its ability to absorb recovered kinetic energy, (ii) charging the battery using the fuel cell is subject to fuel cell losses, and (iii) relying heavily on the battery while the fuel cell is switched off accelerates unnecessary battery wear. State machines can reduce the prevalence of such issues by adding additional sophistication to the if-then statements. One example is allowing the fuel cell to operate at multiple power levels that are selected

Table 2.1: Classification of automotive FCHEV EMS algorithms found in literature

Category	**Subcategory**	**Algorithm Name**	**Examples**
Rule-based	Crisp Logic	Thermostat	[159, 160]
		Hysteresis	[161, 162]
		State Machine	[163, 164, 165, 166, 167, 168, 169, 170, 171]
	Fuzzy Logic	Basic	[172, 173, 174, 175, 176, 177, 178, 179, 180, 181, 182, 183]
		Adaptive	[184, 185, 186, 187]
	Frequency Decoupling	Wavelet Transform	[188, 189]
	Time Series	Moving Average	[189, 190]
Optimisation-based	Offline	Dynamic Programming	[191, 192, 193, 194, 195, 196, 197, 198, 199]
		Stochastic Dynamic Programming	[200, 201, 202, 33]
		Pontryagin's Maximum Principle [a]	[203, 204, 205, 206, 207, 208, 209, 210, 211, 212, 190]
		Linear Programming [b]	[213, 214]
		Quadratic Programming [b]	[161]
		Genetic Algorithms	[215, 216]
		Game Theory	[217]
	Online	ECMS [a] [c]	[218, 219, 220, 221, 222, 223, 224, 173, 225, 226, 227]
		Model Predictive Control [b]	[228, 229, 230, 231, 232, 233, 234]
		Extremum Seeking	[235, 236, 237]
Learning-based	Supervised Learning	Neural Networks	[238, 239, 240]
	Reinforcement Learning	Actor-Critic	[241]
		Q-Learning	[242, 243, 244, 245, 246]

[a] Indirect Method
[b] Direct Method
[c] ECMS stands for Equivalent Consumption Minimisation Strategy

according to the vehicle's power demand.

Designing and testing a state machine that is capable of exploiting all system specifics can become a laborious task. Alternatively, fuzzy logic can achieve comparable behaviour with less design effort. A distinction is made between "Basic" and "Adaptive" fuzzy logic. The former operates using fixed algorithm parameters, whereas the latter adapts the parameters to better accommodate the current duty cycle, e.g. [185] adapt the parameters differently to urban, rural, and motorway driving; [186] adapt the parameters as the fuel cell ages.

Frequency decoupling and time series algorithms split the power in a manner that keeps the power output of the fuel cell steady. The reason here is that the battery can handle power swings faster and more adequately. Moreover, this reduces fuel cell degradation that is induced by load-cycling. Frequency decoupling algorithms decompose power demand into low- and high-frequency components, where lower frequency components are passed to the fuel cell and higher frequencies are passed to the battery [188]. Time series algorithms, such as the moving average algorithm, dampen the fuel cell's output by keeping it close to a historic average.

The tuning of rule-based parameters is a vital and difficult step. This is initially done using computer simulations; for example, genetic algorithms were used to tune state machines and fuzzy logic controllers before performing any real-world experiments [164, 172]. The parameters however do not scale across different vehicle types and thus require re-tuning. This parameter "rigidity" is further exacerbated as the powertrain ages or is subject to duty cycles drastically different than originally designed for. Adaptive fuzzy logic can partially alleviate this problem; however, only a handful of cases can be considered in advance.

Optimisation-Based Methods

Optimisation-based algorithms use mathematical optimisation to make a decision. They seek a decision that achieves a specified objective, e.g. minimise fuel consumption, while being subject to physical and operational constraints, e.g. powertrain limits, and target journey time. The obtained solution is optimal with respect to the mathematical optimisation problem constructed; therefore, it is vital that it accurately reflects the designer's objectives and the real-world system. Mathematical models of the powertrain, track and journey timetable are used to construct the optimisation problem.

This model-centric approach yields an algorithm that can be easily and intuitively adjusted to reflect changes in attributes, e.g. powertrain ageing, generalisation to other vehicles, heavier vehicle load, duty cycle. This benefit is especially meaningful for fuel cells that exhibit considerable changes as they age. For example, it has been shown that updating the model of an ageing fuel cell reduces consumption [161, 247]. Updating a fuel cell model as it ages could also be useful if its peak power capability drops considerably [207], as otherwise it would not meet the power required by the EMS.

Table 2.1 categorises optimisation-based algorithms according to the time at which the optimisation problem is solved, namely offline methods which are computed prior to a journey and online methods which are computed during the journey. Offline methods can afford to use high-fidelity models because, being offline, they have more compute time. Online methods are restricted to low-fidelity models that are computationally lighter to meet their real-time compute deadlines. Furthermore, offline methods compute the optimal solution for the entire journey upfront, whereas online methods often use a rolling horizon, where the optimal solution is only found for a short horizon into the future to save on compute time. This implies that online methods could be suboptimal and shortsighted from the perspective of an entire journey [248, 249], whereas offline methods can better guarantee global optimality for the entire journey. In practice, however, online methods have the edge of adapting to unexpected disturbances and model mismatch.

Some publications combine both methods to reap the benefits of both, namely, they precompute a global trajectory offline and then resort to online methods upon deviating off the trajectory [250, 198, 251].

Offline methods can be classed into five algorithm subcategories: (i) dynamic programming, (ii) indirect methods, (iii) direct methods, (iv) genetic algorithms, and (v) game theory. Online methods can also be classified into direct and indirect methods. The equivalent consumption minimisation strategy (ECMS) is an online indirect method that is derived from a simplified PMP formulation [252]. Model predictive control (MPC) is a leading online direct method that often relies on QP, although alternative optimisation formulations are also possible.

To counteract the shortsightedness of rolling-horizon online methods, the cost function needs to penalise both instantaneous fuel consumption and any future consumption that is needed to maintain a certain battery SoC. To this end, there are two battery operation schemes: i) charge-sustaining operation that preserves battery SoC for future journeys and ii) charge-depleting operation that allows full discharge of the battery. Charge-sustaining operation is advised for hybrid vehicles that cannot recharge from the electric grid, whereas charge-depleting operation is recommended for hybrid vehicles that can recharge from the electric grid. The reason for the latter is because power from the grid is often cheaper than the hydrogen fuel that would be used to recharge the battery using the fuel cell.

Lastly, the Extremum Seeking (ES) algorithm is a model-free online approach that does not rely on powertrain models to compute the cost function but instead relies on physically evaluating the cost of actions on the real system. The commanded action is a perturbed signal that is used to measure the local gradient of the cost function to execute gradient descent. This model-free approach circumvents model mismatch complications but is not suitable for long-horizon planning, hence its limited prevalence in EMS literature.

Learning-based Methods

More recently, EMS algorithms aided by machine learning tools have surfaced. A review paper on this new development can be found in [253]. Some of these attempts use supervised learning to learn optimal solutions from offline optimisation algorithms [238]. This approach allows one to obtain quasi-optimal performance with substantially less computational burden. Unfortunately, similarly to rule-based algorithms, a controller obtained by supervised learning is limited to the training data set. Algorithms based on reinforcement learning (RL) are less rigid than supervised learning because they can continuously adapt to changes by learning from newer data as they come. RL algorithms minimise a cost function that is evaluated on data instead of mathematical models.

Data quality, noise and coverage of scenarios is of up-most importance for all learning-based methods. While this concern can be managed for supervised learning because data selection takes place under expert supervision, it poses a bigger problem for RL algorithms that are continuously adapting during deployment. A popular approach to safeguarding learning-based algorithms is to limit their decisions within provably reliable bounds [254].

2.4.2 EMS and Battery Degradation

The significant cost of traction batteries has led EMS research to consider preserving battery lifetime in addition to basic EMS functionality. It should be noted that literature mainly covers the degradation of carbon-anode batteries, whereas titanate oxide anodes are often assumed to be degradation-free due to their longer cycle life [255].

One of the simplest heuristics to reduce battery degradation is to reduce its utilisation. This can be achieved by penalising charge-throughput

$$\int_{\tau_1}^{\tau_2} |I_{\text{batt}}(t)| dt. \tag{2.1}$$

Real-world tests show that charge-throughput is the leading degradation driver for vehicular applications [256, 257, 258], where the severity of degradation is influenced by operational stress factors such as battery SoC, current, and temperature [259, 260]. This subsection explores all battery degradation models found in the EMS literature. These are summarised in Tab. 2.2 namely, (i) electrochemical degradation models, (ii) empirical models that fit experimental data, and (iii) surrogate models that fit data generated from electrochemical simulations.

Electrochemical degradation models often use computationally taxing partial differential equations, a burden that is passed onto the optimisation problem, which explains its lack of prevalence in EMS literature. The only example found, which models the SEI layer, recognises that its utility is limited to offline analysis [261]. However, their findings are promising, indicating a potential reduction in battery degradation by 27% at the minor expense of only a 1% increase in fuel consumption. Figure 2.10 shows their reported variation in battery SoC against different Pareto coefficients. A lower coefficient prioritises battery preservation, whereas a higher coefficient prioritises fuel consumption. The figure shows how attempting to preserve battery lifetime reduces charge-throughput by reducing SoC swings.

In contrast to electrochemical models, empirical models are computationally lighter at the expense of accuracy [262]. The Arrhenius Model stands out as a leading semi-empirical model. At its core, it uses an exponential formula linking charge throughput and temperature to degradation. The Arrhenius Model can be extended by incorporating additional stress factors such as C-rate and SoC, which yields the more capable Severity Factor Model. For example, [263] used a severity factor model to optimise the operation of electric vehicles, revealing that intermediate discharge rates prolong battery life, while brief high-rate discharges are more efficient at the expense of battery life.

Empirical models are fitted using experimental data from batteries cycled under various stress factors until end-of-life. These campaigns could be carried out using constant

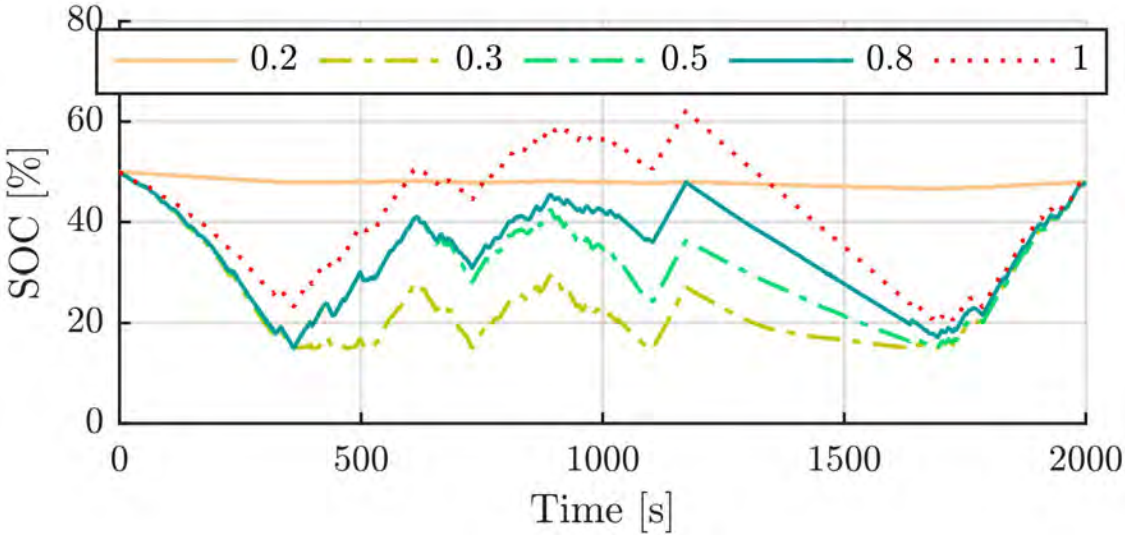

Figure 2.10: Evolution of battery SoC throughout trip for different Pareto coefficients. A lower coefficient emphasizes battery preservation, whereas a higher coefficient emphasizes fuel saving. Reprinted from [261]. © 2020 IEEE.

Table 2.2: Battery degradation models used in degradation-aware EMS literature. Stress factors: temperature is "Temp", current magnitude (C-rate) is "|I|" and current as a vector is "I". DoD is exclusively used for plug-in hybrid electric vehicles

Category	**Subcategory**	**Stress Factors**	**Examples**	**Model Source**
Electrochemical	Single Particle Model	SoC, I, Temp	[261]	[264]
		SoC, I, Temp	x	[265]
Empirical	Arrhenius Model I	|I|, Temp	[266, 267, 268, 263, 255, 269, 270, 193, 271, 229]	[61]
	Arrhenius Model II	|I|, Temp	[196]	x
	Severity Factor	DoD,Temp	[272, 195][a]	x
		SoC, Temp	[273]	[274]
		SoC, Temp	[275]	[276]
		SoC, |I|, Temp	[277, 203, 249]	[278]
		SoC, |I|, Temp	[279, 280]	[281]
	S-N Curve	DoD	[282, 211, 273][a]	x
Surrogate	Polynomial	SoC, I	[32]	[283]
		SoC, I	[284]	[285]
		SoC, I	[286, 287]	x

[a]Plug-in Hybrid Electric Vehicle

Table 2.3: Examples of battery degradation test campaigns

Test Campaign	**Examples**
Static	[61, 288, 289, 290, 291, 281]
Dynamic	[258, 292, 274]

discharge currents (static testing) or using power profiles representative of vehicle duty cycles (dynamic testing). Models built using the former exhibit inferior prediction accuracy because the underlying dataset is not representative of a vehicle duty cycle [262]. This signifies the importance of selecting data that is representative of expected duty cycle conditions. Table 2.3 shows a list of test campaigns commonly used in literature to develop models.

The S-N Curve, shown in Fig. 2.11, is an empirical model that predicts a battery's expected lifespan as a function of DoD assuming it discharges at constant rate to a given depth of discharge (DoD). Many battery datasheets include this information, which makes this model the easiest model to construct amongst those shown in Tab. 2.2. Nevertheless, its prediction accuracy is very poor for dynamic duty cycles because it assumes static discharge and thus is not very suitable for vehicle applications.

Surrogate models aim to achieve the performance of electrochemical models at a lower computational complexity by fitting a regression model to simulated data obtained from the electrochemical model itself. Polynomial models are amongst the most used surrogate models and can cover multiple stress factors, e.g. Fig. 2.12 shows a polynomial that predicts the rate of growth of SEI versus SoC and current. The role of temperature can be integrated by obtaining several polynomials for a range of temperatures. Unlike models built using static discharge tests, the polynomial in Fig. 2.12 accommodates the difference in degradation between charging and discharging; it shows that charging at high SoC is more damaging than discharging.

The most common method to embed a degradation model into an optimisation problem is to directly add it to the cost function. Although apparently simple, this forms a multi-

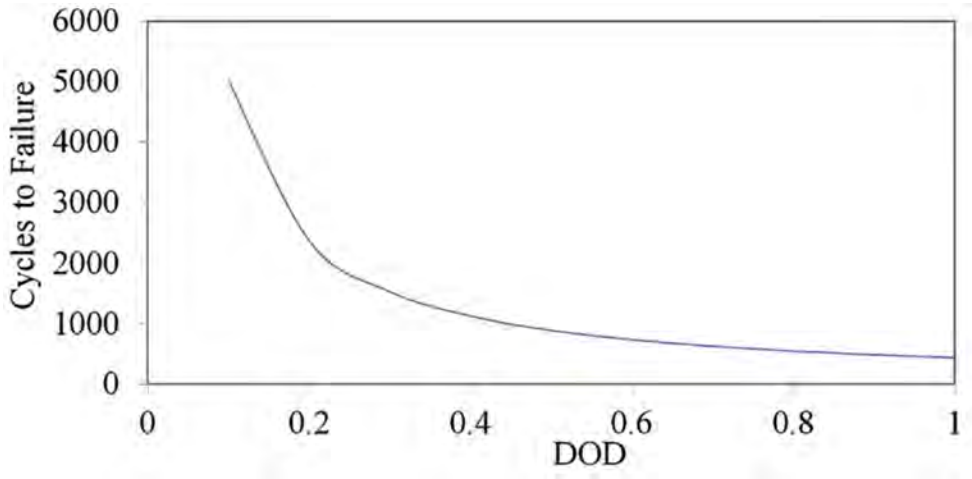

Figure 2.11: S-N Curve shows expected battery life as function of DoD. Reprinted from [211]. © 2015 Elsevier.

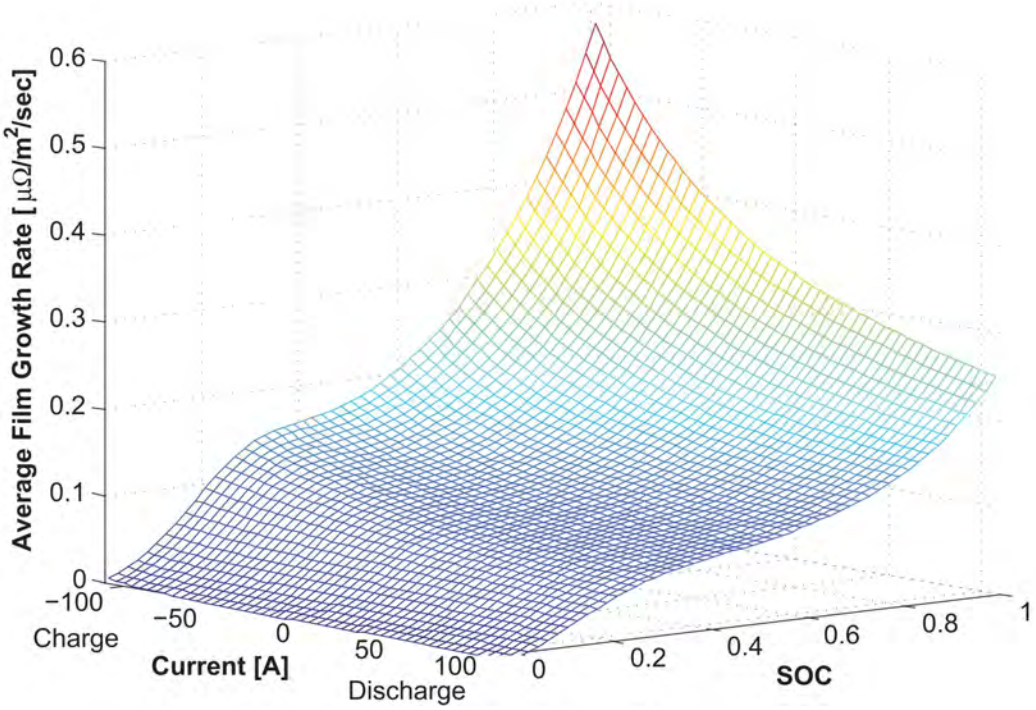

Figure 2.12: SEI growth versus SoC and current. Reprinted from [32]. © 2013 IEEE.

objective optimisation problem that presents the designer with the nontrivial task of tuning the weight factors of competing objectives. An alternative arrangement would be to only minimise one objective (e.g. fuel consumption) while constraining the other objective to a maximum value, known as an epsilon-constraint [293]. For example, [294, 267, 266] limit a unit of battery degradation per unit distance travelled while strictly minimising fuel consumption. Such an epsilon-constraint makes it easier to quantify the level of battery degradation accumulated between maintenance intervals.

Most of the surveyed publications assume an ideal battery thermal management system capable of maintaining battery temperature within a favourable range. However, this assumption seldom holds due to plant limitations and would thus lead to a suboptimal operation when the assumption falters. Indeed, by assuming a fixed battery temperature, the optimal strategy would be to rely heavily on the battery instead of the primary mover [32], while when modelling battery thermals the optimal strategy is blended operation to alleviate thermal stresses on the battery [295, 296].

An accurate but computationally taxing approach to control temperature-related degradation would be to include temperature as a controllable dynamic state. The following achieve this: [255] include thermal dynamics while sizing a battery pack using a Genetic Algorithm; [203] add thermal dynamics to an EMS PMP formulation but admit to the problem's computational intractability; [280] add thermal dynamics to an EMS DP formulation; [296] propose an MPC approach but is only optimal under certain conditions; [297] propose a simplified PMP formulation for battery cooling; [298] use MPC to balance between battery cooling and recovering kinetic energy.

2.4.3 EMS and Fuel Cell Degradation

Similarly to batteries, fuel cell degradation can be influenced by the EMS algorithm employed. The stress factors of interest are those previously mentioned in Fig. 2.8 and summarised in Section (2.2.4).

To reduce load-cycling, a soft-run strategy could be adopted, in which fuel cell power is kept as steady as possible while transients are delegated to the battery [270]. This reduction in fuel cell degradation comes at the expense of increased fuel consumption, as fuel cell output will not match power demand in real time and thus might be unnecessarily maintained at high levels. Moreover, it will lead to increased battery degradation due to increased battery utilisation. On the other hand, a power-following strategy where the fuel cell tracks power demand prioritises consumption over fuel cell lifetime [299].

A soft-run strategy can be implemented using rule-based algorithms such as frequency decoupling and time series as previously introduced in Tab. 2.1. Soft-run can be integrated into optimisation-based algorithms by penalising [300, 205] or constraining [222, 241, 227, 228, 226] the fuel cell output slew rate (rate of change).

A heuristic related to load-cycling is to adopt a soft-run strategy during the early stages of a fuel cell's lifetime and then adopt a power-following strategy as it ages [193]. The motivation here is that fuel cells experience a higher rate of catalyst loss when new, so limiting degradation early on is beneficial, whereas fuel economy can become a priority later on. Nonethess, this heuristic was only verified by simulation and not by real-world experiments.

The frequency of start-stop cycles can be controlled by applying a constraint on the minimum time elapsed before a fuel cell stack can be shut down [206, 233, 197, 301]. This heuristic is computationally demanding to integrate into an optimisation problem because it requires integer variables. Lastly, idling and high power can be discouraged by constraining or penalising these power levels [170].

A heuristic for multi-stack fuel cells is to operate the stacks as evenly as possible near their peak efficiency point and to only partially power down some of the stacks during extended periods of low-power or idling [171]. A calculation method was proposed by [302] to find the threshold for this low-power level.

Table 2.4 lists the fuel cell degradation models employed in EMS literature. The ma-

Table 2.4: Fuel cell degradation models used in degradation-aware EMS literature

Category	Subcategory	Examples	Source
Empirical	Runtime I	[33, 229]	[33]
	Runtime II	[269, 193, 195, 272, 271, 225, 270, 229]	[103]
	Runtime III	[193]	[303]
Electrochemical	Platinum Reduction	[196]	[304]
Surrogate	Polynomial	[305]	[306]

jority of publications found utilise empirical models due to its computational simplicity. These models are based on fuel cell runtime and thus predict degradation by multiplying the rate of hourly degradation by the time spent in operation. The data necessary for this model can be sourced from manufacturer datasheets and real-world testing. A potential drawback of this model is that it does not accurately capture the impact of load-cycling which is very consequential.

2.4.4 Beyond the EMS—Automotive

The majority of hybrid automotive literature focuses on the design of the EMS and assumes the vehicle's speed is under the driver's discretion. This could lead to suboptimal operation should the driver's driving style be suboptimal in itself. To this end, a handful of publications have attempted to optimise both vehicle speed and EMS. The simplest approach to achieve this is sequential, where the vehicle's speed is first optimised after which the resulting power profile is fed to the EMS to be optimised. Examples exist in both the time-domain [234, 198, 307] and the space-domain [308, 309, 250] problem settings.

The aforementioned sequential method is easy to implement because it leverages existing speed optimisation and EMS optimisation methods. Nonetheless, it could fail to yield optimal operation because the speed optimisation step is unaware of the decisions made

by the succeeding EMS optimisation step. To counter this shortcoming, both speed and EMS need to be optimised jointly by a single optimisation problem. Several publications confirm the superior optimality of the joint method [310, 311, 312, 313, 314]. The fuel savings between the sequential and joint methods are often reported to be around 5%. Though these often use computationally intensive algorithms. One publication attempted using convex optimisation though the solution is optimal under certain conditions [36]. Nonetheless, their attempt is very promising because compute time was under 1 second for a journey that is 21 km long.

The concept of joint optimisation has also been extended to other vehicle systems to reap further benefits at the system level. Heating, ventilation and air conditioning (HVAC) is a prime example of such because it is the leading auxiliary load. For instance, HVAC efficiency improves with vehicle speed due to the additional airflow around the HVAC external coil, as shown in Fig. 2.13. This phenomena can be capitalised by scheduling cooling to when the vehicle is in-motion to reduce cooling consumption. Up to 10% reduction in fuel consumption was reported in simulation [315]. Thermal comfort is maintained due to the thermal inertia of the vehicle's interior. Another example of joint optimisation is to include powertrain thermal management into the EMS as done by [316]. Though doing so in the latter publication only delivered marginal fuel savings due to the small amounts of energy consumed by powertrain thermal management systems.

2.4.5 Concluding Remarks on Automotive Literature

The following keys insights were concluded from the automotive review:

- There is a growing focus on forming tractable optimisation-based methods. This promises real-time algorithms that are theoretically more optimal than traditional rule-based methods. It is more tractable to solve optimisation problems formulated using the direct method.
- Research has transitioned beyond the simple EMS problem setting into system-level

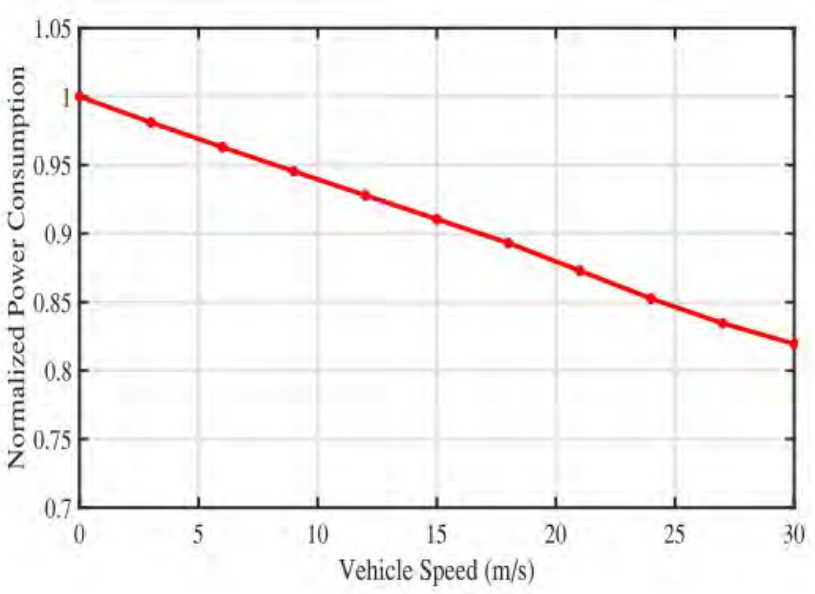

Figure 2.13: Variation of cooling energy consumption with vehicle speed. Reprinted from [315]. © 2021 IEEE.

optimisation such as optimising speed and auxiliaries.

- The energy savings of joint optimisation is around 5% in comparison to sequential optimisation. This motivates adopting joint optimisation.
- There is tangible evidence of the possibility to use convex optimisation for joint speed-EMS optimisation [36]. Compute time was much quicker and for a longer journey when compared to examples from rail in Section 2.3.2. This motivates adopting a convex algorithm for the rail problem setting, as it could be computationally more efficient than existing rail algorithms.

2.5 Gaps in Literature

Based on the reviews of Sections 2.3 and 2.4, Tab. 2.5 contrasts the hypotheses posed by this thesis with the current state of literature to identify gaps.

Table 2.5: Contrasting the hypotheses with state of literature

Hypothesis	Answered in literature?
HO1	No. Existing literature does not specifically compare joint speed-EMS optimisation to conventional ecodriving and coasting. That being said, there is evidence that the joint method is more optimal than the sequential method.
HO2	Partially. Some evidence supporting this hypothesis was found in automotive literature. None was found in rail literature.
HO3	No. Existing literature only does sequential optimisation of speed-EMS-timetable.
HA1	Partially. There is some success of convex optimisation in automotive literature. This result is very promising because it was much quicker and offers better solution optimality than algorithms used in rail literature, especially those mentioned in Section 2.3.2.
HA2	No. Examples found use non-convex sequential optimisation.

3 A PRIMER ON CONVEX OPTIMISATION

This chapter offers a primer on convex optimisation to support formulating convex formulations in Chapter 5. It chapter only covers principles and examples that directly support this thesis, as a comprehensive coverage would become prohibitively long. Unless cited otherwise, much of the first-principles covered here can be found in [35].

Section 3.1 introduces sufficient conditions for an optimisation problem to be convex. Section 3.2 presents some of the basic conditions for a function to be convex. Section 3.3 explores the impact of common mathematical operations on convexity. Section 3.4 deals with convex sets, which is vital in formulating convex problems with constraints. Section 3.5 lists specific examples of convexity that are directly relevant to this thesis. Lastly, Section 3.6 covers how some non-convex problems can be "convexified" (turned convex).

3.1 Introduction

The optimisation problem (3.1) attempts to find the value of $x \in \mathbb{R}^n$ that minimises the objective function (3.1a) while satisfying the equality and inequality constraints (3.1b) and (3.1c).

$$\min_{x} \quad f(x) \tag{3.1a}$$

$$\text{s.t.} \quad h(x) = 0, \tag{3.1b}$$

$$g(x) \leq 0 \tag{3.1c}$$

The following conditions are sufficient for (3.1) to be convex:

$$\text{the objective function } f \text{ is convex,} \tag{3.2a}$$

$$\text{the equality constraint function } h \text{ is linear (affine),} \tag{3.2b}$$

$$\text{the inequality constraint function } g \text{ is convex,} \tag{3.2c}$$

These conditions are "sufficient" and thus might become restrictive in some circumstances. The restrictive circumstances that are directly relevant to this thesis will be explained in this chapter.

3.2 Convex Functions

3.2.1 Basic Properties

A function $f(.)$ is linear if

$$f(\alpha x_1 + \beta x_2) = \alpha f(x_1) + \beta f(x_2) \tag{3.3}$$

$\forall x_1, x_2 \in \mathbb{R}^n$ and $\forall \alpha, \beta \in \mathbb{R}$.

A function $f(.)$ is convex if

$$f(\alpha x_1 + \beta x_2) \leq \alpha f(x_1) + \beta f(x_2) \tag{3.4}$$

$\forall x_1, x_2 \in \mathbb{R}^n$ and $\forall \alpha, \beta \in \mathbb{R}$ with $\alpha + \beta = 1$, and $\alpha, \beta \geq 0$.

The inequality condition in (3.4) is less strict than the equality condition in (3.3) which implies that all linear functions are convex, but the converse is not true.

Figure 3.1 plots the convex quadratic function $f(x) := x^2$ to provide geometric intuition of how a convex function would satisfy (3.4). The red dashed line $\alpha f(x_1) + \beta f(x_2)$ is above

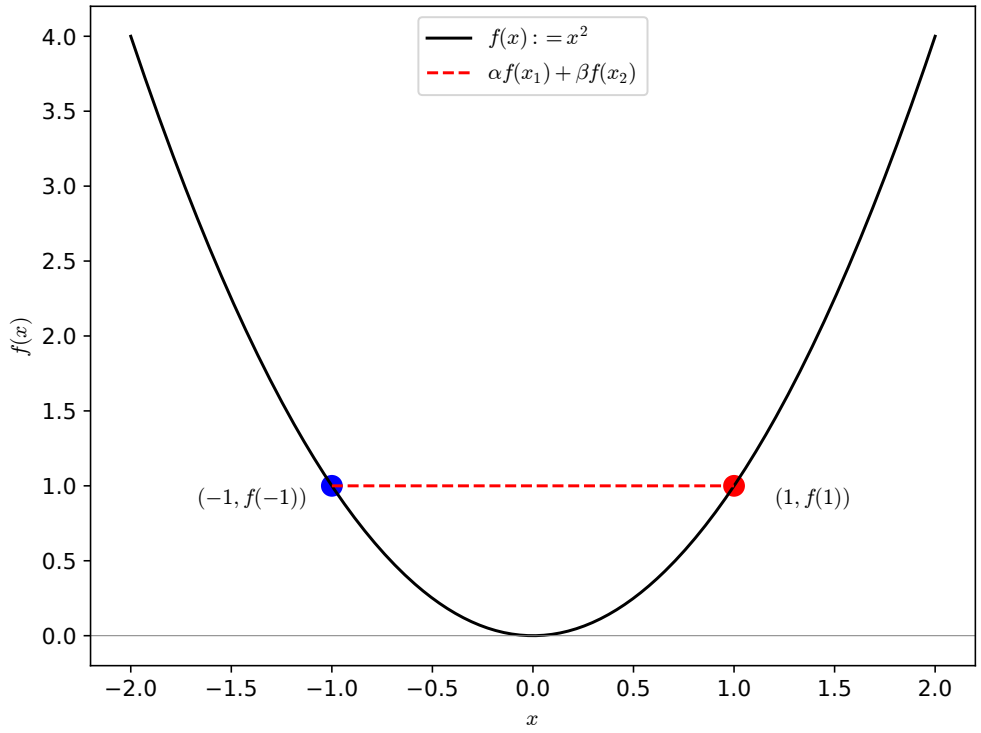

Figure 3.1: Plot of convex function $f(x) := x^2$.

or equal to the black line $f(\alpha x_1 + \beta x_2)$ for all $\{\alpha, \beta \in \mathbb{R} | \alpha + \beta = 1 \text{ and } \alpha, \beta \geq 0\}$. When this condition holds across the function's entire domain it guarantees the existence of a single local minimum that coincides with the global minimum.

Figure 3.2 plots the function $f(x) := sin(x) + \frac{x^2}{10}$. The function is non-convex because it does not satisfy the convexity condition (3.4) throughout its domain. An example of this is between $[-1.2, 3.8]$ where the red dashed line $\alpha f(x_1) + \beta f(x_2)$ falls below $f(\alpha x_1 + \beta x_2)$. This leads to a local maximum in-between that creates a pair of separated local minima. Consequently, a numerical optimisation algorithm could mistake a sub-optimal local minimum for the global minimum.

3.2.2 Second Order Condition

The convexity condition (3.4) ought to hold true across the function's domain which makes it difficult to asses on functions with high dimensions. To this end, the second-order derivative of a function is an alternative to assess convexity.

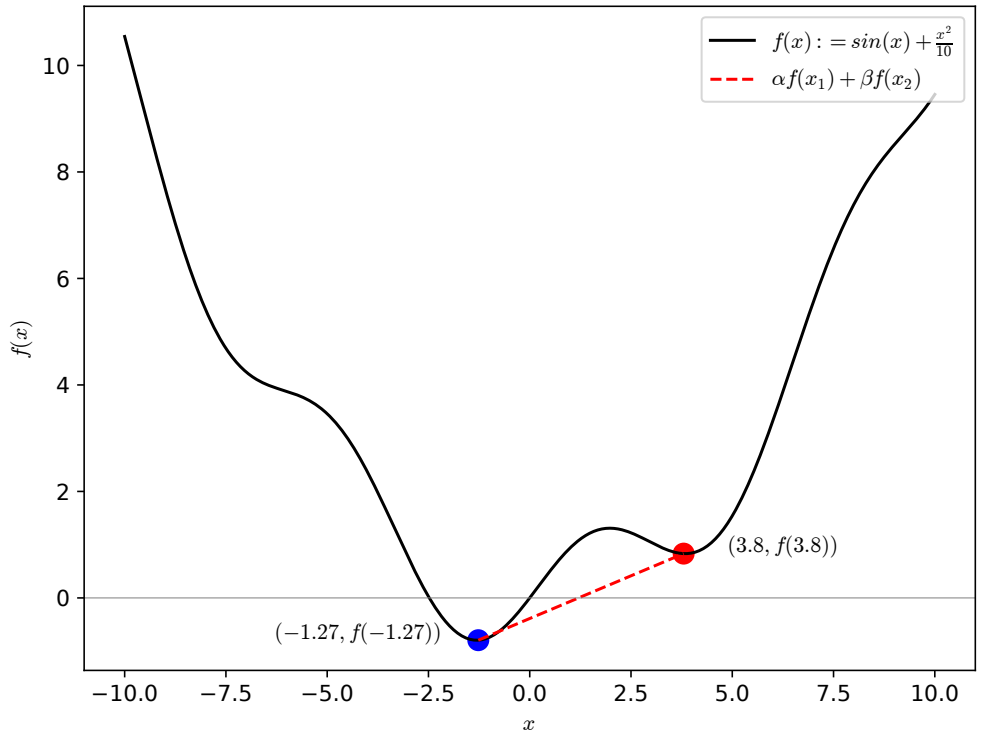

Figure 3.2: Plot of non-convex function $f(x) := sin(x) + \frac{x^2}{10}$.

A function $f(x)$ that is twice differentiable (the second derivative exists across its domain) is convex if $\forall x \in \mathbb{R}$

$$f''(x) \geq 0. \tag{3.5}$$

If the function were to have a multidimensional domain, the Hessian can be assessed instead. As such, a function $f(x)$ whose Hessian exists $\forall x \in \mathbb{R}^n$ is convex if its Hessian matrix is positive semidefinite

$$\nabla^2 f(x) \succeq 0. \tag{3.6}$$

The Hessian is analogous to a function's second-order derivative but uses partial derivatives instead, which enables it to be used for higher-dimensional functions. The Hessian

matrix of the function $f(x)$ with $x \in \mathbb{R}^n$ is

$$\mathbf{H}_f = \begin{bmatrix} \frac{\partial^2 f}{\partial x_1^2} & \frac{\partial^2 f}{\partial x_1 \partial x_2} & \cdots & \frac{\partial^2 f}{\partial x_1 \partial x_n} \\ \frac{\partial^2 f}{\partial x_2 \partial x_1} & \frac{\partial^2 f}{\partial x_2^2} & \cdots & \frac{\partial^2 f}{\partial x_2 \partial x_n} \\ \vdots & \vdots & \ddots & \vdots \\ \frac{\partial^2 f}{\partial x_n \partial x_1} & \frac{\partial^2 f}{\partial x_n \partial x_2} & \cdots & \frac{\partial^2 f}{\partial x_n^2} \end{bmatrix} \tag{3.7}$$

A Hessian matrix is positive semidefinite if all of its eigenvalues are non-negative.

3.3 Convexity and Mathematical Operations

This subsection explores the impact of common mathematical operations on the convexity of functions.

Scaling

Scaling a convex function f by a non-negative constant $\alpha \geq 0$ maintains a convex αf.

Scaling a convex function f by a negative $\gamma < 0$ does not necessarily maintain a convex γf. For example, scaling the covnex $f(x) := x^2$ by -1 leads to the concave $-x^2$, shown in Fig. 3.3.

Linear functions (which are a special condition of convex functions) are an example of convex functions whose convexity is not impacted by negative scaling. For example, scaling the linear $f(x) := x$ by -1 returns the linear $-x$.

Summation

Adding the convex functions f_1, f_2 produces a convex $f_1 + f_2$. Similarly, scaling them by the non-negative constants $\alpha_1, \alpha_2 \geq 0$ produces a convex $\alpha_1 f_1 + \alpha_2 f_2$. This extends to an arbitrary number of functions added.

Since negative scaling does not preserve convexity, scaling the convex functions f_1, f_2

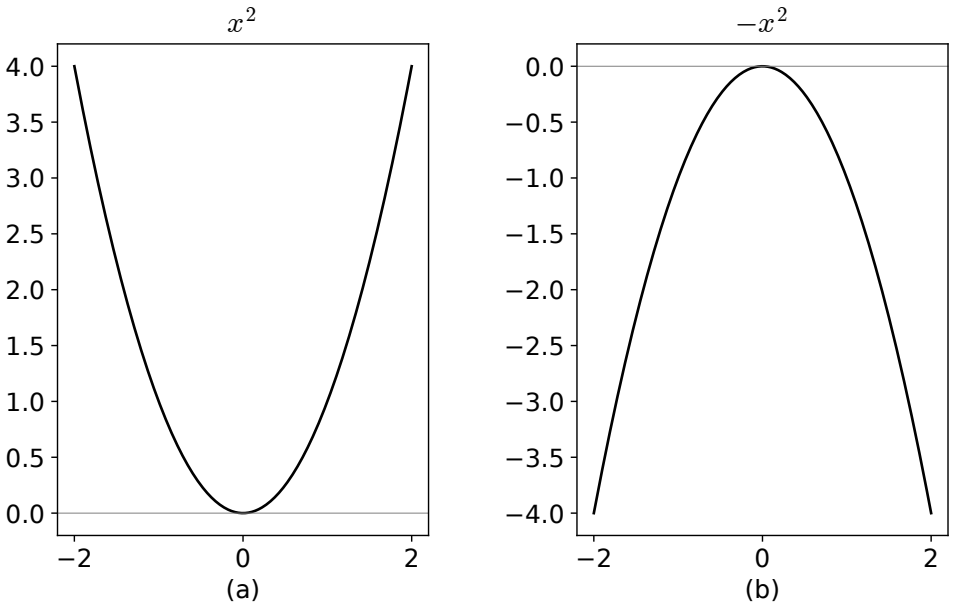

Figure 3.3: Plots of convex x^2 and concave $-x^2$.

by the negative $\gamma_1, \gamma_2 < 0$ and adding them does not necessarily produce a convex $\gamma_1 f_1 + \gamma_2 f_2$.

Adding a constant $\beta \in \mathbb{R}$ to a convex function f does not affect convexity, regardless of the sign β. For example, adding -1 to the convex $f(x) := x^2$ only causes a vertical offset, shown in Fig. 3.4.

Composition

There are various rules for composite functions, with the two below being most relevant to this thesis.

The composite function $f(x) = h(g(x))$ is convex if both functions $h, g : \mathbb{R} \to \mathbb{R}$ are convex. For example, the composite of the convex $h(x) : x^2$ and linear $g(x) := x + 1$ produces the convex composite $f(x) = x^2 + 2x + 1$. To verify this, the second-order derivative is $2 \geq 0$ which meets the second-order convexity condition (3.5).

The composite function $f(x) = h(g(x))$ is convex if $h : \mathbb{R} \to \mathbb{R}$ is convex and non-increasing and $g : \mathbb{R} \to \mathbb{R}$ is concave.

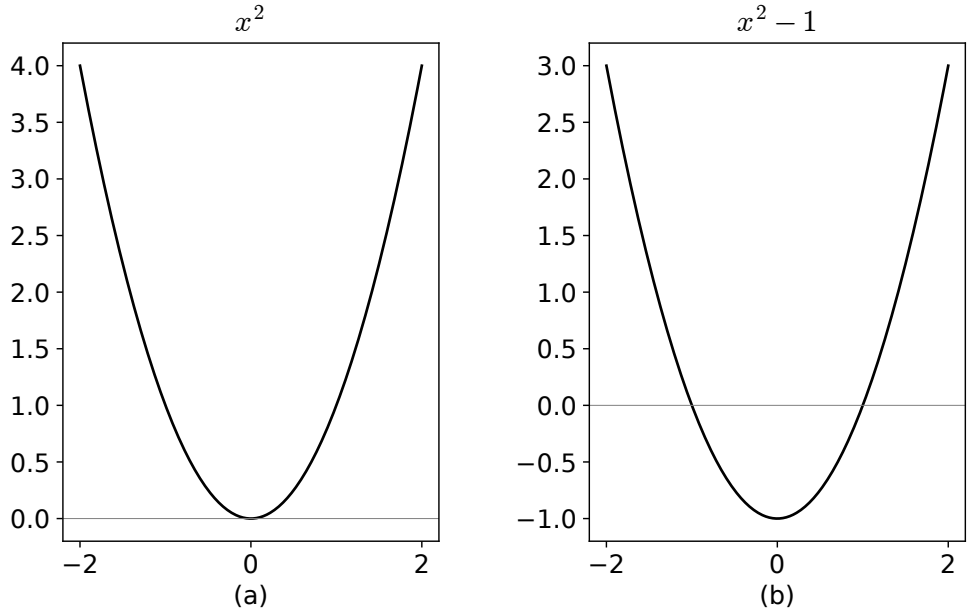

Figure 3.4: Plots of convex x^2 and $x^2 - 1$.

3.4 Convex Sets

The equality and inequality constraints in (3.1) form the feasible set of the solution. The optimal solution to the problem (the problem's global minimum) is defined as that which minimises the cost function within the feasible set. Therefore, understanding the convexity of the feasible set is vital to successfully formulate a convex problem.

Condition for Convex Set

A set is convex if any two points within can be connected by a straight line that remains entirely within the set. This can be described mathematically as follows for the set C

$$\alpha x_1 + \beta x_2 \in C, \tag{3.8}$$

$\forall x_1, x_2 \in C.\ \alpha, \beta \in \mathbb{R}$, $\alpha + \beta = 1$ and $\alpha, \beta \geq 0$.

Convex Sets and Equality Constraints

A set that is created using the equality constraint

$$h(x) = 0 \tag{3.9}$$

will fall exactly on the function line. Therefore, for an equality constraint to form a convex set, it is sufficient and necessary for $h(x)$ to be linear, because that is the only means to satisfy (3.8): connect any pair of points within the set with a straight line that remains within the set.

Convex Sets and Inequality Constraints

A set that is created using the inequality constraint

$$g(x) \leq 0 \tag{3.10}$$

will consist of an area (two dimensions) or hypervolume (higher dimensions). To form a convex set, it is sufficient for $g(x)$ to be a convex function. Though this can be a restrictive condition, as some non-convex $g(x)$ functions can produce a convex set under very specific conditions. Variations of such will be used throughout this thesis and will therefore be explored in Section 3.5.

Figure 3.5 shows examples of convex sets. Figure 3.6 shows examples of non-convex sets. In the figures, sets formed from equality constraints are plotted as solid lines only; sets formed from inequality constraints are shaded area including the function's line.

Intuition Behind Convex Sets

The necessity of convex sets is related to how numerical algorithms explore the feasible set while searching for the global minimum. This is done incrementally over the course of straight steps within the feasible set under the condition that each step reduces the

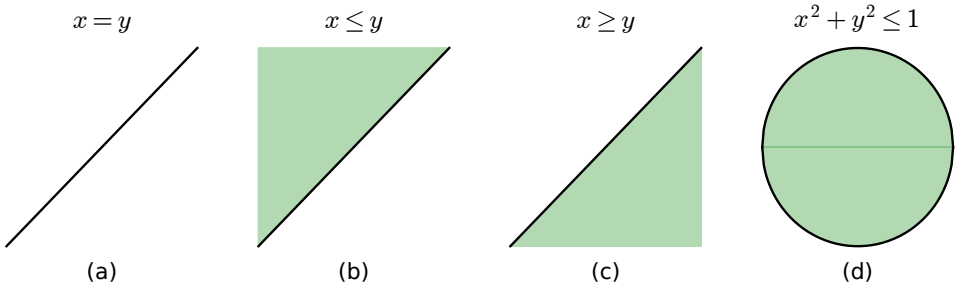

Figure 3.5: Examples of convex sets formed by an equality constraint in (a) and inequality constraints in (b), (c) and (d).

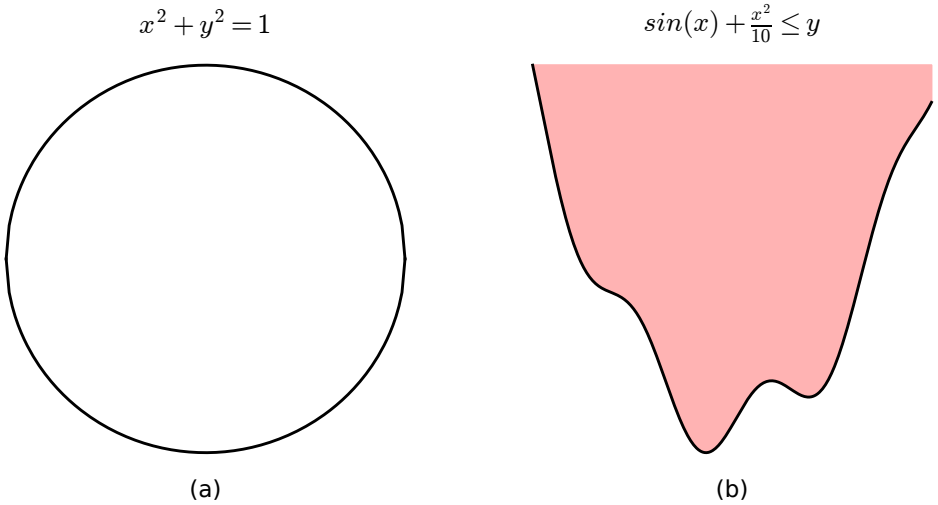

Figure 3.6: Examples of non-convex sets formed by an equality constraint in (a) and inequality constraint in (b).

current cost function value. A convex set that can be fully explored through straight steps that remain within the set (following the condition (3.8)) allows for thorough exploration. In contrast, a non-convex set poses the risk of getting stuck at a local minimum that is not possible to escape in straight steps that remain within the feasible set and reduce the cost function.

3.5 Relevant Functions and Sets

Quadratic Polynomials

The quadratic polynomial

$$f(x) := p_2 x^2 + p_1 x + p_0 \tag{3.11}$$

is convex if its second-order derivative is non-negative

$$f''(x) := 2p_2 \geq 0. \tag{3.12}$$

The quadratic polynomial

$$g(x, y) := p_{02} x^2 + p_{20} y^2 + p_{11} xy + p_{01} x + p_{10} y + p_{00} \tag{3.13}$$

is convex if its Hessian matrix is positive semidefinite

$$\mathbf{H}_g := \begin{bmatrix} 2p_{02} & p_{11} \\ p_{11} & 2p_{20} \end{bmatrix} \succeq 0. \tag{3.14}$$

Square Root

The square root

$$f(x) := \sqrt{x} \tag{3.15}$$

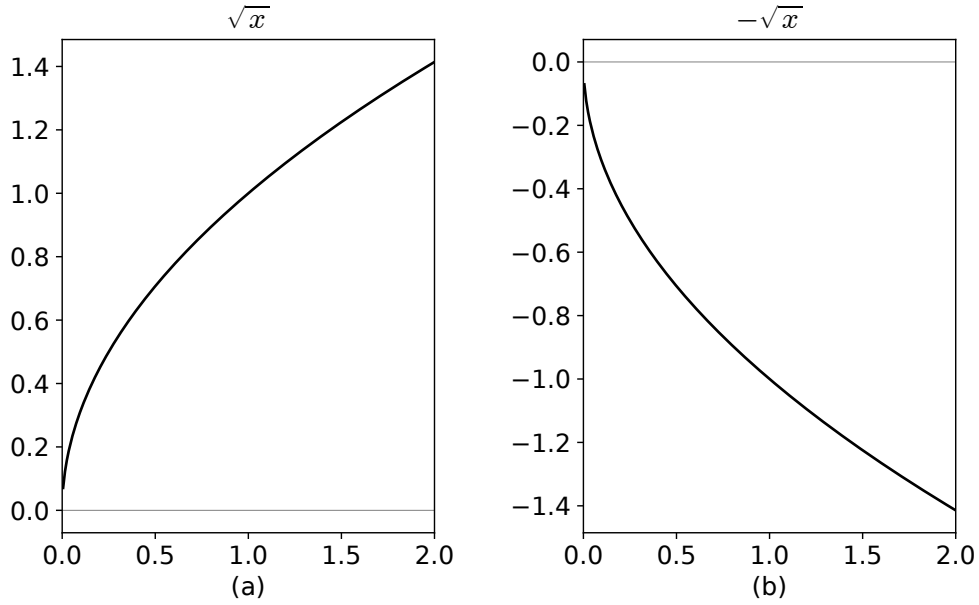

Figure 3.7: Plot of (a) concave $\sqrt{x}$ and (b) convex -$\sqrt{x}$.

is concave for $x > 0$. This is because its second order derivative is always negative

$$f''(x) := -\frac{1}{4x^{3/2}}. \tag{3.16}$$

This means that its negative scaling is convex, namely,

$$g(x) := -\sqrt{x} \tag{3.17}$$

which is consistent with the positive second-order derivative for $x > 0$

$$g''(x) := \frac{1}{4x^{3/2}}. \tag{3.18}$$

Figure 3.7 shows plots for both the concave $\sqrt{x}$ and convex $-\sqrt{x}$.

Reciprocal Function

The reciprocal function

$$h(x) := \frac{1}{x} \tag{3.19}$$

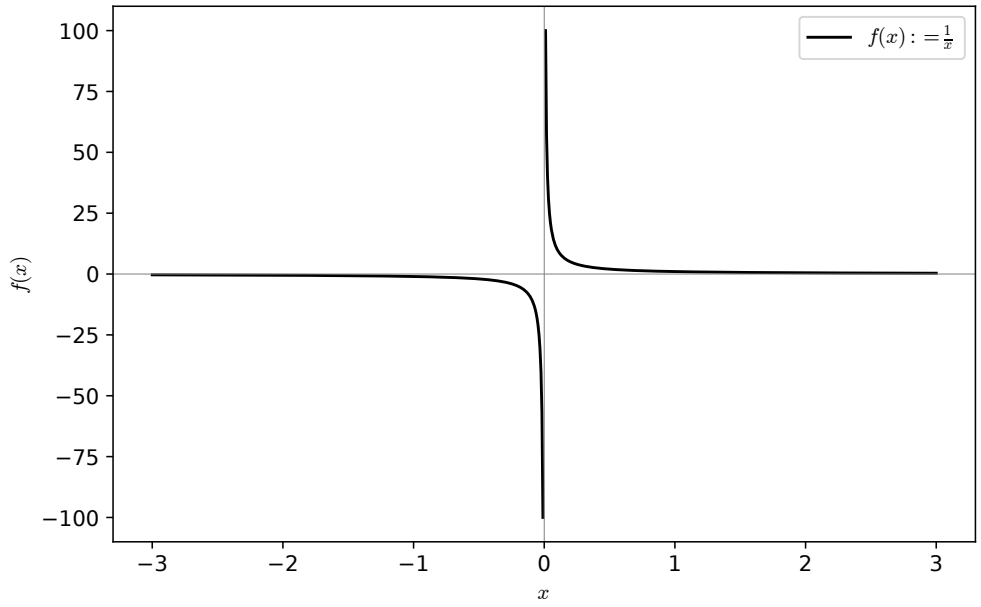

Figure 3.8: Plot of reciprocal function $\frac{1}{x}$.

is not convex throughout its domain, shown in Fig. 3.8. However, it is convex and non-increasing for $x > 0$. Therefore, according to the composite rules in Section (3.3), the composite

$$f(x) := \frac{1}{g(x)} \tag{3.20}$$

is convex for a concave $g(x)$ and $g(x) > 0$.

It is important to note that 3.20 is convex as is, and would turn non-convex if multiplied by another variable. For example

$$f(x, y) := \frac{x}{y} \tag{3.21}$$

is not convex, shown in Fig. 3.9.

Second-Order Cone Constraint

The function

$$f(x, y, z) := x^2 - yz \tag{3.22}$$

$$f(x, y) := \frac{x}{y}$$

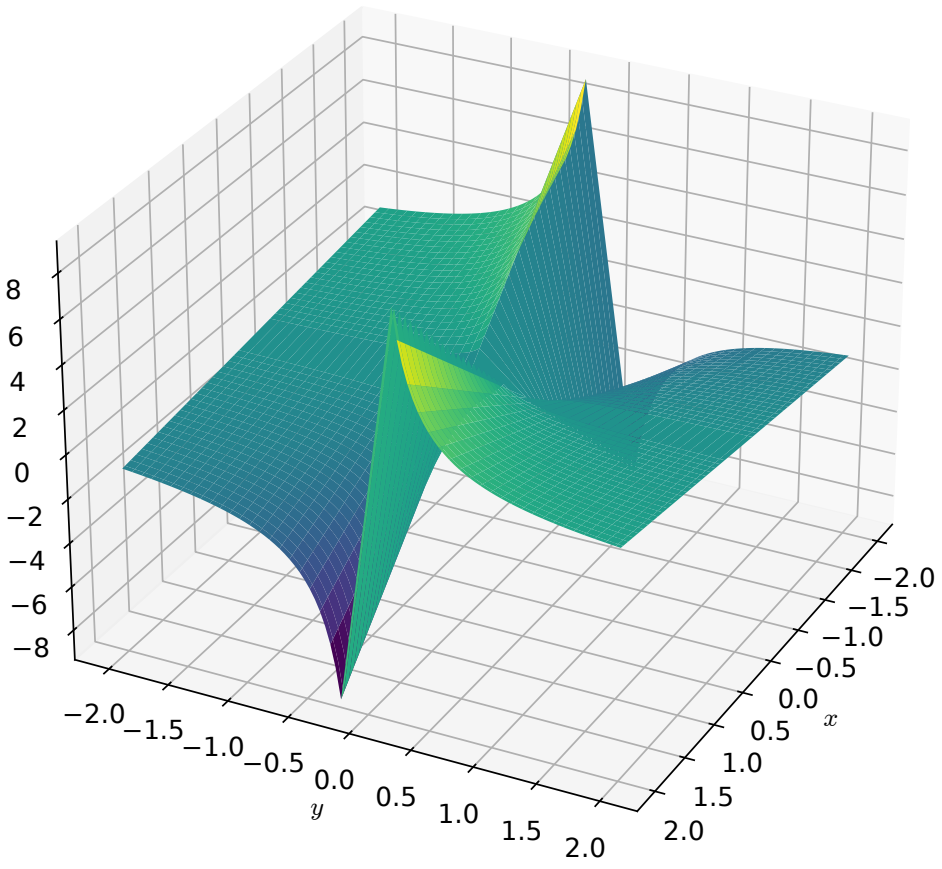

Figure 3.9: Plot of non-convex $\frac{x}{y}$.

is non-convex because its Hessian matrix

$$\mathbf{H}_f = \begin{bmatrix} 2 & 0 & 0 \\ 0 & 0 & -1 \\ 0 & -1 & 0 \end{bmatrix} \tag{3.23}$$

contains a negative eigenvalue: (-1,1,2).

Nonetheless, $f(x)$ can form the convex set

$$x^2 \leq yz \tag{3.24}$$

for $y, z \geq 0$. This is a second-order cone constraint [317].

Bilinear Inequality

The bilinear function

$$f(x, y) := xy \tag{3.25}$$

is non-convex because its Hessian matrix

$$\mathbf{H}_f = \begin{bmatrix} 0 & 1 \\ 1 & 0 \end{bmatrix} \tag{3.26}$$

contains a negative eigenvalue: (-1,1).

Figure 3.10(a) shows the non-convexity of the function $f(x, y)$ in 3D space.

Nonetheless, $f(x, y)$ can form the convex set

$$\alpha \leq xy \tag{3.27}$$

for a non-negative constant $\alpha \geq 0$ and non-negative variables $x, y \geq 0$. Note that this constraint is a special condition of the more general second-order cone constraint (3.24).

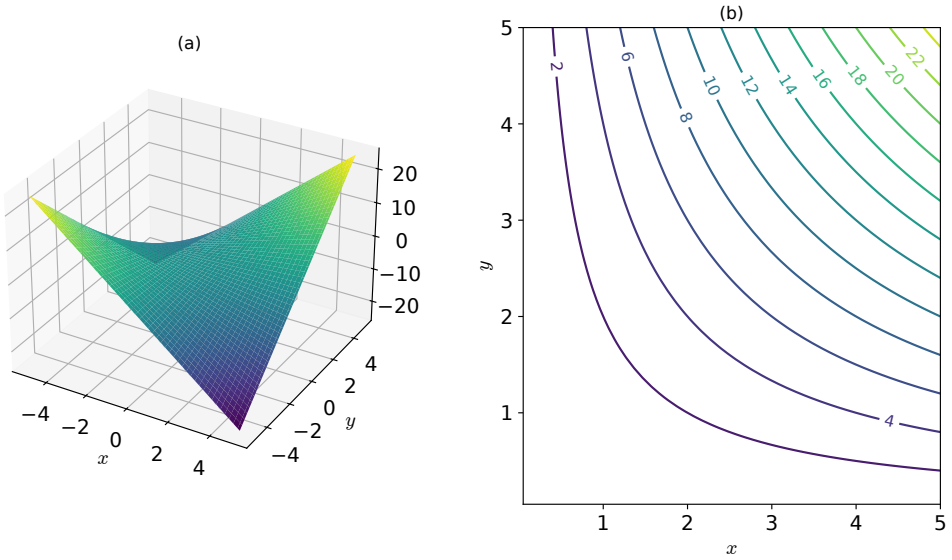

Figure 3.10: (a) 3D plot of non-convex xy, (b) contour lines of xy over positive quadrant.

Figure 3.10(b) shows how (3.27) forms a convex set. It shows that the function's contour line over the positive quadrant $(x, y \geq 0)$ forms a convex area above any given constant $(\alpha \geq 0)$.

3.6 Formulation Convexification

Convexification is defined as transforming a non-convex optimisation problem into a convex one. The primary objective behind doing so is to harness the benefits associated with solving convex problems, such as the global minimum guarantee and lower computational complexity.

The success of a convexified problem largely depends on how closely the optimal solution of the convex version aligns with that of the original non-convex problem. If this alignment is not sufficiently close, it may diminish the practical utility of the convexified version.

Convexifying an optimisation problem does not follow a universal approach. It typically requires an in-depth analysis of the problem to identify non-convex components and then modifying them using techniques specific to the non-convexity at hand. This process can

be complex and often relies on the expertise of the formulation designer.

Convexication by Relaxation

Take the optimisation problem (3.28) with both convex and nonlinear functions f, h. Denote its optimal solution $\boldsymbol{x}^*$. This is a non-convex problem because h does not meet the linearity condition on equality constraints (3.2b).

$$\min_{\boldsymbol{x}} \quad \sum_{i=1}^{n} f(x_i) \tag{3.28a}$$

$$\text{s.t.} \quad h(x_i) = 0, \quad i = 1, \ldots, l \tag{3.28b}$$

The optimisation problem (3.28) can be convexified by relaxing the equality constraint into the inequality shown in (3.29b). This is because the function h meets the convex set condition on inequality constraints (3.2c).

$$\min_{\boldsymbol{x}} \quad \sum_{i=1}^{n} f(x_i) \tag{3.29a}$$

$$\text{s.t.} \quad h(x_i) \leq 0, \quad i = 1, \ldots, l \tag{3.29b}$$

Denote the solution of the new relaxed problem $\boldsymbol{x}^*_{\text{rel}}$. The new relaxed problem is a valid convexification only if $\boldsymbol{x}^* = \boldsymbol{x}^*_{\text{rel}}$. This will be the case if it is shown that objective function f tightens the relaxed constraint to equality at the optimal solution $\boldsymbol{x}^*_{\text{rel}}$.

Convexication by Substitution

Take the optimisation problem (3.30) that has a convex objective function f and a non-linear equality constraint function. Assume that it would not be possible to relax this optimisation problem as in (3.29). A way to convexify this formulation is to substitute

x^2 by the surrogate variable y.

$$\min_{\boldsymbol{x}} \quad \sum_{i=1}^{n} f(x_i) \tag{3.30a}$$

$$\text{s.t.} \quad x_i^2 = 0, \quad i = 1, \ldots, l \tag{3.30b}$$

The formulation (3.31) shows the alternative variant with a linear equality constraint. Notice that the variable x has replaced by y. Therefore, the new problem is solved for the variable $\boldsymbol{y}$. After finding the optimal $\boldsymbol{y}^*$, the optimal $\boldsymbol{x}^*$ can be computed by substituting into the relation between x and y.

$$\min_{\boldsymbol{y}} \quad \sum_{i=1}^{n} g(y_i) \tag{3.31a}$$

$$\text{s.t.} \quad y_i = 0, \quad i = 1, \ldots, l \tag{3.31b}$$

4 TRAIN MODELLING

This chapter introduces the mathematical models that will be used later in Chapter 5 to formulate the train's optimisation problem. This chapter merely derives and presents the models. The convexity of these models will be thoroughly examined and addressed in Chapter 5.

Section 4.1 introduces the modelling domain and vital preliminaries required for the remainder of the chapter. Section 4.2 models longitudinal speed and journey duration. Section 4.3 models the fuel cell hybrid powertrain which includes the traction motor, fuel cell and battery.

4.1 Model Fundamentals

4.1.1 The Modelling Domain

A "journey" is defined as the movement of a train, starting from an initial stationary state and ending with a terminal stationary state. No restrictions are placed on the number of stops in between. Without loss of generality, it is assumed herein that a journey is a train service that serves multiple stations and includes dwelling at stations.

A train's journey can be modelled in the temporal or spatial domain, a choice that controls how the train's state evolves. In the temporal domain, the train's state evolves after the passage of a temporal interval, whereas the state evolves after traversing a spatial interval in the spatial domain.

Modelling a train's movement in the spatial domain rather than the temporal domain yields higher accuracy. This is because the location of the train after a spatial interval is deterministically known, whereas it is contingent on the speed achieved after a temporal interval. Consequently, track characteristics that affect speed can be deterministically

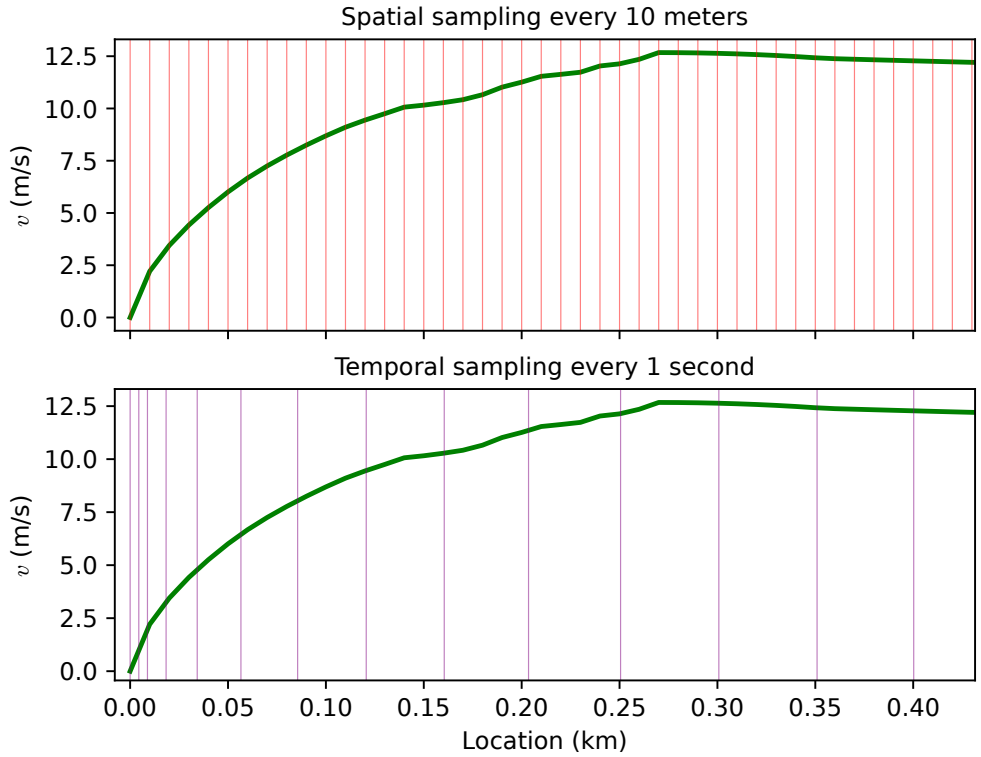

Figure 4.1: Plot of spatial and temporal sampling examples for an accelerating train. Train speed is the solid green line. The location of spatial samples 10 meters apart are orange vertical lines. The location of temporal samples 1 second apart are purple vertical lines.

retrieved and modelled in the spatial domain, whereas they can only be estimated in the temporal domain without prior knowledge of the train's speed.

Figure 4.1 shows spatial samples that are 10 meters apart and temporal samples that are 1 second apart for an accelerating train. The location of spatial samples are uniformly distributed and independent of the train's speed. The location of temporal samples are dependent on train speed; the spacing is initially small and increases as the train accelerates.

Despite the accuracy of the spatial domain for modelling motion, it is incapable of modelling dwelling at stations because a stationary state stops the spatial domain from progressing. On the other hand, the temporal domain would still function while stationary because it only requires the passage of time rather than motion in space. This makes the temporal domain preferable for dwelling.

To leverage the benefits of both domains, this thesis adopts a hybrid approach: the train's motion is modelled in the spatial domain when moving, whereas dwelling at stations is modelled in the temporal domain. Both modelling domains are interleaved over the course of a journey to achieve motion in between stations and dwelling at stations. The use of either domain is exclusive of the other at any given instant. The train's state is exchanged when transitioning between domains to ensure a seamless simulation.

To avoid ambiguity, in the context of this thesis:

- the spatial domain is defined by scalar distance along the track. Adding all the distance modelled in the spatial domain returns the total track distance covered, not to be mistaken for absolute distance from origin.
- the temporal domain is defined by the time spent dwelling at stations. Adding all the time modelled in the temporal domain returns the total time spent dwelling at stations, not to be mistaken for total journey time.

Lastly, discrete dynamics will be used instead of continuous dynamics to enable the use of direct optimisation methods that are computationally more favourable [37] (see the footer of Tab. 2.1). The zero-order hold will be used to discretise dynamics. This will be applied to models in both spatial and temporal domains, where a discrete spatial interval is denoted by Δ_s and a discrete temporal interval is denoted by Δ_t.

4.1.2 Instances and Intervals

Journey Instances

A journey is discretised by sampling it at $N + 1$ instances, including both spatial and temporal instances, starting from the initial stationary state and ending with the terminal stationary state. This produces N domain intervals, mixed between spatial and temporal intervals.

Denote the following set for all indexes of a journey's $N+1$ instances

$$\mathcal{A} = (0, 1, 2, \ldots, N), \tag{4.1}$$

which is ordered chronologically by the order of occurence. The train's state is defined for all of $\mathcal{A}$.

Define the following subset of $\mathcal{A}$

$$\mathcal{B} = \{i \in \mathcal{A} \mid i < N\}, \tag{4.2}$$

which excludes the last instance N. This set is defined for system inputs and domain intervals, as the discretised dynamics implies that the $N-1$ instance is sufficient to describe the terminal state N.

Assigning Domains and Intervals

The modelling domain assigned to an instance depends on the behaviour required at that instance: spatial domain for moving instances or temporal domain for stationary instances. Consequently, the modelling domain chosen for an instance decides the type of interval it receives: spatial interval Δ_{s} or temporal interval Δ_{t}. The domain decision is to be made in advance by consulting the route's information and the working timetable. This is not restrictive, so long no unplanned stops take place.

The above can be described procedurally as follows. Start by denoting the longitudinal scalar speed of the train by v. A speed value is not required, only whether the train is to be moving or stationary at any given instance. Each instance $i \in \mathcal{B}$ is assigned **<u>either</u>**:

- **a spatial interval** $\Delta_{\mathrm{s},i} > 0$ if it is required for the train to
  - start to move from stationary ($v_i = 0$ and $v_{i+1} > 0$), or

  - keep moving ($v_i > 0$ and $v_{i+1} > 0$), or
  - come to a stop ($v_i > 0$ and $v_{i+1} = 0$),

- **a temporal interval** $\Delta_{\mathrm{t},i} > 0$ if the train is required to remain stationary given it is already stationary ($v_i = 0$ and $v_{i+1} = 0$).

The magnitude of the discrete intervals, Δ_s and Δ_t, is a modelling choice to be made. Finer intervals would increase model fidelty, though would increase the size of $\mathcal{B}$ to maintain the journey's length and duration, thus increasing compute time. A practical rule of thumb is to reduce interval magnitude until sufficient dynamic behaviour is achieved and simulation results stabilise.

4.1.3 Additional Sets

This subsection defines further sets that will be used throughout this thesis.

Denote the spatial domain set

$$\mathcal{S} = \{j \in \mathcal{B} \mid \Delta_{\mathrm{s},j} \text{ is defined}\}, \tag{4.3}$$

which is a subset of $\mathcal{B}$ that was assigned spatial intervals. The set $\mathcal{S}$ leaves behind instances at which Δ_t was defined instead of Δ_s.

Denote the temporal domain set

$$\mathcal{T} = \{k \in \mathcal{B} \mid \Delta_{\mathrm{t},k} \text{ is defined}\}, \tag{4.4}$$

which is a subset of $\mathcal{B}$ that was assinged temporal intervals. The set $\mathcal{T}$ leaves behind instances at which Δ_s was defined instead of Δ_t.

The union of the sets $\mathcal{S}$ and $\mathcal{T}$ is equal to $\mathcal{B}$, that is, $\mathcal{B} = \mathcal{S} \cup \mathcal{T}$. This is because $\mathcal{B}$ is a set of all instances to which a domain interval was assigned. Furthermore, $\mathcal{A} = \mathcal{S} \cup \mathcal{T} \cup \{N\}$, as N was excluded from $\mathcal{B}$ prior to defining the sets $\mathcal{S}$ and $\mathcal{T}$.

Denote the zero speed set

$$\mathcal{V}^0 = \{l \in \mathcal{A} \mid v_l = 0\}, \tag{4.5}$$

which is a subset of $\mathcal{A}$ at which instantaneous speed is zero. By definition, this set will include all of $\mathcal{T}$, instances of $\mathcal{S}$ at which the train starts moving from stationary, the initial instance 0 and the terminal instance N.

Denote a subset of $\mathcal{A}$ that is defined a timing point

$$\mathcal{M} = \{m \in \mathcal{A} \mid \text{timing point is defined at } m\ \} \tag{4.6}$$

where the train is required to reach $m \in \mathcal{M}$ by a defined time. This serves the purpose of defining the train's arrival time at station stops or passing points. In Great Britain, this concept is referred to as "TIPLOC".

It is attempted to use the same instance identifiers (i, j, k, l, m, n) to improve readability and consistency, where $i \in \mathcal{B}$, $j \in \mathcal{S}$, $k \in \mathcal{T}$, $l \in \mathcal{V}^0$, $m \in \mathcal{M}$ and $n \in \mathcal{A}$. At times this might be difficult, thus notation will be repeated in each context to dispel any ambiguity.

4.2 Train Longitudinal Dynamics

4.2.1 Longitudinal Speed

This subsection models the train's longitudinal speed and therefore only applies to moving instances $\forall j \in \mathcal{S}$.

The train is modelled as a point mass m with equivalent inertial mass m_{eq} travelling at longitudinal speed v while being controlled by traction motor force F_{trc} and mechanical brake force F_{brk} [318].

The external forces acting on the train F_{ext} are modelled as

$$F_{\text{ext},j} = a + bv_j + cv_j^2 + mg\sin(\theta_j) \tag{4.7}$$

where $a + bv + cv^2$ is the Davis Equation and $mg\sin(\theta)$ represents gravitational pull from the level horizon.

The train speed at instance $j+1$ can be predicted by adding mechanical work $F\Delta_{\text{s}}$ to kinetic energy $\frac{1}{2}m_{\text{eq}}v^2$ at j, namely

$$\frac{1}{2}m_{\text{eq}}v_{j+1}^2 = \frac{1}{2}m_{\text{eq}}v_j^2 + (F_{\text{trc},j} + F_{\text{brk},j})\Delta_{\text{s},j} - F_{\text{ext},j}\Delta_{\text{s},j}, \tag{4.8}$$

where the right handside is the summation of energy at sampling instance j and the left handside represents the resulting kinetic energy at sampling instance $j+1$. This calculation is recursively computed forwards to calculate the speed of the train over the course of a journey.

4.2.2 Journey Duration

Denote the time required to traverse the interval $[i, i+1)$ for $i \in \mathcal{B}$ by $\delta_{\text{t},i}$. Also, denote the time it takes to reach instance $n \in \mathcal{A}$ from the begining of the journey by $t(n)$.

Then, for $n \in \mathcal{A}$ and $n > 0$, the time needed to reach n is

$$t(n) := \sum_{i=0}^{n-1} \delta_{\text{t},i}. \tag{4.9}$$

According to (4.9), the time required to finish a journey (reach last instance N in $\mathcal{A}$) is

$$t(N) := \sum_{i=0}^{N-1} \delta_{\text{t},i}. \tag{4.10}$$

Interval Duration δ_{t}

For $k \in \mathcal{T}$ the interval duration $\delta_{\mathrm{t},k}$ is the predetermined $\Delta_{\mathrm{t},k}$, defined previously in Section 4.1.2. On the contrary, the interval duration for instances $j \in \mathcal{S}$ depends on speed. The simplest model to find duration for interval $[j, j+1)$ is

$$\frac{\Delta_{\mathrm{s},j}}{v_j}. \tag{4.11}$$

However, this would return an infinite result for instances in $\mathcal{S}$ at which the train is stationary and starting to move, i.e. $v_j = 0$ and $v_{j+1} > 0$. Moreover, this model poorly reflects reality, where speed is continuously changing during an interval. To address both of these concerns, use the average speed of consecutive instances

$$v_{\mathrm{avg},j} = \frac{v_j + v_{i+j}}{2}, \tag{4.12}$$

where both instances $j \in \mathcal{S}$ and $j+1 \in \mathcal{S}$ are consecutive. Recall that $\mathcal{S}$ excludes any consecutive stationary instances which safeguards v_{avg} from returning zero.

To conclude

$$\delta_{\mathrm{t},i} = \begin{cases} \frac{\Delta_{\mathrm{s},i}}{v_{\mathrm{avg},i}} & i \in \mathcal{S} \\ \Delta_{\mathrm{t},i} & i \in \mathcal{T} \end{cases} \tag{4.13}$$

4.3 Fuel Cell Hybrid Powertrain

This section covers the powertrain components shown in Fig. 1.3, namely the traction motor, fuel cell, battery, and auxiliary load. Their individual behaviour as well as their interaction with each other and the train is to be modelled.

4.3.1 Power Flow

The powertrain components are electrically connected by the power flow equality

$$P_{\mathrm{m},i} + P_{\mathrm{aux},i} = P_{\mathrm{fc},i} + P_{\mathrm{bat},i} \quad \forall i \in \mathcal{B}. \tag{4.14}$$

P_{m} is the electric power flow at the motor's terminals, P_{aux} is electric auxiliary load, P_{fc} is fuel cell electric power output, and P_{bat} is the electric power flow at the battery's terminals. P_{aux} is assumed to be predetermined for the entire journey.

Note that no traction effort is exerted in $\mathcal{T}$, therefore (4.14) can be further simplified to

$$P_{\mathrm{aux},k} = P_{\mathrm{fc},k} + P_{\mathrm{bat},k} \quad \forall k \in \mathcal{T} \tag{4.15}$$

and then

$$P_{\mathrm{m},j} + P_{\mathrm{aux},j} = P_{\mathrm{fc},j} + P_{\mathrm{bat},j} \quad \forall j \in \mathcal{S}. \tag{4.16}$$

The power flow equality plays a vital role of describing how electric power supplies (fuel cell and battery) meet electric loads (traction and auxiliary). Moreover, it models the flow of power to recharge the battery using the fuel cell or traction motor during regenerative braking.

Without loss of generality, it is assumed that there is a single large unit for each variant of the powertrain components. The load is then distributed equally if there were multiple smaller units. For instance, fuel cell power is equally divided amongst a multi-stack fuel cell.

In what follows, further details are covered for each component individually. This includes interaction with the train, models of efficiency, and physical constraints.

4.3.2 Traction Motor

Mechanical to Electric Efficiency

In order to use the longitudinal speed model (4.8) with the power flow equality (4.16), mechanical traction force F_{trc} from the former should be dynamically coupled with motor electric power P_{m} from the latter. For $j \in \mathcal{S}$, this can be achieved by first deriving mechanical traction power

$$P_{\text{trc},j} = F_{\text{trc},j} v_{\text{avg},j} \tag{4.17}$$

and then converting mechanical traction power P_{trc} to electric P_{m} by dividing over efficiency

$$P_{\text{m},j} = \frac{F_{\text{trc},j} v_{\text{avg},j}}{\eta_{\text{m}}(F_{\text{trc},j} v_{\text{avg},j})}, \tag{4.18}$$

where $\eta_{\text{m}}(F_{\text{trc}} v_{\text{avg}})$ is the motor's efficiency at converting electric power to the requested mechanical power.

Motor efficiency is usually described as a discrete lookup table, which implies that (4.18) is only defined at discrete power points. Figure 4.2 shows an example of the discrete efficiency curve. It peaks at a unique region, thus forming a strictly concave curve. This curve characteristic is typical of traction motors.

Note that v_{avg} from (4.12) is used here instead of v, because this would return a more accurate result with speed changing between sampling instances. It also safeguards against returning zero power for $\{j \in \mathcal{S} \mid v_j = 0 \text{ and } v_{j+1} > 0\}$.

Motor Constraints

The motor's traction force and power outputs are subject to physical constraints $\forall j \in \mathcal{S}$.

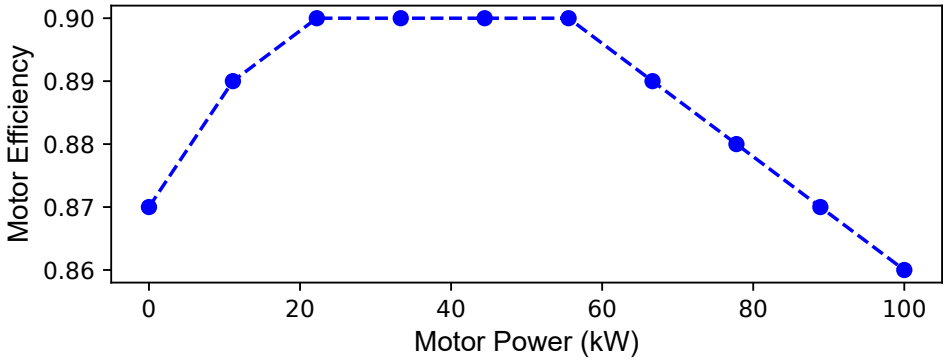

Figure 4.2: Plot of motor efficiency against mechanical power output. Data is of an induction motor for electric vehicles. Data for AC75 from ADVISOR software [319].

The traction force constraint is described by

$$\underline{F_{\text{trc}}} \leq \ F_{\text{trc},j} \leq \overline{F_{\text{trc}}}, \tag{4.19}$$

where $\overline{F_{\text{trc}}}$ is the limit on positive traction force and $\underline{F_{\text{trc}}}$ is the limit on regenrative braking force.

The power constraint is

$$\underline{P_{\text{trc}}} \leq P_{\text{trc},j} \leq \overline{P_{\text{trc}}}, \tag{4.20}$$

where $\overline{P_{\text{trc}}}$ is the limit on positive motoring power and $\underline{P_{\text{trc}}}$ is the limit on regenrative braking power.

The combination of both constraints limits the motor's feasible operation region to that shown in Fig. 4.3, where the blue dashed line is the linear constraint (4.19) and the red dashed line is the hyperbolic constraint of (4.20).

4.3.3 Fuel Cell

Chemical to Electric Efficiency

The fuel cell's conversion of chemical energy to net electric output (after powertrain auxiliaries) is to be modelled. This will be used in Chapter 5 to penalise hydrogen

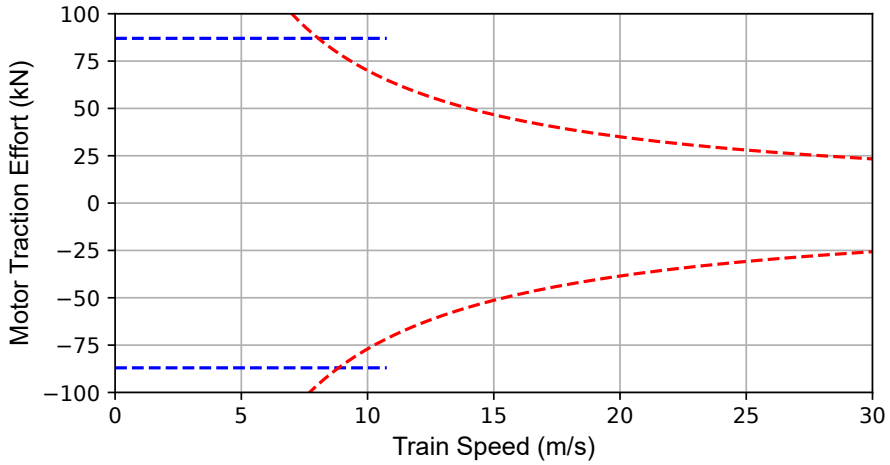

Figure 4.3: Plot of motor constraints. The blue dashed line is the linear constraint of (4.19) and the red dashed line is the hyperbolic constraint of (4.20).

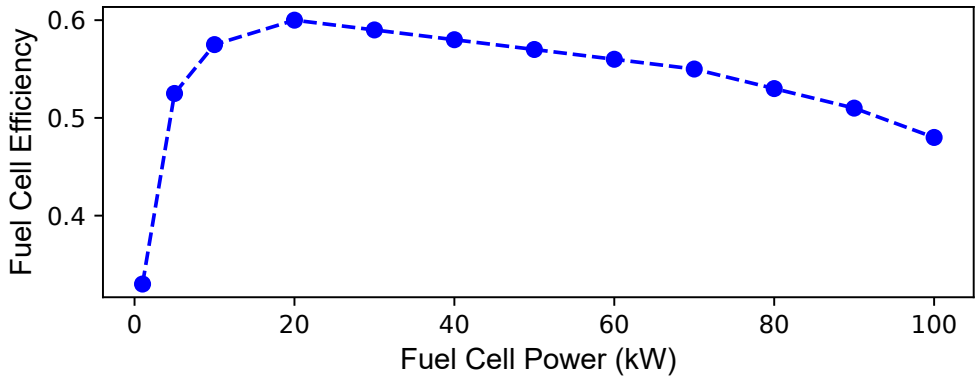

Figure 4.4: Plot of fuel cell efficiency against electric power output. Data from [319].

consumption. The fuel cell power variable P_{fc} will couple this model with the power flow equality in (4.15) and (4.16).

Start by denoting fuel cell efficiency at a given net power output (after powertrain auxiliaries) as $\eta_{\text{fc}}(P_{\text{fc}})$. Similarly to motor efficiency, this is given as a discrete lookup table. Also, fuel cell efficiency has been theoretically proven to always exhibit a concave form [320]. Figure 4.4 shows this.

The rate of converting chemical energy to electric output can be found by dividing fuel cell power by efficiency $\forall i \in \mathcal{B}$

$$\frac{P_{\text{fc},i}}{\eta_{\text{fc}}(P_{\text{fc},i})}. \tag{4.21}$$

Similarly to the traction motor, this is only defined at discrete power points because the efficiency model is discrete. The rate of hydrogen consumption can be computed by multiplying the lower heating value (LHV)

$$\frac{P_{\mathrm{fc},i}}{\eta_{\mathrm{fc}}(P_{\mathrm{fc},i})} \times \mathrm{LHV} \tag{4.22}$$

and multiplying the duration of an interval $\delta_{\mathrm{t},i}$ to find amount of hydrogen consumed over the interval $[i, i+1)$

$$\frac{P_{\mathrm{fc},i}}{\eta_{\mathrm{fc}}(P_{\mathrm{fc},i})} \times \mathrm{LHV} \times \delta_{\mathrm{t},i}. \tag{4.23}$$

Lastly, the hydrogen consumed over an entire journey can be found by the summation

$$\sum_{i \in \mathcal{B}} \frac{P_{\mathrm{fc},i}}{\eta_{\mathrm{fc}}(P_{\mathrm{fc},i})} \times \mathrm{LHV} \times \delta_{\mathrm{t},i}. \tag{4.24}$$

Fuel Cell Constraints

Fuel cell power is subject to lower and upper bounds $\forall i \in \mathcal{B}$

$$0 \leq P_{\mathrm{fc},i} \leq \overline{P_{\mathrm{fc}}}, \tag{4.25}$$

however, it is undesirable to leave the fuel cell idling to extend its lifetime thus a positive minimum power constraint is adopted

$$\underline{P_{\mathrm{fc}}} \leq P_{\mathrm{fc},i} \leq \overline{P_{\mathrm{fc}}}. \tag{4.26}$$

4.3.4 Battery

A battery model would primarily be used to predict state-of-charge, denoted by ζ. This model should also take into account charging and discharging losses. The battery power

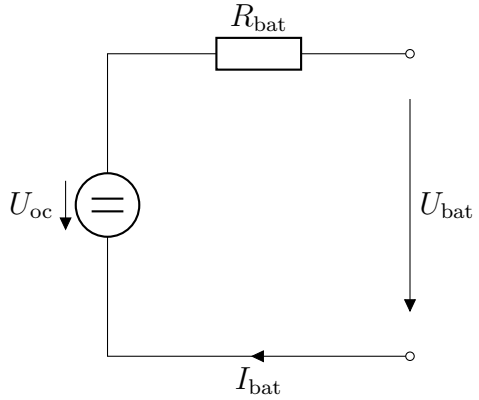

Figure 4.5: Battery equivalent circuit model.

variable P_{bat} will couple state-of-charge to the power flow equalities (4.15) and (4.16).

The battery is modelled using an equivalent circuit model that has a voltage source and resistor, shown in Fig. 4.5 and explained in [321]. The voltage source U_{oc} represents the battery's open-circuit voltage when no load is applied. As the battery is charged/discharged, energy is wasted across the resistor R_{bat}, representing the battery's losses during use.

Both U_{oc} and R_{bat} are fixed. While this model is simplistic, its fidelity has been shown to be adequate for simulating the state-of-charge of battery trains [322]. This model is particularly adequate because the focus is estimating slower dynamics such as state-of-charge rather than fast electrochemical dynamics.

The equivalent circuit model can be used to calculate the change in state-of-charge over interval $[i, i+1)$, denoted $\delta_{\zeta,i}$, by solving for battery current $I_{\text{bat},i}$ at a given power level $P_{\text{bat},i}$.

After finding $\delta_{\zeta,i}$ for the instance $i \in \mathcal{B}$, Columb Counting is used to compute the next state-of-charge

$$\zeta_{i+1} = \zeta_i - \delta_{\zeta,i}. \tag{4.27}$$

The battery's state-of-charge is to be maintained between lower $\underline{\zeta}$ and upper limits $\overline{\zeta}$

$\forall n \in \mathcal{A}$

$$\underline{\zeta} \leq \zeta_n \leq \overline{\zeta}. \tag{4.28}$$

To solve $I_{\text{bat},i}$ at a given power level $P_{\text{bat},i}$, start by implementing Kirchhoff's law as below

$$U_{\text{bat},i} = U_{\text{oc}} - I_{\text{bat},i} R_{\text{bat}}, \tag{4.29}$$

which upon multiplying by I_{bat} becomes

$$P_{\text{bat},i} = U_{\text{oc}} I_{\text{bat},i} - I_{\text{bat},i}^2 R_{\text{bat}}, \tag{4.30}$$

now $I_{\text{bat},i}$ can be found for a given $P_{\text{bat},i}$ using

$$I_{\text{bat},i}(P_{\text{bat},i}) := \frac{U_{\text{oc}} - \sqrt{U_{\text{oc}}^2 - 4R_{\text{bat}} P_{\text{bat},i}}}{2R_{\text{bat}}}, \tag{4.31}$$

where the following limit applies on P_{bat}

$$P_{\text{bat}} \leq \frac{U_{\text{oc}}^2}{4R_{\text{bat}}}. \tag{4.32}$$

Note that (4.32) is merely an upper numerical limit to avoid negative values under the square root. The following physical constraints of the battery are likely to be lower

$$\underline{P_{\text{bat}}} \leq P_{\text{bat},i} \leq \overline{P_{\text{bat}}}. \tag{4.33}$$

Since current is the flow rate of electric charge, $I_{\text{bat}} = \frac{\delta_{\text{q}}}{\delta_{\text{t}}}$, (4.31) can be expressed as

$$\delta_{\text{q},i}(P_{\text{bat},i}, \delta_{\text{t},i}) := \frac{U_{\text{oc}} - \sqrt{U_{\text{oc}}^2 - 4R_{\text{bat}} P_{\text{bat},i}}}{2R_{\text{bat}}} \delta_{\text{t},i}. \tag{4.34}$$

A change in units from coloumbs to battery state-of-charge would convert δ_{q} to the required δ_ζ. This is done by dividing over battery capacity Q_{Ah} (in ampere hour $\text{A} \cdot \text{h}$),

dividing over 3600 to convert from $\mathrm{A}\cdot\mathrm{h}$ to $\mathrm{A}\cdot\mathrm{s}$, and multiplying by 100 convert to a 100% scale

$$\delta_{\zeta,i}(P_{\mathrm{bat},i}, \delta_{\mathrm{t},i}) := \frac{U_{\mathrm{oc}} - \sqrt{U_{\mathrm{oc}}^2 - 4R_{\mathrm{bat}}P_{\mathrm{bat},i}}}{2R_{\mathrm{bat}}} \times \delta_{\mathrm{t},i} \times \frac{100}{3600Q_{\mathrm{Ah}}}. \tag{4.35}$$

According to the adopted sign convention, a positive P_{bat} discharges the battery and a negative P_{bat} charges the battery.

5 OPTIMISING OPERATION

This chapter covers a core contribution: formulating an optimisation problem for optimising the operation of fuel cell hybrid trains. The optimisation problem is developed from the ground up, beginning with a speed-only formulation in Section 5.1, followed by an EMS-only formulation in Section 5.2. These are merged into a joint speed-EMS formulation in Section 5.3. Lastly, a joint speed-EMS-timetable formulation is developed in Section 5.4.

The chapter progressively builds from smaller to larger formulations to allow for the analysis of non-convexities at a smaller scale prior to progressing to larger formulations. Non-convexities will be addressed within each respective section. The end result of this chapter is proving the algorithmic hypotheses HA1 and HA2.

Preliminaries

- The instance identifiers (i, j, k, l, n) are maintained, where $i \in \mathcal{B}$, $j \in \mathcal{S}$, $k \in \mathcal{T}$, $l \in \mathcal{V}^0$ and $n \in \mathcal{A}$.
- A boldface notation is adopted for optimised vectors. For instance, $\boldsymbol{F}_{\text{trc}}$ is an ordered vector of traction force instances, $\boldsymbol{F}_{\text{trc}} = [\ F_{\text{trc},j} \mid j \in \mathcal{S}\ ]$.
- Each optimisation problem is assigned an alphanumeric label. The alphabatic part refers to the problem as a whole, whereas the numeric part refers to a specific equation within the problem.
- Optimisation problem constraints are typed in a double-column format to conserve space. Constraints are clustered according to the set from which they are called.

5.1 Speed Optimisation

This section derives a formulation to optimise speed according to conventional ecodriving: maximum rate acceleration, cruise, coasting, and maximum rate deceleration. It can be generated using various optimisation techniques and formulations. The variant derived here minimises positive traction effort in the objective function while attempting to achieve defined timing points, similar to Eqn. 20 in [109]. The first subsection below presents a basic non-convex variant followed by a convexified variant.

5.1.1 Basic Speed Formulation

To penalise positive traction, start by denoting it as F^{+}_{trc}

$$F^{+}_{\text{trc}} = \begin{cases} F_{\text{trc}} & F_{\text{trc}} \geq 0 \\ 0 & F_{\text{trc}} < 0 \end{cases} \tag{5.1}$$

The positive traction work performed over the interval $[j, j+1)\ \forall j \in \mathcal{S}$ is

$$F^{+}_{\text{trc},j}\Delta_{\text{s},j} \tag{5.2}$$

The optimisation formulation (BSP) minimises positive traction for a journey with arrival timing points defined as τ_m seconds since beginning of the journey at instances $m \in \mathcal{M}$. The timing points in $\mathcal{M}$ will be used to define the required arrival time at intermediate stations and terminal station. The formulation's label stands for "Basic Speed". The optimised vector variables are:

- $\boldsymbol{F}_{\text{trc}}$, $\boldsymbol{F}^{+}_{\text{trc}}$, $\boldsymbol{P}_{\text{trc}}$, $\boldsymbol{F}_{\text{brk}}$, $\boldsymbol{v}_{\text{avg}}$ are optimised only for $\mathcal{S}$ because they are only relevant to intervals during which the train is moving,
- $\boldsymbol{\delta}_{\text{t}}$ is optimised for $\mathcal{S}$ and is assigned the predetermined Δ_{t} for instances in $\mathcal{T}$,

- $\boldsymbol{v}$ is optimised for $\mathcal{A}$ because it is a system state.

$$\min_{\boldsymbol{F}_{\mathrm{trc}},\, \boldsymbol{F}^{+}_{\mathrm{trc}},\, \boldsymbol{P}_{\mathrm{trc}},\, \boldsymbol{F}_{\mathrm{brk}},\, \boldsymbol{v},\, \boldsymbol{v}_{\mathrm{avg}},\, \boldsymbol{\delta}_{\mathrm{t}}} \quad \sum_{j \in \mathcal{S}} F^{+}_{\mathrm{trc},j} \Delta_{\mathrm{s},j} \tag{BSP.1}$$

subject to

given as parameters

$$\Delta_{\mathrm{s},j} \quad \forall j \in \mathcal{S} \tag{BSP.2}$$

$$\Delta_{\mathrm{t},k} \quad \forall k \in \mathcal{T} \tag{BSP.3}$$

$$\forall j \in \mathcal{S}$$

$$(4.8) \tag{BSP.4}$$

$$P_{\mathrm{trc},j} = F_{\mathrm{trc},j} v_{\mathrm{avg},j} \tag{BSP.5}$$

$$v_{\mathrm{avg},j} = \frac{v_j + v_{j+1}}{2} \tag{BSP.6}$$

$$\delta_{\mathrm{t},j} = \frac{\Delta_{\mathrm{s},j}}{v_{\mathrm{avg},j}} \tag{BSP.7}$$

$$0 \leq F^{+}_{\mathrm{trc},j} \tag{BSP.8}$$

$$F_{\mathrm{trc},j} \leq F^{+}_{\mathrm{trc},j} \tag{BSP.9}$$

$$\underline{F_{\mathrm{trc}}} \leq F_{\mathrm{trc},j} \leq \overline{F_{\mathrm{trc}}} \tag{BSP.10}$$

$$\underline{F_{\mathrm{brk}}} \leq F_{\mathrm{brk},j} \leq 0 \tag{BSP.11}$$

$$\underline{P_{\mathrm{trc}}} \leq P_{\mathrm{trc},j} \leq \overline{P_{\mathrm{trc}}} \tag{BSP.12}$$

$$\forall k \in \mathcal{T}$$

$$\delta_{\mathrm{t},k} = \Delta_{\mathrm{t},k} \tag{BSP.13}$$

$$\forall l \in \mathcal{V}^0$$

$$v_l = 0 \tag{BSP.14}$$

$$\forall n \in \mathcal{A}$$

$$0 \leq v_n \leq \overline{v_n} \tag{BSP.15}$$

$$\forall m \in \mathcal{M}$$

$$t(m) = \tau_m \tag{BSP.16}$$

Optimisation Problem 1: Basic Speed (BSP)

The intervals Δ_{s} and Δ_{t} are typed in a separate box in (BSP.2) and (BSP.3) to emphasise that they are given as parameters.

The optimisation problem (BSP) will successfully minimise positive traction effort if F^{+}_{m} were to assume the definition (5.1). This is achieved because the objective function pushes down on F^{+}_{m} while the combination of (BSP.8) and (BSP.9) enable it to mimic the non-negative fraction of F_{trc}. The equality constraint (BSP.5) relates traction force with

traction power to limit the latter in the bound (BSP.12).

The equality constraint (BSP.4) informs the optimisation problem of the speed dynamics and is referenced using the equation number instead of typing to conserve space. The zero speed equality constraint (BSP.14) is vital to enforce zero speed according to $\mathcal{V}^0$, as otherwise the optimisation problem would prevent the train from stopping to conserve kinetic energy. This is different to (BSP.15) which bounds v $\forall n \in \mathcal{A}$ according to the speed limits of the track.

The average speed constraint (BSP.6) and both spatial (BSP.7) and temporal (BSP.13) equalities are used to calculate the timing points in (BSP.16) according to (4.9).

The formulation presents the following non-convexities because they are non-linear equality constraints: (BSP.4), (BSP.7), and (BSP.5). These are addressed in the following subsection.

5.1.2 Convexifying Speed Formulation

Convexifying (BSP.4)

The equality constraint (BSP.4) is non-linear in v due to the squared operation v^2 therein. It can be linearized by substituting the non-linear v^2 terms with the surogate variable z (as done in (3.31))

$$\frac{1}{2}m_{\text{eq}}z_{j+1} = \frac{1}{2}m_{\text{eq}}z_j + (F_{\text{trc},j} + F_{\text{brk},j})\Delta_{\text{s},j} - F_{\text{ext},j}\Delta_{\text{s},j}, \tag{5.4}$$

where the v^2 in F_{ext} is also substituted for z

$$F_{\text{ext},j} = a + bv_j + cz_j + mg\sin(\theta_j). \tag{5.5}$$

The Davis Equation in F_{ext} requires both v and z and thus the non-linear equality con-

straint $v^2 = z$ should be introduced which can be relaxed into the convex inequality

$$v^2 \leq z. \tag{5.6}$$

Convexifying (BSP.7)

The equality constraint (BSP.7) is non-linear due to the presence of v_{avg} in the denominator. To convexify this, define the surrogate variable

$$\lambda_{v,j} = \frac{1}{v_{\text{avg},j}} \tag{5.7}$$

then substitute into (BSP.7) to yield the linear

$$\delta_{\text{t},j} = \Delta_{\text{s},j}\lambda_{v,j}. \tag{5.8}$$

The non-linear equality (5.7) poses a new source of non-convexity, though it can be mitigated by relaxing it into the bilinear inequality (recall (3.27))

$$1 \leq v_{\text{avg},j}\lambda_{v,j} \tag{5.9}$$

for $v_{\text{avg},j}, \lambda_{v,j} \geq 0$. It will be proven that this relaxed constraint will hold tightly with equality at the optimal solution. Note that the product of both variables in (5.9) must be positive to comply with the positive lower bound of 1. This is not restrictive because $v_{\text{avg},j}$ will only return positive values $\forall j \in \mathcal{S}$.

Eliminating (BSP.5)

The motor power constraint (BSP.5) is non-convex because it is a non-linear equality, though it is necessary to convert traction force F_{trc} into traction power P_{trc} which is then bound in (BSP.12).

Upon multiplying (BSP.12) by the newly formed surrogate λ_v (which represents $\frac{1}{v_{\text{avg}}}$), P_{trc} can then be replaced by F_{trc} due to the mechanical relation $F = \frac{P}{v}$

$$\underline{P_{\text{trc}}}\lambda_v \leq F_{\text{trc}} \leq \overline{P_{\text{trc}}}\lambda_v. \tag{5.10}$$

The new linear bounds negate the need for the non-convex (BSP.5) which means it can be eliminated.

5.1.3 Convex Speed Formulation

The formulation (CSP) is a convexified variant of (BSP) by implementing the changes proposed in the last subsection. The new label "CSP" stands for "Convex Speed". The newly added vector variables are:

- $\boldsymbol{\lambda_v}$ is optimised only for $\mathcal{S}$ because it is only to be used with a positive v_{avg},
- $\boldsymbol{z}$ is optimised for $\mathcal{A}$ because it is a system state.

The convexified formulation (CSP) is only equivalent to the original (BSP) if the relaxed constraints (CSP.16) and (CSP.7) were to tighten and hold at equality. This is indeed the case because the formulation has the incentive to achieve the timing points τ_m for minimum traction effort. The following elaborates on this:

- (CSP.7) holds at equality because
  - λ_v is pushed down to achieve timing points constraint (CSP.19). As λ_v is reduced, the train would appear to travel faster in (CSP.6) without a traction cost. Therefore, the optimal solution would rather reduce λ_v before resorting to additional traction effort to accelerate the train, and
  - as λ_v drops, v_{avg} will be pushed up at some point to maintain the lower bound 1 (constraint left-hand side). Subsequently, λ_v can drop further to make the train appear faster and tighten (CSP.7).

$$\min_{\boldsymbol{F}_{\mathrm{trc}},\, \boldsymbol{F}^{+}_{\mathrm{trc}},\, \boldsymbol{F}_{\mathrm{brk}},\, \boldsymbol{v},\, \boldsymbol{v}_{\mathrm{avg}},\, \boldsymbol{\delta}_{\mathrm{t}},\, \boldsymbol{z},\, \boldsymbol{\lambda}_{\boldsymbol{v}}} \quad \sum_{j \in \mathcal{S}} F^{+}_{\mathrm{trc},j} \Delta_{\mathrm{s},j} \tag{CSP.1}$$

subject to

given as parameters

$$\Delta_{\mathrm{s},j} \quad \forall j \in \mathcal{S} \tag{CSP.2}$$

$$\Delta_{\mathrm{t},k} \quad \forall k \in \mathcal{T} \tag{CSP.3}$$

$$\forall j \in \mathcal{S}$$

$$(5.4) \tag{CSP.4}$$

$$v_{\mathrm{avg},j} = \frac{v_j + v_{j+1}}{2} \tag{CSP.5}$$

$$\delta_{\mathrm{t},j} = \Delta_{\mathrm{s},j} \lambda_{v,j} \tag{CSP.6}$$

$$1 \leq v_{\mathrm{avg},j} \lambda_{v,j} \tag{CSP.7}$$

$$0 \leq \lambda_{\mathrm{v},j} \tag{CSP.8}$$

$$0 \leq F^{+}_{\mathrm{trc},j} \tag{CSP.9}$$

$$F_{\mathrm{trc},j} \leq F^{+}_{\mathrm{trc},j} \tag{CSP.10}$$

$$\underline{F_{\mathrm{trc}}} \leq F_{\mathrm{trc},j} \leq \overline{F_{\mathrm{trc}}} \tag{CSP.11}$$

$$\underline{P_{\mathrm{trc}}} \lambda_{v,j} \leq F_{\mathrm{trc},j} \leq \overline{P_{\mathrm{trc}}} \lambda_{v,j} \tag{CSP.12}$$

$$\underline{F_{\mathrm{brk}}} \leq F_{\mathrm{brk},j} \leq 0 \tag{CSP.13}$$

$$\forall k \in \mathcal{T}$$

$$\delta_{\mathrm{t},k} = \Delta_{\mathrm{t},k} \tag{CSP.14}$$

$$\forall l \in \mathcal{V}^0$$

$$v_l = 0 \tag{CSP.15}$$

$$\forall n \in \mathcal{A}$$

$$v_n^2 \leq z_n \tag{CSP.16}$$

$$0 \leq v_n \leq \overline{v_n} \tag{CSP.17}$$

$$0 \leq z_n \leq \overline{z_n} \tag{CSP.18}$$

$$\forall m \in \mathcal{M}$$

$$t(m) = \tau_m \tag{CSP.19}$$

Optimisation Problem 2: Convex Speed (CSP)

- (CSP.16) holds at equality
  - since v_{avg} was being pushed up in (CSP.7), it will also pull up v in (BSP.6) up until it reaches z, and,
  - z is pushed down in (CSP.4) because of its link to the traction penalty (CSP.1) through the variable F_{trc}.

5.2 EMS Optimisation

To implement the results of the speed formulation from the previous section, an accompanying energy management system is needed to control the hybrid powertrain such that it meets traction power demands. This section presents a formulation for optimising the EMS given interval durations $\boldsymbol{\delta}_{\text{t}}$, traction force $\boldsymbol{F}_{\text{trc}}$, and $\boldsymbol{v}_{\text{avg}}$.

The formulation herein directly penalises hyrdogen consumption in the objective function. Furthermore, it adds a charge-sustaining constraint on the battery and prohibits fuel cell idling to preserve its lifetime.

5.2.1 Basic EMS Formulation

Given $\boldsymbol{\delta}_{\text{t}}$, $\boldsymbol{F}_{\text{trc}}$ and $\boldsymbol{v}_{\text{avg}}$ from the preceding speed formulation, first find the electric traction power $\boldsymbol{P}_{\text{m}}$ using (4.18). Then the optimal EMS power split could be found using (BEM). Its label "BEM" refers to "Basic Energy Management". The optimised vector variables are:

- $\boldsymbol{P}_{\text{fc}}$, $\boldsymbol{P}_{\text{bat}}$, $\boldsymbol{\delta}_{\boldsymbol{\zeta}}$ are only optimised for $\mathcal{B}$,
- $\boldsymbol{\zeta}$ is optimised for $\mathcal{A}$.

Note that $\boldsymbol{P}_{\text{m}}$ and $\boldsymbol{\delta}_{\text{t}}$ are not optimised, since they are given as inputs. They are typed in (BEM.2), (BEM.4) and (BEM.5) only to emphasise their presence. Furthermore, the auxiliary load $\boldsymbol{P}_{\text{aux}}$ in (BEM.3) is not optimised and is given as a reference profile.

$$\min_{\boldsymbol{P}_{\mathrm{fc}},\, \boldsymbol{P}_{\mathrm{bat}},\, \boldsymbol{\zeta},\, \boldsymbol{\delta_\zeta}} \quad \sum_{i \in \mathcal{B}} \frac{P_{\mathrm{fc},i}}{\eta_{\mathrm{fc}}(P_{\mathrm{fc},i})} \times \mathrm{LHV} \times \delta_{\mathrm{t},i} \tag{BEM.1}$$

subject to

given as parameters

$$P_{\mathrm{m},i} \quad \forall i \in \mathcal{B} \tag{BEM.2}$$

$$P_{\mathrm{aux},i} \quad \forall i \in \mathcal{B} \tag{BEM.3}$$

$$\delta_{\mathrm{t},j} = \frac{\Delta_{\mathrm{s},j}}{v_{\mathrm{avg},j}} \quad \forall j \in \mathcal{S} \tag{BEM.4}$$

$$\delta_{\mathrm{t},k} = \Delta_{\mathrm{t},k} \quad \forall k \in \mathcal{T} \tag{BEM.5}$$

$i \in \mathcal{B}$

$$\delta_{\zeta,i} = \frac{U_{\mathrm{oc}} - \sqrt{U_{\mathrm{oc}}^2 - 4R_{\mathrm{bat}}P_{\mathrm{bat},i}}}{2R_{\mathrm{bat}} \times \frac{3600Q_{\mathrm{Ah}}}{100} \times \delta_{\mathrm{t},i}} \tag{BEM.6}$$

$$\zeta_{i+1} = \zeta_i - \delta_{\zeta,i} \tag{BEM.7}$$

$$\underline{P_{\mathrm{fc}}} \leq P_{\mathrm{fc},i} \leq \overline{P_{\mathrm{fc}}} \tag{BEM.8}$$

$$\underline{P_{\mathrm{bat}}} \leq P_{\mathrm{bat},i} \leq \overline{P_{\mathrm{bat}}} \tag{BEM.9}$$

$\forall j \in \mathcal{S}$

$$P_{\mathrm{m},j} + P_{\mathrm{aux},j} = P_{\mathrm{fc},j} + P_{\mathrm{bat},j} \tag{BEM.10}$$

$\forall k \in \mathcal{T}$

$$P_{\mathrm{aux},k} = P_{\mathrm{fc},k} + P_{\mathrm{bat},k} \tag{BEM.11}$$

$\forall n \in \mathcal{A}$

$$\underline{\zeta} \leq \zeta_{\mathrm{n}} \leq \overline{\zeta} \tag{BEM.12}$$

other

$$\zeta_{\mathrm{N}} = \zeta_0 \tag{BEM.13}$$

Optimisation Problem 3: Basic Energy Management (BEM)

The objective function (BEM.1) penalises fuel consumption as defined in (4.24).

The power flow constraints (BEM.10) and (BEM.11) play an important role in meeting the required power $\boldsymbol{P}_{\mathrm{m}}$, $\boldsymbol{P}_{\mathrm{aux}}$. The fuel cell lower power constraint $\underline{P_{\mathrm{fc}}}$ in (BEM.8) is strictly positive to preserve lifetime.

The change in battery state-of-charge variable $\boldsymbol{\delta_\zeta}$ is modelled through the equality constraint (BEM.6). The lower and upper bounds on state-of-charge in (BEM.12) are applied $\forall n \in \mathcal{A}$ because it is a dynamic state and not a control input. The equality constraint (BEM.13) is a charge-sustaining requirement on the battery's state-of-charge.

The formulation (BEM) presents two non-convexities:

1. the discrete lookup table η_{fc} in the objective function (BEM.1),
2. the non-linear equality constraint (BEM.6),

which will be both addressed in the next subsection.

It is worth mentioning that δ_{t} could have presented an extra non-convexity for both of these expressions if it were to be an optimised variable because it is directly multiplied by other variables. However, it poses no issue in this context because it is given as a fixed input.

5.2.2 Convexifying EMS Formulation

Convexifying (BEM.1)

$\frac{P_{\mathrm{fc}}}{\eta_{\mathrm{fc}}(P_{\mathrm{fc}})}$ leads to a non-convex formulation due to the discontinuity introduced in the discrete efficiency lookup table. However, its discrete points are expected to follow a convex shape. This is because the denominator $\eta_{\mathrm{fc}}(P_{\mathrm{fc}})$ is concave and positive, shown in Fig. 4.4, which satisfies the condition for a convex reciprocal according to (3.20). This characteristic of fuel cell efficiency can be generalised to other fuel cells, as it was theoretically proven that efficiency is always concave [320].

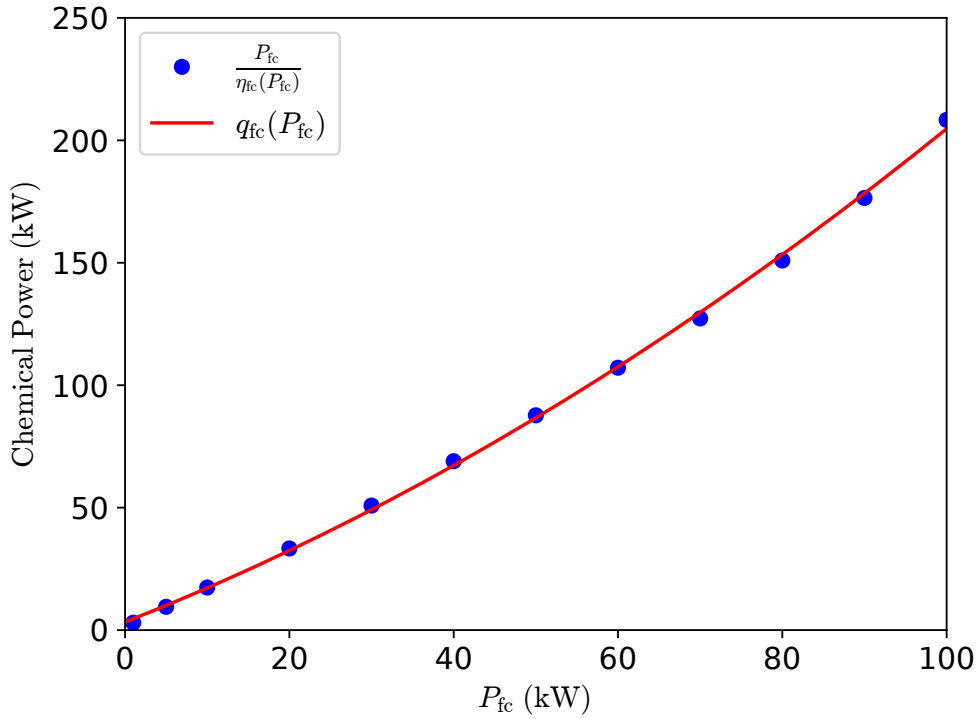

Figure 5.1: Plot of discrete $\frac{P_{\text{fc}}}{\eta_{\text{fc}}(P_{\text{fc}})}$ and its quadratic polynomial approximation q_{fc}.

Given that the discrete $\frac{P_{\text{fc}}}{\eta_{\text{fc}}(P_{\text{fc}})}$ follows a convex pattern, it implies that it could be accurately approximated by the continious quadratic polynomial

$$q_{\text{fc}}(P_{\text{fc},i}) := p_2 P_{\text{fc},i}^2 + p_1 P_{\text{fc},i} + p_0 \quad \forall i \in \mathcal{B}, \tag{5.13}$$

which is convex for $p_2 \geq 0$. Figure 5.1 plots the quadratic polynomial along the original discrete data and indeed shows a high approximation rate.

Convexifying (BEM.6)

The equality constraint (BEM.6) does not form a convex set due to the non-linearity of the square root operation over P_{bat}. This can be convexified by relaxing the constraint into

$$\delta_{\zeta,i} \geq \frac{U_{\text{oc}} - \sqrt{U_{\text{oc}}^2 - 4R_{\text{bat}}P_{\text{bat},i}}}{2R_{\text{bat}}} \times \delta_{\text{t},i} \times \frac{100}{3600Q_{\text{Ah}}}. \tag{5.14}$$

The inequality (5.14) forms a convex set because the lower inequality side is convex and thus satisfies the condition on convex inequalities (3.10). The numerator $U_{\text{oc}} -$

$\sqrt{U_{\text{oc}}^2 - 4R_{\text{bat}}P_{\text{bat}}}$ is convex because scaling the concave square root by -1 produces a convex function. Moreover, $P_{\text{bat},i}$ is the only optimised variable on the right-hand side, since $\delta_{\text{t},i}$ on the right-hand side is a given input within the context of (BEM).

The relaxed constraint (5.14) shall hold with equality at the optimal solution. This can be shown to be true by observing its potential use back in (BEM). Firstly, the optimisation problem will not arbitrarly raise δ_ζ, because that would discharge the battery and trigger the charge-sustaining constraint (BEM.13) which in turn will cost fuel to recharge the battery. Instead, the objective function will push down on δ_ζ to save fuel. Furthermore, there is an incentive for δ_ζ to go negative to recharge the battery by "free energy". All of these tendencies will tighten the relaxed constraint towards equality.

Although the relaxed constraint (5.14) forms a convex set, it will not be accepted by commercial convex solvers, because they typically lack support for square root constraints. The full reason for this limitation goes beyond the scope of this thesis. In a nutshell, it is related to limiting the type of mathematical expressions accepted, which improves algorithmic efficiency. More details on this can be found in [323, Chapter 7].

One approach around the square-root limitation is to build a custom convex solver. Another is to use a non-linear solver that supports general constraints; however, this would fail to leverage the computational benefits of convex models. Instead, it is proposed to rewrite the constraint into a form that can be accepted by the majority of convex solvers, a quadratic constraint.

Rewriting (5.14) as Quadratic

To facilitate derivation, start by defining the constant ω

$$\omega := 2R_{\text{bat}} \times \frac{3600Q_{\text{Ah}}}{100} \tag{5.15}$$

which is used to rewrite (5.14) as the neater

$$\omega \frac{\delta_{\zeta,i}}{\delta_{\mathrm{t},i}} \geq U_{\mathrm{oc}} - \sqrt{U_{\mathrm{oc}}^2 - 4R_{\mathrm{bat}}P_{\mathrm{bat},i}}, \tag{5.16}$$

then move U_{oc} to the left-hand side

$$\omega \frac{\delta_{\zeta,i}}{\delta_{\mathrm{t},i}} - U_{\mathrm{oc}} \geq -\sqrt{U_{\mathrm{oc}}^2 - 4R_{\mathrm{bat}}P_{\mathrm{bat},i}}, \tag{5.17}$$

square both sides to drop the square-root (which also flips the inequality)

$$\omega^2 \frac{\delta_{\zeta,i}^2}{\delta_{\mathrm{t},i}^2} - 2U_{\mathrm{oc}}\omega \frac{\delta_{\zeta,i}}{\delta_{\mathrm{t},i}} + U_{\mathrm{oc}}^2 \leq U_{\mathrm{oc}}^2 - 4R_{\mathrm{bat}}P_{\mathrm{bat},i}, \tag{5.18}$$

U_{oc}^2 can now be cancelled from both sides to yield the final convex form

$$\omega^2 \frac{\delta_{\zeta,i}^2}{\delta_{\mathrm{t},i}^2} - 2U_{\mathrm{oc}}\omega \frac{\delta_{\zeta,i}}{\delta_{\mathrm{t},i}} \leq -4R_{\mathrm{bat}}P_{\mathrm{bat},i}. \tag{5.19}$$

For a given δ_{t}, the final form (5.19) has a quadratic left-hand side and a linear right-hand side. The quadratic part is convex because its coefficient $\frac{\omega^2}{\delta_{\mathrm{t},i}^2}$ is non-negative by definition. Moreover, the non-linear quadratic part is on the lower inequality side which satisfies the convex inequality condition (3.10).

The constraint (5.19) is merely a reformed alternative to (5.14) and would thus hold tightly with equality at the optimal solution.

5.2.3 Convex EMS Formulation

The EMS formulation (CEM) is a convexified variant of (BEM) by implementing the changes proposed in the previous subsection. The new label refers to "Convex Energy Management". The only change to the constraints is introducing the relaxed inequality (CEM.6) which will hold with equality at the optimal solution as explained in the previous subsection.

$$\min_{\boldsymbol{P}_{\mathrm{fc}},\, \boldsymbol{P}_{\mathrm{bat}},\, \boldsymbol{\zeta},\, \boldsymbol{\delta_\zeta}} \quad \sum_{i \in \mathcal{B}} q_{\mathrm{fc}}(P_{\mathrm{fc},i}) \times \mathrm{LHV} \times \delta_{\mathrm{t},i} \tag{CEM.1}$$

subject to

given as parameters

$$P_{\mathrm{m},i} \quad \forall i \in \mathcal{B} \tag{CEM.2}$$

$$P_{\mathrm{aux},i} \quad \forall i \in \mathcal{B} \tag{CEM.3}$$

$$\delta_{\mathrm{t},j} = \frac{\Delta_{\mathrm{s},j}}{v_{\mathrm{avg},j}} \quad \forall j \in \mathcal{S} \tag{CEM.4}$$

$$\delta_{\mathrm{t},k} = \Delta_{\mathrm{t},k} \quad \forall k \in \mathcal{T} \tag{CEM.5}$$

$$\forall i \in \mathcal{B}$$

$$\omega^2 \frac{\delta_{\zeta,i}^2}{\delta_{\mathrm{t},i}^2} - 2U_{\mathrm{oc}}\omega \frac{\delta_{\zeta,i}}{\delta_{\mathrm{t},i}} \leq -4R_{\mathrm{bat}}P_{\mathrm{bat},i} \tag{CEM.6}$$

$$\zeta_{i+1} = \zeta_i - \delta_{\zeta,i} \tag{CEM.7}$$

$$\underline{P_{\mathrm{fc}}} \leq P_{\mathrm{fc},i} \leq \overline{P_{\mathrm{fc}}} \tag{CEM.8}$$

$$\underline{P_{\mathrm{bat}}} \leq P_{\mathrm{bat},i} \leq \overline{P_{\mathrm{bat}}} \tag{CEM.9}$$

$$\forall j \in \mathcal{S}$$

$$P_{\mathrm{m},j} + P_{\mathrm{aux},j} = P_{\mathrm{fc},j} + P_{\mathrm{bat},j} \tag{CEM.10}$$

$$\forall k \in \mathcal{T}$$

$$P_{\mathrm{aux},k} = P_{\mathrm{fc},k} + P_{\mathrm{bat},k} \tag{CEM.11}$$

$$\forall n \in \mathcal{A}$$

$$\underline{\zeta} \leq \zeta_{\mathrm{n}} \leq \overline{\zeta} \tag{CEM.12}$$

other

$$\zeta_{\mathrm{N}} = \zeta_0 \tag{CEM.13}$$

Optimisation Problem 4: Convex Energy Management (CEM)

5.3 Joint Speed and EMS Optimisation

This section builds a joint speed-EMS formulation to optimise all speed and EMS variables at the same time. This would improve the optimality of the solution by better exploring and thus taking advantage of the dynamic interaction between all variables.

Nevertheless, a joint formulation comes at a higher computational cost. For example, feeding $\boldsymbol{\delta}_\mathrm{t}$ as a fixed input to (CEM) enabled convexifying the constraint (BEM.6) into (CEM.6). This will no longer be the case for a joint formulation because $\boldsymbol{\delta}_\mathrm{t} \in \mathcal{S}$ should now be optimised.

Section 5.3.1 attempts creating a joint formulation by merging the convex speed (CSP) and convex EMS (CEM). This returns a non-convex joint formulation which is analysed and convexified in Section 5.3.2. The final convex formulation is presented in Section 5.3.3.

5.3.1 Merging Speed and EMS Formulations

Directly merging the convex speed (CSP) and the convex EMS (CEM) formulations produces the joint formulation (BJN). Its label refers to "Basic Joint".

$$\min_{\boldsymbol{F}_{\text{trc}},\, \boldsymbol{F}_{\text{brk}},\, \boldsymbol{v},\, \boldsymbol{v}_{\text{avg}},\, \boldsymbol{\delta}_{\text{t}},\, \boldsymbol{z},\, \boldsymbol{\lambda}_{v},\, \boldsymbol{P}_{\text{m}},\, \boldsymbol{P}_{\text{fc}},\, \boldsymbol{P}_{\text{bat}},\, \boldsymbol{\zeta},\, \boldsymbol{\delta}_{\zeta}} \quad \sum_{i \in \mathcal{B}} q_{\text{fc}}(P_{\text{fc},i}) \times \text{LHV} \times \delta_{\text{t},i} \tag{BJN.1}$$

subject to

given as parameters

$$\Delta_{\text{s},j} \quad \forall j \in \mathcal{S} \tag{BJN.2}$$

$$\Delta_{\text{t},k} \quad \forall k \in \mathcal{T} \tag{BJN.3}$$

$$P_{\text{aux},i} \quad \forall i \in \mathcal{B} \tag{BJN.4}$$

$\forall i \in \mathcal{B}$

$$\omega^2 \frac{\delta_{\zeta,i}^2}{\delta_{\text{t},i}^2} - 2U_{\text{oc}}\omega\frac{\delta_{\zeta,i}}{\delta_{\text{t},i}} \leq -4R_{\text{bat}}P_{\text{bat},i} \tag{BJN.5}$$

$$\zeta_{i+1} = \zeta_i - \Delta_{\zeta,i} \tag{BJN.6}$$

$$\underline{P_{\text{fc}}} \leq P_{\text{fc},i} \leq \overline{P_{\text{fc}}} \tag{BJN.7}$$

$$\underline{P_{\text{bat}}} \leq P_{\text{bat},i} \leq \overline{P_{\text{bat}}} \tag{BJN.8}$$

$\forall j \in \mathcal{S}$

(5.4) (BJN.9)

$$v_{\text{avg},j} = \frac{v_j + v_{j+1}}{2} \tag{BJN.10}$$

$$\delta_{\text{t},j} = \Delta_{\text{s}}\lambda_{v,j} \tag{BJN.11}$$

$$P_{\text{m},j} = \frac{F_{\text{trc},j}v_{\text{avg},j}}{\eta_{\text{m}}(F_{\text{trc},j}v_{\text{avg},j})} \tag{BJN.12}$$

$$P_{\text{m},j} + P_{\text{aux},j} = P_{\text{fc},j} + P_{\text{bat},j} \tag{BJN.13}$$

$$1 \leq v_{\text{avg},j}\lambda_{v,j} \tag{BJN.14}$$

$$0 \leq \lambda_{v,j} \tag{BJN.15}$$

$$\underline{F_{\text{trc}}} \leq F_{\text{trc},j} \leq \overline{F_{\text{trc}}} \tag{BJN.16}$$

$$\underline{P_{\text{trc}}}\lambda_{v,j} \leq F_{\text{trc},j} \leq \overline{P_{\text{trc}}}\lambda_{v,j} \tag{BJN.17}$$

$$\underline{F_{\text{brk}}} \leq F_{\text{brk},j} \leq 0 \tag{BJN.18}$$

$\forall k \in \mathcal{T}$

$$\delta_{\text{t},k} = \Delta_{\text{t},k} \tag{BJN.19}$$

$$P_{\text{aux},k} = P_{\text{fc},k} + P_{\text{bat},k} \tag{BJN.20}$$

$\forall l \in \mathcal{V}^0$

$$v_l = 0 \tag{BJN.21}$$

$$z_l = 0 \tag{BJN.22}$$

$\forall n \in \mathcal{A}$

$$v_n^2 \leq z_n \tag{BJN.23}$$

$$0 \leq v_n \leq \overline{v_n} \tag{BJN.24}$$

$$0 \leq z_n \leq \overline{z_n} \tag{BJN.25}$$

$$\underline{\zeta} \leq \zeta_{\text{n}} \leq \overline{\zeta} \tag{BJN.26}$$

$\forall m \in \mathcal{M}$

$$t(m) = \tau_m \tag{BJN.27}$$

other

$$\zeta_{\text{N}} = \zeta_0 \tag{BJN.28}$$

Optimisation Problem 5: Basic Joint (BJN)

Firstly, note that the positive traction variable $\boldsymbol{F}^{+}_{\mathrm{trc}}$ has been eliminated. It was used to penalise (CSP), whereas now hydrogen consumption can be directly penalised using $q_{\mathrm{fc}}(P_{\mathrm{fc}})$.

Secondly, the constraint (BJN.12), which is based on (4.18), has been introduced, to convert traction force F_{trc} to motor electric power P_{m}. This is done to couple longitudinal dynamics (BJN.9) with the powertrain (BJN.13).

Although (CSP) and (CEM) were convex in their own right, their merger (BJN) has introduced the following non-convexities:

1. the bilinear multiplication between the variables P_{fc} and δ_{t} in the objective function is non-convex for instances that belong to $\mathcal{S}$. It is convex for instances that belong to $\mathcal{T}$ because δ_{t} is predetermined as Δ_{t}.

2. the bilinear multiplication between F_{trc} and v in the equality constraint (BJN.12) is non-convex for instances that belong to $\mathcal{S}$. Moreover, the efficiency model therein is discrete, which also creates non-convexity.

3. the variable δ_{ζ} is divided by δ_{t} in (BJN.5) which is non-convex for instances in $\mathcal{S}$. In contrast, it is convex for instances that belong to $\mathcal{T}$ because δ_{t} is predetermined as Δ_{t}.

5.3.2 Convexifying Speed and EMS Merger

This section addresses the aforementioned non-convexities of (BJN) to produce a convex joint speed-EMS formulation. Since the non-convexities were concerning instances in $\mathcal{S}$, the focus here shifts to finding alternative models that are convex for $\mathcal{S}$. The convex alternatives to be developed in this section for $\mathcal{S}$ can be used in conjunction with the already convex models for $\mathcal{T}$, as the modelling domains are used exclusively of each other for any given instance.

The convexification strategy for $\mathcal{S}$ is inspired by the linear work penalty $\sum_{j\in\mathcal{S}} F^{+}_{\mathrm{trc},j}\Delta_{\mathrm{s},j}$

in (CSP.1). This penalty is linear for $\mathcal{S}$ because it is assigned a predetermined $\Delta_{\mathrm{s},j}$ for all $j \in \mathcal{S}$. Comparing this to the non-convexities in (BJN), suggests that models built using the predetermined $\Delta_{\mathrm{s},j}$ instead of the variable $\delta_{\mathrm{t},j}$, and using work instead of power, are likely to be convex for $\mathcal{S}$.

Therefore, it will be attempted to convexify (BJN) by transforming its models for $\mathcal{S}$ from power to work. Upon examining (BJN), it becomes evident that implementing this approach requires changes to (BJN.13), (BJN.12), (BJN.1) and (BJN.5). This is explored in the following subsections in the same order.

Rewriting Power Flow (BJN.13) **as Work**

To transform the electric power equality (BJN.13) into terms of work and $\Delta_{\mathrm{s},j}$ for all $j \in \mathcal{S}$, start by multiplying by $\delta_{\mathrm{t},j}$

$$P_{\mathrm{m},j}\delta_{\mathrm{t},j} + P_{\mathrm{aux},j}\delta_{\mathrm{t},j} = P_{\mathrm{fc},j}\delta_{\mathrm{t},j} + P_{\mathrm{bat},j}\delta_{\mathrm{t},j}, \tag{5.22}$$

which returns the electric energy balance over the interval $[j, j+1)$.

Substitute $\delta_{\mathrm{t},j} = \frac{\Delta_{\mathrm{s},j}}{v_{\mathrm{avg},j}}$ as defined in (4.13) except for $P_{\mathrm{aux},j}\delta_{\mathrm{t},j}$

$$P_{\mathrm{m},j}\frac{\Delta_{\mathrm{s},j}}{v_{\mathrm{avg},j}} + P_{\mathrm{aux},j}\delta_{\mathrm{t},j} = P_{\mathrm{fc},j}\frac{\Delta_{\mathrm{s},j}}{v_{\mathrm{avg},j}} + P_{\mathrm{bat},j}\frac{\Delta_{\mathrm{s},j}}{v_{\mathrm{avg},j}}. \tag{5.23}$$

There is no risk for the denominator v_{avg} to return a zero with $\mathcal{S}$ as explained in (4.12). It was chosen to keep $P_{\mathrm{aux},j}\delta_{\mathrm{t},j}$ because auxiliary power is given as a reference power profile and not optimised.

The equality (5.23) contains the spatial interval Δ_{s} but lacks a force variable to get work $F\Delta_{\mathrm{s}}$. To this end, define the "analogous" force variable $\forall j \in \mathcal{S}$

$$F_{x,j} := \frac{P_{x,j}}{v_{\mathrm{avg},j}}, \tag{5.24}$$

where x refers to one of: motor, fuel cell or battery. It is called "analogous" because it draws an analogy to the mechanical relation $F = \frac{P}{v}$ yet it is applied to electric quantities.

Now substitute (5.24) into (5.23)

$$F_{\mathrm{m},j}\Delta_{\mathrm{s},j} + P_{\mathrm{aux},j}\delta_{\mathrm{t},j} = F_{\mathrm{fc},j}\Delta_{\mathrm{s},j} + F_{\mathrm{bat},j}\Delta_{\mathrm{s},j}. \tag{5.25}$$

The equality (5.25) describes the balance of "electric work". Using work for electric quantities is not intuitive, though mathematically, $F_{\mathrm{x},j}\Delta_{\mathrm{s},j}$ represents the electric energy flow for the interval $[j, j+1)$ for $j \in \mathcal{S}$.

To conclude this subsection, the work equality (5.25) shall replace (BJN.13). To successfully implement this change, P_x should be replaced by F_x for all powertrain components for $\mathcal{S}$. This will be explored after the next subsection which demonstrates the equivalence of power- and work-based models using a numerical example.

Numeric Intuition behind $F_x\Delta_{\mathrm{s}}$

This short subsection presents a numerical example to provide insight into how $F_{x,j}\Delta_{\mathrm{s},j}$ and $P_{x,j}\delta_{\mathrm{t},j}$ return the same energy magnitude for $j \in \mathcal{S}$. Take an instance $j \in \mathcal{S}$, at which $\Delta_{\mathrm{s},j} = 10\,\mathrm{m}$, $v_{\mathrm{avg},j} = 10\,\mathrm{m\cdot s^{-1}}$ and $P_{\mathrm{fc},j} = 50\,\mathrm{kW}$. This means that the "analogous" force of the fuel cell is $F_{\mathrm{fc},j} = \frac{50\,\mathrm{kW}}{10\,\mathrm{m\cdot s^{-1}}} = 5\,\mathrm{kN}$. Also, the interval $[j, j+1)$ lasts $\frac{10\,\mathrm{m}}{10\,\mathrm{m\cdot s^{-1}}} = 1\,\mathrm{s}$ long. Energy found using $F_{\mathrm{fc}}\Delta_{\mathrm{s}}$: $5\,\mathrm{kN} \times 10\,\mathrm{m} = 50\,\mathrm{kJ}$ is equivalent to that using $P_{\mathrm{fc}}\delta_{\mathrm{t}}$: $50\,\mathrm{kW} \times 1\,\mathrm{s} = 50\,\mathrm{kJ}$.

Convexifying (BJN.12)

To couple (BJN.12) with the work equality (5.25), motor electric power $P_{\mathrm{m},j}$ should be transformed into the motor analogous force $F_{\mathrm{m},j}$ for all $j \in \mathcal{S}$. This has the added benefit that the numerator in (BJN.12) will become linear, which will facilitate convexification. To do so, repeat the same steps that were used to rewrite the power equality (BJN.13)

into the work equality (5.25).

First, multiply (BJN.12) by $\delta_{\mathrm{t},j} = \frac{\Delta_{\mathrm{s},j}}{v_{\mathrm{avg},j}}$

$$P_{\mathrm{m},j}\frac{\Delta_{\mathrm{s},j}}{v_{\mathrm{avg},j}} = \frac{F_{\mathrm{trc},j}v_{\mathrm{avg},j}}{\eta_{\mathrm{m}}(F_{\mathrm{trc},j}v_{\mathrm{avg},j})}\frac{\Delta_{\mathrm{s},j}}{v_{\mathrm{avg},j}}, \tag{5.26}$$

replace $P_{\mathrm{m},j}$ by the analogous terms $F_{\mathrm{m},j}v_{\mathrm{avg},j}$, defined in (5.24),

$$F_{\mathrm{m},j}v_{\mathrm{avg},j}\frac{\Delta_{\mathrm{s},j}}{v_{\mathrm{avg},j}} = \frac{F_{\mathrm{trc},j}v_{\mathrm{avg},j}}{\eta_{\mathrm{m}}(F_{\mathrm{trc},j}v_{\mathrm{avg},j})}\frac{\Delta_{\mathrm{s},j}}{v_{\mathrm{avg},j}}, \tag{5.27}$$

cancel out excessive $v_{\mathrm{avg},j}$ terms

$$F_{\mathrm{m},j}\Delta_{\mathrm{s},j} = \frac{F_{\mathrm{trc},j}}{\eta_{\mathrm{m}}(F_{\mathrm{trc},j}v_{\mathrm{avg},j})}\Delta_{\mathrm{s},j}. \tag{5.28}$$

optionally, cancel out the common $\Delta_{\mathrm{s},j}$

$$F_{\mathrm{m},j} = \frac{F_{\mathrm{trc},j}}{\eta_{\mathrm{m}}(F_{\mathrm{trc},j}v_{\mathrm{avg},j})}. \tag{5.29}$$

Excluding the discrete efficiency term in the denominator, the numerators in (5.29) have become linear, namely $F_{\mathrm{m},j}$ and $F_{\mathrm{trc},j}$.

The discrete $\frac{F_{\mathrm{trc},j}}{\eta_{\mathrm{m}}(F_{\mathrm{trc},j}v_{\mathrm{avg},j})}$ on the right-hand side of (5.29) forms a convex pattern because motor efficiency is concave and positive, which satisfies the condition for a convex reciprocal (3.20). This implies that it can be accurately approximated by the convex quadratic polynomial

$$q_{\mathrm{m}}(F_{\mathrm{trc}}, v_{\mathrm{avg}}) := p_{02}F_{\mathrm{trc}}^2 + p_{20}v_{\mathrm{avg}}^2 + p_{11}F_{\mathrm{trc}}v_{\mathrm{avg}} + p_{01}F_{\mathrm{trc}} + p_{10}v_{\mathrm{avg}}, \tag{5.30}$$

though it is proposed to use the much simpler

$$q_{\mathrm{m}}(F_{\mathrm{trc}}) := p_{02}F_{\mathrm{trc}}^2 + p_{01}F_{\mathrm{trc}}, \tag{5.31}$$

which drops the speed variable v_{avg}, because it plays a negligible effect on the approximated discrete points and thus on the approximation rate. In fact, a closer inspection of the approximated expression, $\frac{F_{\text{trc},j}}{\eta_{\text{m}}(F_{\text{trc},j}v_{\text{avg},j})}$, reveals that $v_{\text{avg},j}$ only plays a minor role in the denominator, whereas $F_{\text{trc},j}$ plays a major role in both the numerator and denominator. Note that $q_{\text{m}}(F_{\text{trc},j})$ excludes a constant offset to ensure that traction consumption is zero if traction force were zero, i.e. $q_{\text{m}}(0) = p_{02} \times (0)^2 + p_{01} \times (0) = 0$. This goes against typical polynomial fitting that includes a constant coefficient, see p_0 in (3.11).

Figure 5.2 depicts the actual discrete values of $\frac{F_{\text{trc},j}}{\eta_{\text{m}}(F_{\text{trc},j}v_{\text{avg},j})}$ against the approximated polynomial $q_{\text{m}}(F_{\text{trc},j})$. Moreover, Fig. 5.3 shows that the approximation error is primarily under 10% for both positive and negative traction spans. This level of accuracy is vital for informing the optimisation problem of traction losses. For example, failing to model regenerative braking losses would encourage the optimisation problem to excessively use negative traction thinking that the recovered kinetic energy would save fuel, whereas in reality the motor would be capturing less kinetic energy than planned.

Upon substituting $q_{\text{m}}(F_{\text{trc},j})$ into (5.29) we get the non-linear equality

$$F_{\text{m},j} = q_{\text{m}}(F_{\text{trc},j}), \tag{5.32}$$

which is to be convexified by relaxing it into

$$F_{\text{m},j} \geq q_{\text{m}}(F_{\text{trc},j}). \tag{5.33}$$

The inequality (5.33) forms a convex set because the convex quadratic term exists on the lower inequality side, thus satisfying the convexity condition on inequality constraints (3.10). It will be explained in the final formulation how this relaxation holds tightly at the optimal solution.

To conclude, (BJN.12) has been convexified by replacing it with (5.33).

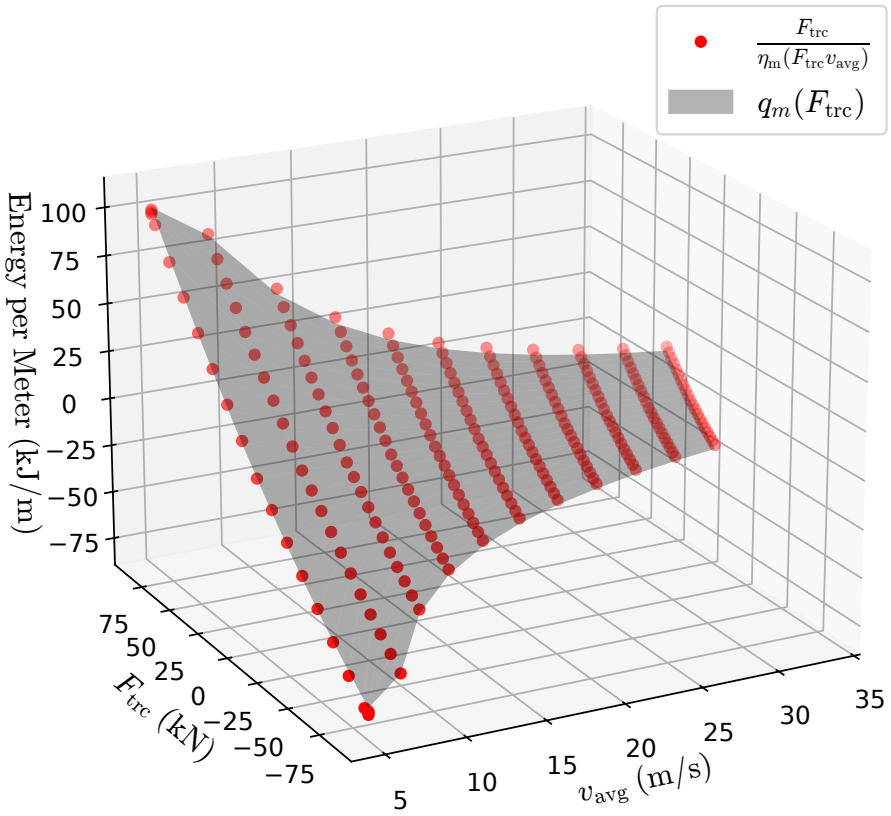

Figure 5.2: Plot of motor polynomial $q_{\text{m}}(F_{\text{trc}})$ and discrete values $\frac{F_{\text{trc}}}{\eta_{\text{m}}(F_{\text{trc}}v_{\text{avg}})}$.

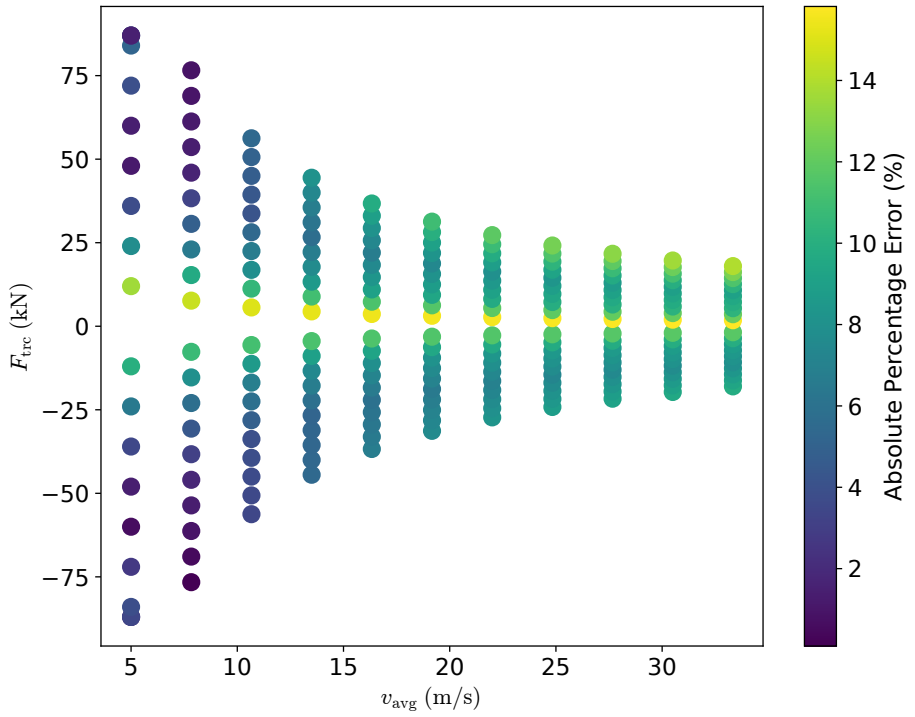

Figure 5.3: Absolute percentage error between the actual discrete values $\frac{F_{\text{trc}}}{\eta_{\text{m}}(F_{\text{trc}}v_{\text{avg}})}$ and the approximated polynomial $q_{\text{m}}(F_{\text{trc}})$ across the operation domain.

Convexifying (BJN.1)

To couple the objective function (BJN.1) with the work equality (5.25), fuel cell power $P_{\text{fc},j}$ should be transformed into fuel cell analogous force $F_{\text{fc},j}$ for all $j \in \mathcal{S}$. This will also convexify the objective function as has resulted previosuly for (BJN.12). Nonetheless, the existing penalty on $\mathcal{T}$ should remain unmodified because it is already convex. To achieve this, split the existing penalty summation over $\mathcal{B}$ into separate summations for $\mathcal{S}$ and $\mathcal{T}$. This way it becomes possible to implement changes on $\mathcal{S}$ without affecting the existing penalty on $\mathcal{T}$.

Split (BJN.1) into

$$\sum_{j\in\mathcal{S}} q_{\text{fc}}(P_{\text{fc},j}) \times \text{LHV} \times \delta_{\text{t},j} + \sum_{k\in\mathcal{T}} q_{\text{fc}}(P_{\text{fc},k}) \times \text{LHV} \times \delta_{\text{t},k}. \tag{5.34}$$

Now roll back $q_{\text{fc}}(P_{\text{fc},j})$ in the $\mathcal{S}$ summation to its discrete expression prior to the polynomial approximation, which is (4.23),

$$\sum_{j\in\mathcal{S}} \frac{P_{\text{fc},j}}{\eta_{\text{fc}}(P_{\text{fc},j})} \times \text{LHV} \times \delta_{\text{t},j} + \sum_{k\in\mathcal{T}} q_{\text{fc}}(P_{\text{fc},k}) \times \text{LHV} \times \delta_{\text{t},k}. \tag{5.35}$$

Substitute $\delta_{\text{t},j} = \frac{\Delta_{\text{s},j}}{v_{\text{avg},j}}$ and replace $P_{\text{fc},j}$ by the analogous terms $F_{\text{fc},j}v_{\text{avg},j}$, defined in (5.24),

$$\sum_{j\in\mathcal{S}} \frac{F_{\text{fc},j}v_{\text{avg},j}}{\eta_{\text{fc}}(F_{\text{fc},j}v_{\text{avg},j})} \times \text{LHV} \times \frac{\Delta_{\text{s},j}}{v_{\text{avg},j}} + \sum_{k\in\mathcal{T}} q_{\text{fc}}(P_{\text{fc},k}) \times \text{LHV} \times \delta_{\text{t},k}. \tag{5.36}$$

Now cancel the excessive $v_{\text{avg},j}$ present in the $\mathcal{S}$ summation

$$\sum_{j\in\mathcal{S}} \frac{F_{\text{fc},j}}{\eta_{\text{fc}}(F_{\text{fc},j}v_{\text{avg},j})} \times \text{LHV} \times \Delta_{\text{s},j} + \sum_{k\in\mathcal{T}} q_{\text{fc}}(P_{\text{fc},k}) \times \text{LHV} \times \Delta_{\text{t},k}. \tag{5.37}$$

The hydrogen consumption penalty (5.37) would become convex if the discrete $\frac{F_{\text{fc},j}}{\eta_{\text{fc}}(F_{\text{fc},j}v_{\text{avg},j})}$ in the $\mathcal{S}$ summation were to be replaced by a convex quadratic polynomial as present in the $\mathcal{T}$ summation. However, this new polynomial ought to use F_{fc} unlike P_{fc} in the $\mathcal{T}$ summation,

$$q_{\text{fc}}(F_{\text{fc}}) := p_{02}F_{\text{fc}}^2 + p_{01}F_{\text{fc}} + p_{00}. \tag{5.38}$$

The polynomial (5.38) only uses F_{fc} as its independent variable instead of both F_{fc} and v_{avg}. This was found to return adequate accuracy because in the discrete $\frac{F_{\text{fc},j}}{\eta_{\text{fc}}(F_{\text{fc},j}v_{\text{avg},j})}$, v_{avg} only plays a minor role in the denominator, whereas F_{fc} plays a major role in both the numerator and denominator. Figure 5.4 shows actual values against the approximated polynomial. Figure 5.5 shows that the polynomial's approximation error is primarily less than 10%.

To conclude, the following is to replace (BJN.1)

$$\sum_{j\in\mathcal{S}} q_{\text{fc}}(F_{\text{fc},j}) \times \text{LHV} \times \Delta_{\text{s},j} + \sum_{k\in\mathcal{T}} q_{\text{fc}}(P_{\text{fc},k}) \times \text{LHV} \times \delta_{\text{t},k}. \tag{5.39}$$

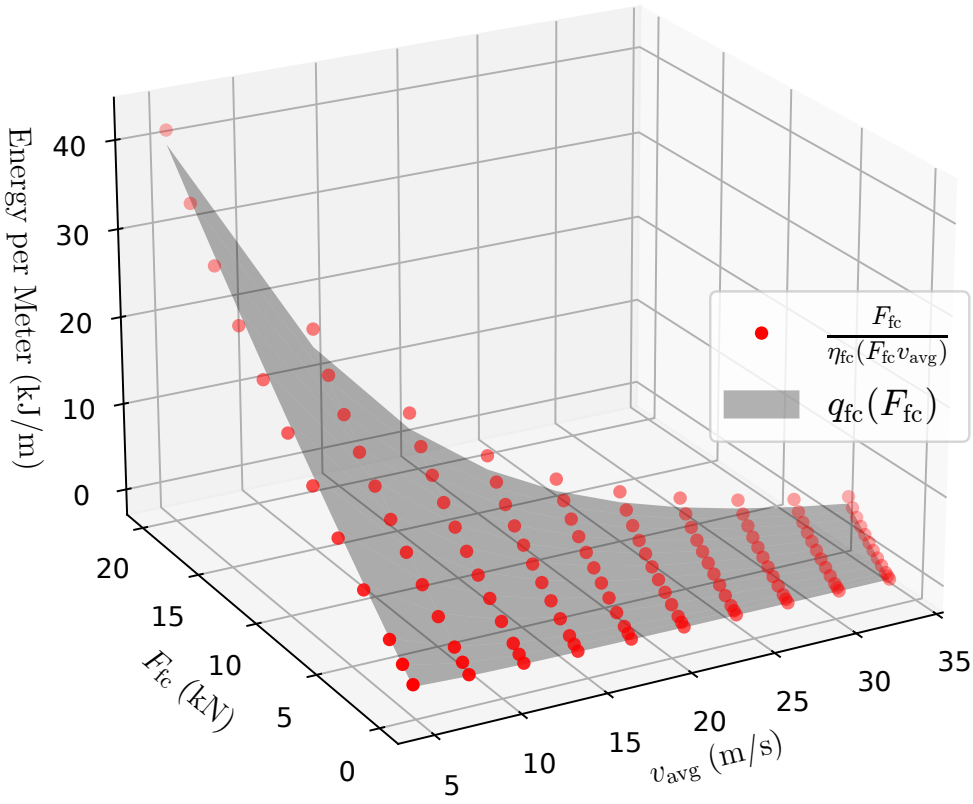

Figure 5.4: Plot of fuel cell polynomial $q_{\text{fc}}(F_{\text{fc}})$ and discrete values $\frac{F_{\text{fc}}}{\eta_{\text{fc}}(F_{\text{fc}}v_{\text{avg}})}$.

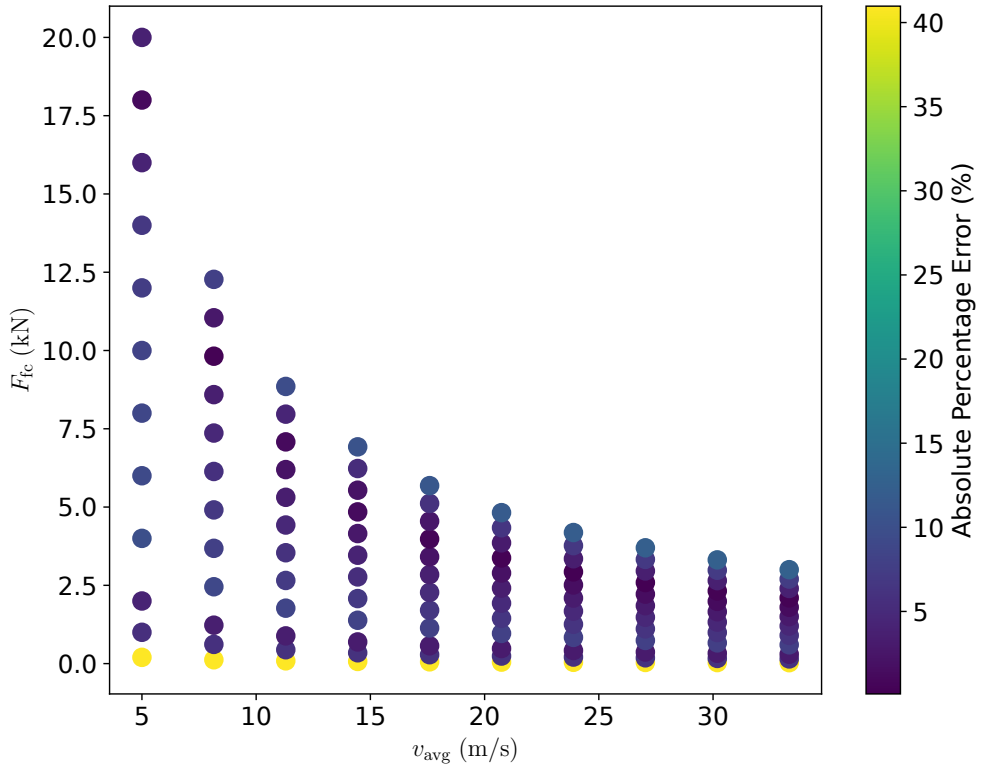

Figure 5.5: Absolute percentage error between the actual discrete values $\frac{F_{\text{fc}}}{\eta_{\text{fc}}(F_{\text{fc}}v_{\text{avg}})}$ and the approximated polynomial $q_{\text{fc}}(F_{\text{fc}})$ across the operation domain.

Note that the notation q_{fc} has been overloaded, where (5.13) is $q_{\text{fc}}(P_{\text{fc}})$ and (5.38) is $q_{\text{fc}}(F_{\text{fc}})$. These polynomials are not to be mistaken for each other, as they use different variables and coefficients.

Convexifying (BJN.5)

The battery constraint (BJN.5) should be coupled with (5.25) for instances in $\mathcal{S}$. This is done by transforming the battery power $P_{\text{bat},j}$ into the analogous battery force $F_{\text{bat},j}$ for all $j \in \mathcal{S}$. This transformation will also facilitate convexifying (BJN.5) as has resulted previously for motor constraint (BJN.12) and fuel cell penalty (BJN.1).

Start by multiplying (BJN.5) by the variable $\delta_{\text{t},j}$ (not its definition yet)

$$\omega^2 \frac{\delta_{\zeta,j}^2}{\delta_{\text{t},j}} - 2U_{\text{oc}}\omega\delta_{\zeta,j} \leq -4R_{\text{bat}}P_{\text{bat},j}\delta_{\text{t},j}, \tag{5.40}$$

now replace $\frac{\delta_{\zeta,j}^2}{\delta_{\mathrm{t},j}}$ (most left term of the inequality) by the surrogate variable $\lambda_{\zeta,j}$

$$\omega^2\lambda_{\zeta,j} - 2U_{\mathrm{oc}}\omega\delta_{\zeta,j} \leq -4R_{\mathrm{bat}}P_{\mathrm{bat},j}\delta_{\mathrm{t},j}, \tag{5.41}$$

substitute the definition $\delta_{\mathrm{t},j} = \frac{\Delta_{\mathrm{s},j}}{v_{\mathrm{avg},j}}$

$$\omega^2\lambda_{\zeta,j} - 2U_{\mathrm{oc}}\omega\delta_{\zeta,j} \leq -4R_{\mathrm{bat}}P_{\mathrm{bat},j}\frac{\Delta_{\mathrm{s},j}}{v_{\mathrm{avg},j}}, \tag{5.42}$$

introduce the analogous battery force $F_{\mathrm{bat},j}$ in place of $\frac{P_{\mathrm{bat},j}}{v_{\mathrm{avg},j}}$, defined in (5.24),

$$\omega^2\lambda_{\zeta,j} - 2U_{\mathrm{oc}}\omega\delta_{\zeta,j} \leq -4R_{\mathrm{bat}}F_{\mathrm{bat},j}\Delta_{\mathrm{s},j}, \tag{5.43}$$

the inequality is now linear and thus swapping the inequality sign with an equality sign would return the convex set

$$\omega^2\lambda_{\zeta,j} - 2U_{\mathrm{oc}}\omega\delta_{\zeta,j} = -4R_{\mathrm{bat}}F_{\mathrm{bat},j}\Delta_{\mathrm{s},j}. \tag{5.44}$$

Note that the tightening operation that returned (5.44) does not alter the optimal solution because it is merely undoing the relaxation introduced back in (5.14).

Now that (5.44) is linear, we return our attention to the newly introduced surrogate variable

$$\lambda_{\zeta,j} = \frac{\delta_{\zeta,j}^2}{\delta_{\mathrm{t},j}} \tag{5.45}$$

Using the surrogate variable $\lambda_{\zeta,j}$ requires the equality constraint (5.45), which is non-convex because it non-linearly divides optimised variables. However, it can be convexified by relaxing it and rearranging it into the form of the second-order cone constraint (3.24)

$$\delta_{\zeta,j}^2 \leq \delta_{\mathrm{t},j}\lambda_{\zeta,j} \tag{5.46}$$

This second-order cone constraint is convex if $\delta_{\mathrm{t},j}$ and $\lambda_{\zeta,j}$ are non-negative. This is true because time $\delta_{\mathrm{t},j}$ is naturally non-negative.

The relaxation between (5.45) and (5.46) will not alter the optimal solution. This is easiest to prove by observing a relaxed variant of (5.45) without altering its form,

$$\lambda_{\zeta,j} \geq \frac{\delta_{\zeta,j}^2}{\delta_{\mathrm{t},j}}, \tag{5.47}$$

now observe that the right-hand side in (5.41) pushes down on the left-handside just as was proven previously for (5.19). Since $\lambda_{\zeta,j}$ is on the left-hand side of (5.41), it will therefore push down and tighten its relaxed definition (5.47). By equivalence, the second-order cone constraint (5.46) will also tighten and hold with equality at the optimal solution.

To conclude, (BJN.5) will be convexified for $\mathcal{S}$ by replacing it with the linear equality (5.44) and the second-order cone inequality (5.46).

Adapting Fuel Cell and Battery Bounds

The analogous force variables for the fuel cell F_{fc} and the battery F_{bat} are not directly compatible with the power bounds (BJN.8) and (BJN.7), because they were originally written for the power variables P_{fc} and P_{bat}.

To work around this non-compatibility, start by replacing the power variable by the definition of analogous force, defined in (5.24),

$$\underline{P} \leq F_x v_{\mathrm{avg}} \leq \overline{P} \tag{5.48}$$

then clear F_x on its own by dividing over v_{avg}

$$\frac{\underline{P}}{v_{\mathrm{avg}}} \leq F_x \leq \frac{\overline{P}}{v_{\mathrm{avg}}} \tag{5.49}$$

and replace $\frac{1}{v_{\text{avg}}}$ by the already defined surrogate variable λ_v to produce the linear bounds

$$\underline{P}\lambda_v \leq F_x \leq \overline{P}\lambda_v \tag{5.50}$$

Using this process, for $j \in \mathcal{S}$, (BJN.7) becomes

$$\underline{P_{\text{fc}}}\lambda_v \leq F_{\text{fc},j} \leq \overline{P_{\text{fc}}}\lambda_v, \tag{5.51}$$

and (BJN.8) becomes

$$\underline{P_{\text{bat}}}\lambda_v \leq F_{\text{bat},j} \leq \overline{P_{\text{bat}}}\lambda_v. \tag{5.52}$$

5.3.3 Convex Joint Speed-EMS Formulation

The new formulation (CJN) convexifies (BJN) by implementing the changes proposed in Section (5.3.2). The new label of (CJN) refers to "Convex Joint". The changes are:

- the objective function was split to convexify the $\mathcal{S}$ penalty by introducing a new polynomial $q_{\text{fc}}(F_{\text{fc}})$. This is different to the $\mathcal{T}$ penalty which is $q_{\text{fc}}(P_{\text{fc}})$.
- the work equality (CJN.20) introduces the new analogous variables $F_{\text{m}},\ F_{\text{fc}},$ and F_{bat}. These are bounded in (CJN.29) and (CJN.30). A bound on the analogous F_{m} is not required because it is already lower bounded by mechanical traction F_{trc} in (CJN.23) which in turn is lower bounded in (CJN.26) and (CJN.27). The equivalent power equality for $\mathcal{T}$, (CJN.6), remains unchanged.
- the change in state-of-charge for $\mathcal{S}$ is modelled by the linear (CJN.21) and convex second-order cone (CJN.24). The equivalent model for $\mathcal{T}$, (CJN.7), remains unchanged.

Table 5.1: The variables optimised for $\mathcal{S}$ and $\mathcal{T}$ in (CJN). ① speed is set to zero because train remains stationary for $\mathcal{T}$. ② given as Δ_{t} for $\mathcal{T}$.

	$\boldsymbol{F}_{\mathrm{trc}}$	$\boldsymbol{F}_{\mathrm{brk}}$	$\boldsymbol{v}$	$\boldsymbol{v}_{\mathrm{avg}}$	$\boldsymbol{\delta}_{\mathrm{t}}$	$\boldsymbol{z}$	$\boldsymbol{\lambda}_{\mathrm{v}}$	$\boldsymbol{P}_{\mathrm{fc}}$	$\boldsymbol{P}_{\mathrm{bat}}$	$\boldsymbol{\zeta}$	$\boldsymbol{\delta}_{\boldsymbol{\zeta}}$	$\boldsymbol{F}_{\mathrm{m}}$	$\boldsymbol{F}_{\mathrm{fc}}$	$\boldsymbol{F}_{\mathrm{bat}}$	$\boldsymbol{\lambda}_{\boldsymbol{\zeta}}$
$\mathcal{S}$	✓	✓	✓	✓	✓	✓	✓	-	-	✓	✓	✓	✓	✓	✓
$\mathcal{T}$	-	-	①	-	②	①	-	✓	✓	✓	✓	-	-	-	-

Seamless State Transition

Table 5.1 lists all of the variables optimised in (CJN) and whether each is defined for $\mathcal{S}$ or $\mathcal{T}$. This depiction will help explain the seamless state transition between modelling domains. Recall that this transition is vital to using hybrid modelling, where both spatial and temporal domains are used, discussed previously in Section 4.1.1.

In the joint problem setting, state is defined as the tuple (v, z, ζ) which is defined for both $\mathcal{S}$ and $\mathcal{T}$ according to Tab. 5.1. This means that state (v_i, z_i, ζ_i) for $i \in \mathcal{B}$ will seamlessly transfer to the next state $(v_{i+1}, z_{i+1}, \zeta_{i+1})$ for $i+1 \in \mathcal{B}$, regardless of the domain that was assigned to i and $i+1$. Moreover, so long the state is defined, this transition will occur seamlessly regardless of the underlying state evolution model. For example, the state ζ will seamlessly transition between instances, regardless of whether the state evolution δ_ζ was computed using (CJN.7) for $\mathcal{T}$ or (CJN.21) for $\mathcal{S}$. The same applies to train speed v and z.

Solution Optimality and Polynomial Approximation

The optimality of (CJN) is dependent on the approximation accuracy of the used polynomials. To this end, the error rates were shown to be largely less than 10% in Fig. 5.3 and Fig. 5.5.

Solution Optimality and Constraint Relaxation

For (CJN) to find the real global optimal solution, the relaxed constraints ought to hold at equality at the obtained solution.

(CJN) inherits three constraint relaxations from previous formulations, namely (CJN.13) and (CJN.22) from (CSP) and (CJN.7) from (CEM). No changes have occurred to the incentives that push these inequalities to hold at equality: they collectively rely on minimising fuel consumption, conserving battery charge, and completing the journey by a target time.

Two new relaxations have been introduced into (CJN), namely (CJN.23) and (CJN.24). The optimal solution will tighten these relaxed inequalities to hold with equality. The following elaborates on this

1. (CJN.23) holds with equality because $F_{\mathrm{m},j}$ pushes down on $F_{\mathrm{trc},j}$ to reduce its demand on the fuel cell and battery in (CJN.20) to conserve fuel. In return, $F_{\mathrm{trc},j}$ will push up on $F_{\mathrm{m},j}$ to accelerate the train in (CJN.17) and achieve the timing points constraints (CJN.31).

2. Section 5.3.2 explains why (CJN.24) holds at equality. This is not repeated here for brevity.

As such, the hypothesis HA1 has been proven.

$$\min_{\substack{\boldsymbol{F}_{\mathrm{trc}},\,\boldsymbol{F}_{\mathrm{brk}},\,\boldsymbol{v},\,\boldsymbol{v}_{\mathrm{avg}},\,\boldsymbol{\delta}_{\mathrm{t}},\,\boldsymbol{z},\,\boldsymbol{\lambda}_{v}\\ \boldsymbol{P}_{\mathrm{fc}},\,\boldsymbol{P}_{\mathrm{bat}},\,\boldsymbol{\zeta},\,\boldsymbol{\delta}_{\zeta}\\ \boldsymbol{F}_{\mathrm{m}},\,\boldsymbol{F}_{\mathrm{fc}},\,\boldsymbol{F}_{\mathrm{bat}},\,\boldsymbol{\lambda}_{\zeta}}} \begin{array}{l}\sum_{j\in\mathcal{S}}\, q_{\mathrm{fc}}(F_{\mathrm{fc},j})\times\mathrm{LHV}\times\Delta_{\mathrm{s},j}\ +\\ \sum_{k\in\mathcal{T}}\, q_{\mathrm{fc}}(P_{\mathrm{fc},k})\times\mathrm{LHV}\times\delta_{\mathrm{t},k}\end{array} \tag{CJN.1}$$

subject to

given as parameters

$$\Delta_{\mathrm{s},j} \quad \forall j\in\mathcal{S} \tag{CJN.2}$$

$$\Delta_{\mathrm{t},k} \quad \forall k\in\mathcal{T} \tag{CJN.3}$$

$$P_{\mathrm{aux},i} \quad \forall i\in\mathcal{B} \tag{CJN.4}$$

$\forall k\in\mathcal{T}$

$$\delta_{\mathrm{t},k} = \Delta_{\mathrm{t},k} \tag{CJN.5}$$

$$P_{\mathrm{aux},k} = P_{\mathrm{fc},k} + P_{\mathrm{bat},k} \tag{CJN.6}$$

$$\omega^2\frac{\delta_{\zeta,k}^2}{\delta_{\mathrm{t},k}^2} - 2U_{\mathrm{oc}}\omega\frac{\delta_{\zeta,k}}{\delta_{\mathrm{t},k}} \le -4R_{\mathrm{bat}}P_{\mathrm{bat},k} \tag{CJN.7}$$

$$\underline{P_{\mathrm{fc}}} \le P_{\mathrm{fc},k} \le \overline{P_{\mathrm{fc}}} \tag{CJN.8}$$

$$\underline{P_{\mathrm{bat}}} \le P_{\mathrm{bat},k} \le \overline{P_{\mathrm{bat}}} \tag{CJN.9}$$

$\forall i\in\mathcal{B}$

$$\zeta_{i+1} = \zeta_i - \Delta_{\zeta,i} \tag{CJN.10}$$

$\forall l\in\mathcal{V}^0$

$$v_l = 0 \tag{CJN.11}$$

$$z_l = 0 \tag{CJN.12}$$

$\forall n\in\mathcal{A}$

$$v_n^2 \le z_n \tag{CJN.13}$$

$$0 \le v_n \le \overline{v_n} \tag{CJN.14}$$

$$0 \le z_n \le \overline{z_n} \tag{CJN.15}$$

$$\underline{\zeta} \le \zeta_{\mathrm{n}} \le \overline{\zeta} \tag{CJN.16}$$

$\forall j\in\mathcal{S}$

$$(5.4) \tag{CJN.17}$$

$$v_{\mathrm{avg},j} = \frac{v_j + v_{j+1}}{2} \tag{CJN.18}$$

$$\delta_{\mathrm{t},j} = \Delta_{\mathrm{s}}\lambda_{v,j} \tag{CJN.19}$$

$$F_{\mathrm{m},j}\Delta_{\mathrm{s},j} + P_{\mathrm{aux},j}\delta_{\mathrm{t},j} = F_{\mathrm{fc},j}\Delta_{\mathrm{s},j} + F_{\mathrm{bat},j}\Delta_{\mathrm{s},j} \tag{CJN.20}$$

$$\omega^2\lambda_{\zeta,j} - 2U_{\mathrm{oc}}\omega\delta_{\zeta,j} = -4R_{\mathrm{bat}}F_{\mathrm{bat},j}\Delta_{\mathrm{s},j} \tag{CJN.21}$$

$$1 \le v_{\mathrm{avg},j}\lambda_{v,j} \tag{CJN.22}$$

$$q_{\mathrm{m}}(F_{\mathrm{trc},j}) \le F_{\mathrm{m},j} \tag{CJN.23}$$

$$\delta_{\zeta,j}^2 \le \delta_{\mathrm{t},j}\lambda_{\zeta,j} \tag{CJN.24}$$

$$0 \le \lambda_{v,j},\ \lambda_{\zeta,j} \tag{CJN.25}$$

$$\underline{F_{\mathrm{trc}}} \le F_{\mathrm{trc},j} \le \overline{F_{\mathrm{trc}}} \tag{CJN.26}$$

$$\underline{P_{\mathrm{trc}}}\lambda_{v,j} \le F_{\mathrm{trc},j} \le \overline{P_{\mathrm{trc}}}\lambda_{v,j} \tag{CJN.27}$$

$$\underline{F_{\mathrm{brk}}} \le F_{\mathrm{brk},j} \le 0 \tag{CJN.28}$$

$$\underline{P_{\mathrm{fc}}}\lambda_{v,j} \le F_{\mathrm{fc},j} \le \overline{P_{\mathrm{fc}}}\lambda_{v,j} \tag{CJN.29}$$

$$\underline{P_{\mathrm{bat}}}\lambda_{v,j} \le F_{\mathrm{bat},j} \le \overline{P_{\mathrm{bat}}}\lambda_{v,j} \tag{CJN.30}$$

$\forall m\in\mathcal{M}$

$$t(m) = \tau_m \tag{CJN.31}$$

other

$$\zeta_{\mathrm{N}} = \zeta_0 \tag{CJN.32}$$

Optimisation Problem 6: Convex Joint (CJN)

5.4 Joint Speed, EMS and Timetable Optimisation

This section presents a formulation to jointly optimise speed-EMS-timetable for a single train. The motive to include timetable optimisation is to fully leverage the dynamic interaction between the timetable and the hybrid powertrain. The formulation optimises running time between stations given a fixed total journey time.

Observe from (CJN) that the duration constraint (CJN.31) is constraining the intermediate stations $\{m \in \mathcal{M} | m < N\}$. Therefore, dropping these intermediate station constraints returns a single constraint on total journey time $t(N) = \tau_N$. The resulting formulation is shown in (CTT). This new formulation maintains the incentive to tighten the previously relaxed constraints. This is because the duration constraint (CTT.31) still maintains incentive to "move" the train up until the terminal instance N which is adequate. As such, the hypothesis HA2 has been proven.

$$\min_{\substack{\boldsymbol{F}_{\mathrm{trc}},\,\boldsymbol{F}_{\mathrm{brk}},\,\boldsymbol{v},\,\boldsymbol{v}_{\mathrm{avg}},\,\boldsymbol{\delta}_{\mathrm{t}},\,\boldsymbol{z},\,\boldsymbol{\lambda}_{v}\\ \boldsymbol{P}_{\mathrm{fc}},\,\boldsymbol{P}_{\mathrm{bat}},\,\boldsymbol{\zeta},\,\boldsymbol{\delta}_{\zeta}\\ \boldsymbol{F}_{\mathrm{m}},\,\boldsymbol{F}_{\mathrm{fc}},\,\boldsymbol{F}_{\mathrm{bat}},\,\boldsymbol{\lambda}_{\zeta}}} \begin{array}{l}\sum_{j\in\mathcal{S}}\, q_{\mathrm{fc}}(F_{\mathrm{fc},j})\times\mathrm{LHV}\times\Delta_{\mathrm{s},j}\ +\\ \sum_{k\in\mathcal{T}}\, q_{\mathrm{fc}}(P_{\mathrm{fc},k})\times\mathrm{LHV}\times\delta_{\mathrm{t},k}\end{array} \tag{CTT.1}$$

subject to

given as parameters

$$\Delta_{\mathrm{s},j} \quad \forall j\in\mathcal{S} \tag{CTT.2}$$

$$\Delta_{\mathrm{t},k} \quad \forall k\in\mathcal{T} \tag{CTT.3}$$

$$P_{\mathrm{aux},i} \quad \forall i\in\mathcal{B} \tag{CTT.4}$$

$\forall k\in\mathcal{T}$

$$\delta_{\mathrm{t},k} = \Delta_{\mathrm{t},k} \tag{CTT.5}$$

$$P_{\mathrm{aux},k} = P_{\mathrm{fc},k} + P_{\mathrm{bat},k} \tag{CTT.6}$$

$$\omega^2\frac{\delta_{\zeta,k}^2}{\delta_{\mathrm{t},k}^2} - 2U_{\mathrm{oc}}\omega\frac{\delta_{\zeta,k}}{\delta_{\mathrm{t},k}} \le -4R_{\mathrm{bat}}P_{\mathrm{bat},k} \tag{CTT.7}$$

$$\underline{P_{\mathrm{fc}}} \le P_{\mathrm{fc},k} \le \overline{P_{\mathrm{fc}}} \tag{CTT.8}$$

$$\underline{P_{\mathrm{bat}}} \le P_{\mathrm{bat},k} \le \overline{P_{\mathrm{bat}}} \tag{CTT.9}$$

$\forall i\in\mathcal{B}$

$$\zeta_{i+1} = \zeta_i - \Delta_{\zeta,i} \tag{CTT.10}$$

$\forall l\in\mathcal{V}^0$

$$v_l = 0 \tag{CTT.11}$$

$$z_l = 0 \tag{CTT.12}$$

$\forall n\in\mathcal{A}$

$$v_n^2 \le z_n \tag{CTT.13}$$

$$0 \le v_n \le \overline{v_n} \tag{CTT.14}$$

$$0 \le z_n \le \overline{z_n} \tag{CTT.15}$$

$$\underline{\zeta} \le \zeta_{\mathrm{n}} \le \overline{\zeta} \tag{CTT.16}$$

$\forall j\in\mathcal{S}$

$$(5.4) \tag{CTT.17}$$

$$v_{\mathrm{avg},j} = \frac{v_j + v_{j+1}}{2} \tag{CTT.18}$$

$$\delta_{\mathrm{t},j} = \Delta_{\mathrm{s}}\lambda_{v,j} \tag{CTT.19}$$

$$F_{\mathrm{m},j}\Delta_{\mathrm{s},j} + P_{\mathrm{aux},j}\delta_{\mathrm{t},j} = F_{\mathrm{fc},j}\Delta_{\mathrm{s},j} + F_{\mathrm{bat},j}\Delta_{\mathrm{s},j} \tag{CTT.20}$$

$$\omega^2\lambda_{\zeta,j} - 2U_{\mathrm{oc}}\omega\delta_{\zeta,j} = -4R_{\mathrm{bat}}F_{\mathrm{bat},j}\Delta_{\mathrm{s},j} \tag{CTT.21}$$

$$1 \le v_{\mathrm{avg},j}\lambda_{v,j} \tag{CTT.22}$$

$$q_{\mathrm{m}}(F_{\mathrm{trc},j}) \le F_{\mathrm{m},j} \tag{CTT.23}$$

$$\delta_{\zeta,j}^2 \le \delta_{\mathrm{t},j}\lambda_{\zeta,j} \tag{CTT.24}$$

$$0 \le \lambda_{v,j},\ \lambda_{\zeta,j} \tag{CTT.25}$$

$$\underline{F_{\mathrm{trc}}} \le F_{\mathrm{trc},j} \le \overline{F_{\mathrm{trc}}} \tag{CTT.26}$$

$$\underline{P_{\mathrm{trc}}}\lambda_{v,j} \le F_{\mathrm{trc},j} \le \overline{P_{\mathrm{trc}}}\lambda_{v,j} \tag{CTT.27}$$

$$\underline{F_{\mathrm{brk}}} \le F_{\mathrm{brk},j} \le 0 \tag{CTT.28}$$

$$\underline{P_{\mathrm{fc}}}\lambda_{v,j} \le F_{\mathrm{fc},j} \le \overline{P_{\mathrm{fc}}}\lambda_{v,j} \tag{CTT.29}$$

$$\underline{P_{\mathrm{bat}}}\lambda_{v,j} \le F_{\mathrm{bat},j} \le \overline{P_{\mathrm{bat}}}\lambda_{v,j} \tag{CTT.30}$$

only$N$

$$t(N) = \tau_N \tag{CTT.31}$$

other

$$\zeta_{\mathrm{N}} = \zeta_0 \tag{CTT.32}$$

Optimisation Problem 7: Convex Joint Speed-EMS-Timetable (CTT)

6 SIMULATION RESULTS

This chapter presents a series of simulation results to compare and asses the optimised performance. These will be used to prove the operational hypotheses.

To start, Section 6.1 describes the case study used throughout this chapter and Section 6.2 defines metrics that will be used to compare outcomes. Section 6.3 compares conventional ecodriving that emphasises coasting to jointly optimising speed and EMS. Section 6.4 explores the impact of adding measures against degradation on fuel consumption. Section 6.5 compares following a given timetable to jointly optimising speed-EMS-timetable. Section 6.6 presents results for optimising both timetable running time and total journey time. Lastly, Section 6.7 presents numerical results to verify various aspects of the optimisation, such as polynomial accuracy and constraint relaxation.

6.1 Case Study

The rail line simulated is the 63-km-long Tees Valley Line which runs between Saltburn and Bishop Auckland in northern England, shown in Fig. 6.1. This line is currently operated by the train operating company Northern. This case study was chosen because Northern published a series of reports regarding converting this line from a diesel service to a hydrogen service [324, 325].

To serve the Tees Valley Line, the train manufacturer Alstom proposed retrofitting a fuel cell hybrid powertrain into an existing Class 321. Due to the lack of public data about Alstom's offering, the train parameters chosen are partially similar to the HydroFLEX which is based on the Class 319 [326]. These can be found in Appendix A.

The case study is optimised with $\Delta_s = 10$. The dwell times and working timetable can be found in Appendix B. To ensure a fair comparison, all simulations were subject to the same charge-sustaining constraint, where the initial and terminal state-of-charge was

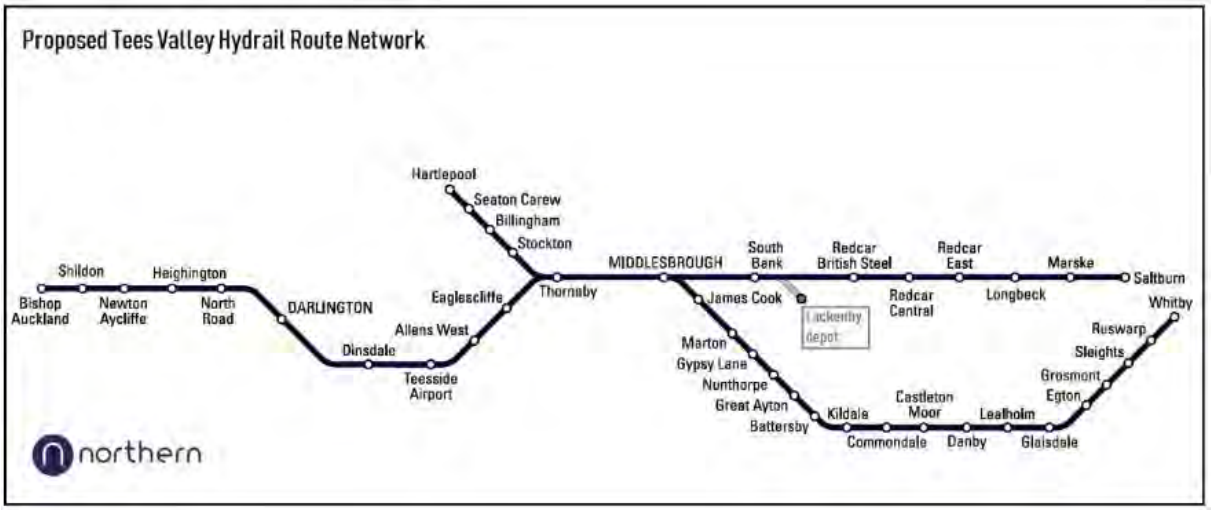

Figure 6.1: Tees Valley Line. Reprinted from [325].

similarly set to 50%. The solver used is the Gurobi barrier algorithm [327].

6.2 Comparison Metrics

This section introduces metrics that will be used to compare between operating strategies. These metrics are produced after optimisation and simulation. Therefore, computational complexity is of no concern and are thus derived using the original non-convex models of Chapter 4. Note that the small symbol Σ is used as a prefix to signify that a metrics is a sum over the journey. This is not to be confused for the mathematical summation operation that is assigned the bigger symbol $\sum$.

Fuel Consumption

Based on (4.24), denote a journey's total hydrogen consumption by

$$\Sigma \mathrm{H}_2 := \sum_{i \in \mathcal{B}} \frac{P_{\mathrm{fc},i}}{\eta_{\mathrm{fc}}(P_{\mathrm{fc},i})} \times \mathrm{LHV} \times \delta_{\mathrm{t},i}. \tag{6.1}$$

Since efficiency η_{fc} is in the form of a discrete lookup table (see Fig. 4.4), linear interpolation is used to fetch values that fall between the defined efficiency values.

Traction Work

Denote total positive traction work for a journey

$$\Sigma W^{+}_{\mathrm{trc}} := \sum_{j \in \mathcal{S}} F^{+}_{\mathrm{trc},j} \Delta_{\mathrm{s},j}, \tag{6.2}$$

and total negative traction work

$$\Sigma W^{-}_{\mathrm{trc}} := \sum_{j \in \mathcal{S}} F^{-}_{\mathrm{trc},j} \Delta_{\mathrm{s},j}, \tag{6.3}$$

where

$$F^{+}_{\mathrm{trc},j} := \begin{cases} F_{\mathrm{trc},j} & F_{\mathrm{trc},j} \geq 0 \\ 0 & F_{\mathrm{trc},j} < 0 \end{cases} \tag{6.4}$$

and

$$F^{-}_{\mathrm{trc},j} := \begin{cases} 0 & F_{\mathrm{trc},j} \geq 0 \\ F_{\mathrm{trc},j} & F_{\mathrm{trc},j} < 0 \end{cases} \tag{6.5}$$

Mechanical Braking Work

Denote total mechanical braking work for a journey

$$\Sigma W_{\mathrm{brk}} := \sum_{j \in \mathcal{S}} F_{\mathrm{brk},j} \Delta_{\mathrm{s},j}. \tag{6.6}$$

Battery Charge-Throughput

Based on (2.1) and (4.31), denote the total battery charge-throughput for a journey

$$\Sigma Q_{\mathrm{bat}} := \sum_{i \in \mathcal{B}} |I_{\mathrm{bat},i}| \delta_{\mathrm{t},i}, \tag{6.7}$$

which according to Section 2.1.4 is the main driver behind cyclic battery degradation. The resulting unit is Coulombs.

Fuel Cell Load-Cycling

Based on Equation 13 in [33], denote fuel cell degradation due to load-cycling over a journey by

$$\Sigma D_{\mathrm{fc}} := \sum_{i \in \mathcal{B}} \alpha \frac{|P_{\mathrm{fc},i+1} - P_{\mathrm{fc},i}|}{\delta_{\mathrm{t},i}}, \tag{6.8}$$

where α is the load-cycling degradation factor. The unit of α is $\mu\mathrm{V} \cdot \mathrm{kW}^{-1}$. Since the expression is linear, an accurate value for α is not required for qualitative comparison. We assume the same value from [33] (α =0.041 $\mu\mathrm{V} \cdot \mathrm{kW}^{-1}$). The degradation measure (6.8) represents drop in stack voltage; therefore, higher values represent more degradation. Recall from Fig. 2.4 how stack voltage drops with ageing.

6.3 Conventional Ecodriving vs. Joint Optimisation

This section compares conventional ecodriving that emphasises coasting to joint speed-EMS optimisation. The former is achieved by first optimising speed according to (CSP) then optimising the EMS using (CEM). The former is achieved using (CJN). The purpose of this comparison is to prove hypothesis HO1.

Table 6.1 shows the resulting metrics according to those defined in Section 6.2. It shows that the joint method consumed 15.1% less fuel than the conventional method, despite consuming 15.8% more positive traction. This is because the joint method relied 87.5% less on wasteful mechanical braking and relied 342% more on regenerative braking (negative traction). Therefore, the joint method offset its higher positive traction figure by bigger regenerative braking returns.

Table 6.1: Simulation metrics for conventional ecodriving and joint formulations.

	ΣH_2 (kg)	ΣW^+_{trc} (MJ)	ΣW^-_{trc} (MJ)	ΣW_{brk} (MJ)	ΣQ_{bat} (MC)	ΣD_{fc} (mV)
Conventional	20.1	677.8	72.7	161.2	1.91	0.75
Joint	17.1	785.5	321.4	20.1	1.82	0.50
Difference to conventional (%)	-15.1	+15.8	+342	-87.5	-4.2	-33.6

We examine plots of the simulation to understand how the joint method succeeded at leveraging regenerative braking to its advantage. Figure 6.2 shows a plot for the entire journey. Alternatively, Figure 6.3 shows a smaller excerpt from the journey for clarity. The P_{trc} subplot confirms that the joint method applied positive traction ($P_{trc} > 0$) for longer while departing stations. This enabled it to form a different speed profile v that was compatible with earlier and longer regenerative braking ($P_{trc} < 0$) while coming to a stop at stations. The F_{brk} subplots show that it used less wasteful mechanical braking while coming to a stop because it had already started regenerative braking earlier.

On the contrary to the joint method, the conventional method pulled back on positive traction as early as possible while departing stations. This is to commence coasting as early as possible ($P_{trc} = 0$). It delayed all forms of braking as much as possible to maximise coasting. The short braking span left towards the end forced it to supplement regenerative braking with wasteful mechanical braking.

Figure 6.4 is an alternative depiction for the explanation above. It plots the accumulative sum of the comparison metrics. The ΣW^-_{trc} subplot shows the joint method accumulating more regenerative braking energy each time it stops. The conventional method wastefully accumulates more mechanical braking work ΣW_{brk} each time it stops. The accumulative fuel subplot ΣH_2 shows how the gap in consumed fuel widens as the journey progresses.

To conclude, the results show that the joint method successfully leverages regenerative braking thereby consuming less fuel and proving hypothesis HO1. It leverages regenerative

braking more effectively because it uncovers the dynamic coupling between speed and EMS at the time of optimising them jointly. On the other hand, the conventional method uncovers the benefit of regenerative braking at the time of EMS optimisation which occurs after being given a speed profile, thus is only able to influence regenerative braking to a limited extent.

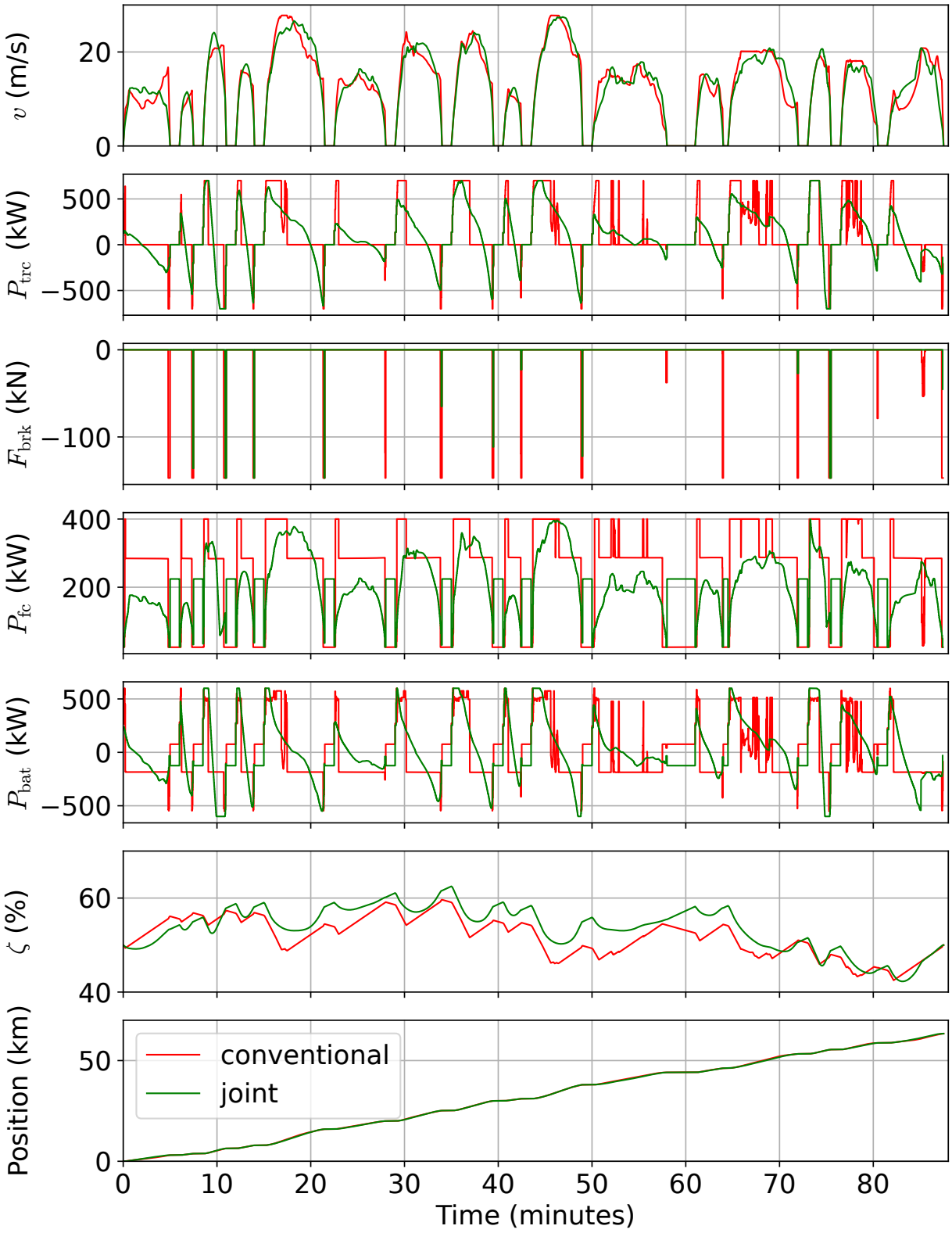

Figure 6.2: Simulation result of the entire journey for conventional ecodriving and joint formulations.

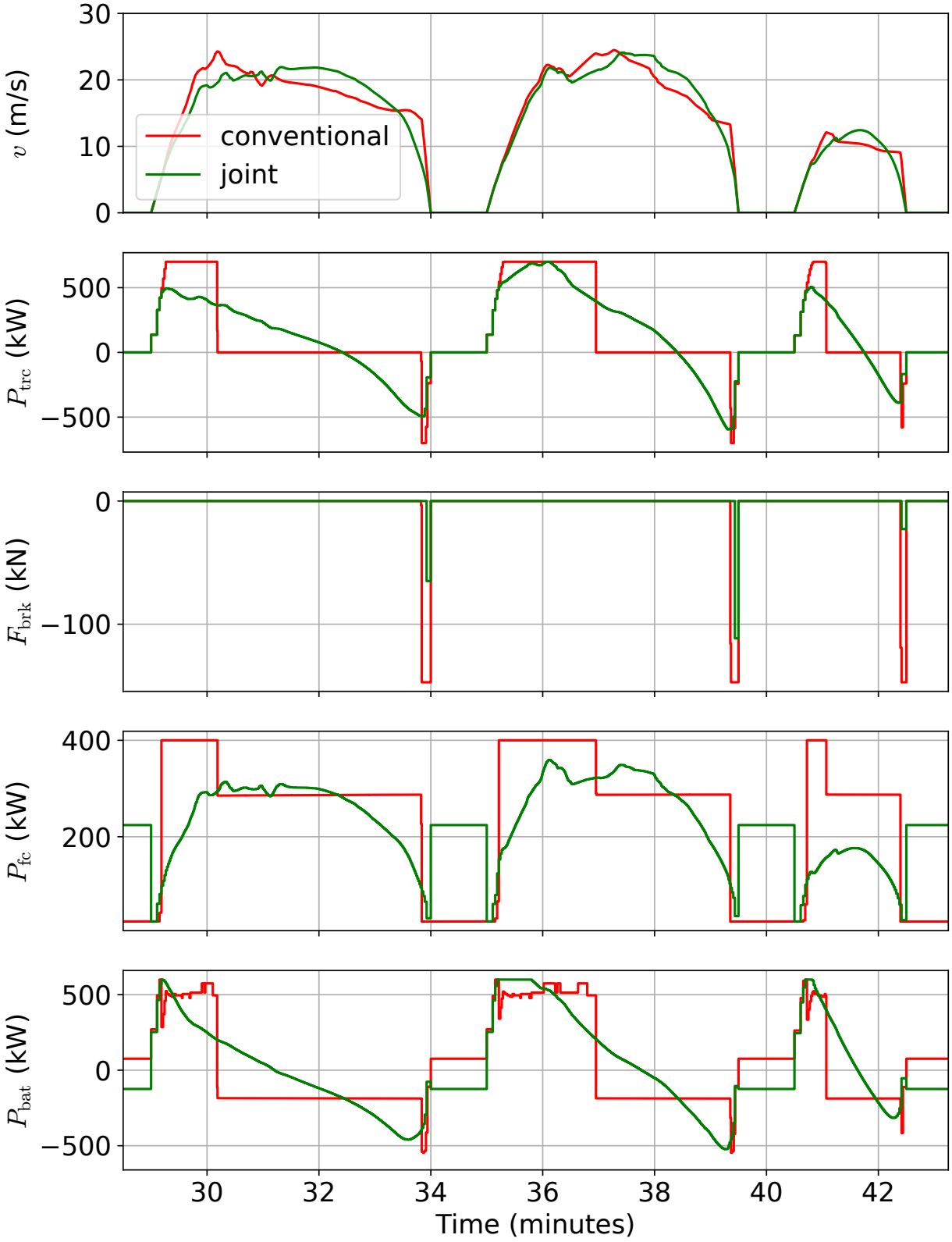

Figure 6.3: Excerpt from simulation result for conventional ecodriving and joint formulations.

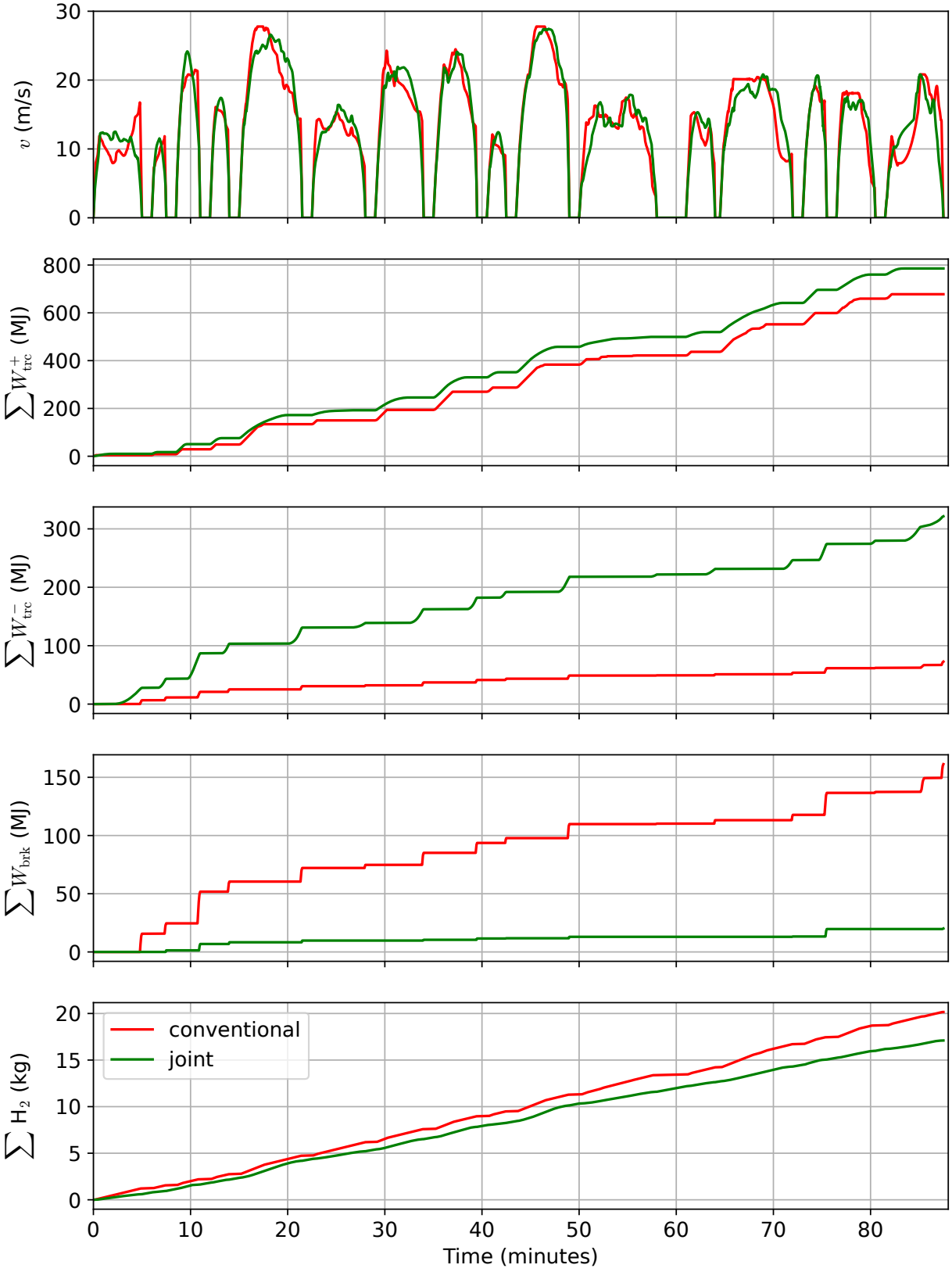

Figure 6.4: Plot of train speed and accumulative summation for conventional ecodriving and joint formulations.

6.4 Measures Against Fuel Cell Degradation

This section assesses the impact of a protective measure against fuel cell degradation on fuel consumption. The protective measure assessed is reducing harmful fuel cell load-cycling. This assessment is for the purpose of proving hypothesis HO2.

The assessment is performed on the standard joint formulation (CJN) by fixing fuel cell power during i) dwell time and ii) third of the way between each pair of consecutive stations. The remaining distance between consecutive stations is left unfixed to allow for some optimisation flexibility. Figure 6.5 shows both free and "fixed" fuel cell power profiles. The latter fluctuates a lesser number of times thereby reducing harmful load-cycling, as shown in the third subplot ΣD_{fc}.

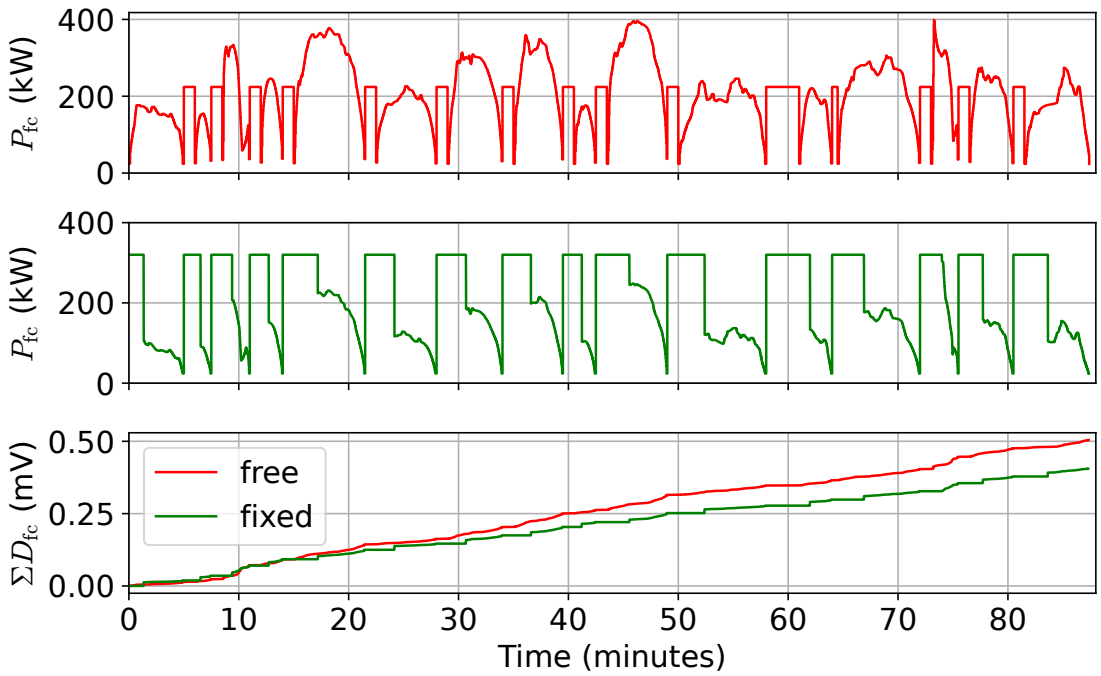

Figure 6.5: Fuel cell power and accumulative load-cycle degradation for free and fixed comparison.

Table 6.2 lists the resulting comparison metrics between free and fixed results. The fixed consumes marginally more fuel at 1.3% while load-cycling drops a substantial 19.7%. Moreover, rather unexpectedly, the battery charge-throughput dropped by 2.1% as well,

thereby alleviating some battery degradation as well. This occurred because the fixed fuel cell power output has offset some of the battery output.

Table 6.2: Simulation metrics for joint formulation with free and fixed fuel cell power.

	ΣH_2 (kg)	ΣW^+_{trc} (MJ)	ΣW^-_{trc} (MJ)	ΣW_{brk} (MJ)	ΣQ_{bat} (MC)	ΣD_{fc} (mV)
Free	17.1	785.5	321.4	20.1	1.82	0.50
Fixed	17.3	783.3	321.3	18.8	1.78	0.40
Difference to free(%)	+1.3	-0.28	-0.05	-6.1	-2.1	-19.7

Figure 6.6 plots the journey results for both free and fixed formulations. It shows that speed v, traction P_{trc}, and mechanical braking F_{brk} remained largely the same. The biggest difference is in fuel cell power P_{fc} which was imposed by fixing the power level. Battery power P_{bat} for the fixed variant has dropped in some places to offset for the fixed fuel cell power output.

To conclude, it was shown that adding protective constraints negatively affects fuel consumption thereby proving HO2. Nonetheless, the percentage reduction in harmful load-cycling was substantially bigger than increase in fuel consumption. Although the protective measure was meant for the fuel cell, the results also suggest that it might protect the traction battery from degradation as well. These encouraging results are due to the ability of the joint method to optimise all variables while simultaneously observing the fixed power constraint.

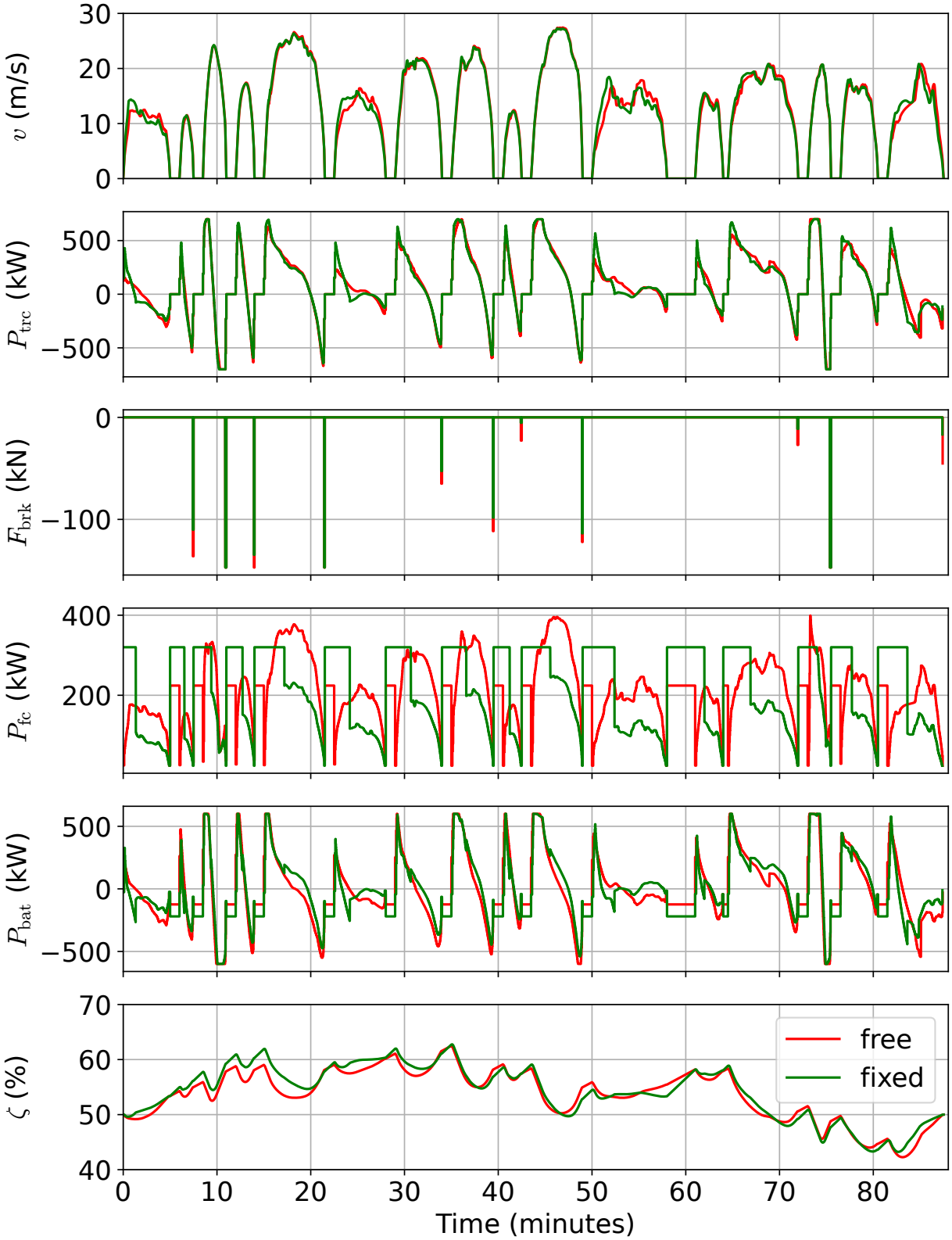

Figure 6.6: Journey simulation result for free and fixed fuel cell power.

6.5 Timetable Joint Optimisation

This section compares the joint speed-EMS (CJN) to the joint speed-EMS-timetable (CTT). In the figures, the former will be called "timetabled" referring to it being given a timetable, while the latter will be called "free" referring to it freely self-optimising its own timetable. The free formulation only follow uses the dwell time parameters from Appendix B, as it optimises its own running time between intermediate stations. Both formulations hold fuel cell power constant as in Section 6.4.

Table 6.3 lists the comparison metrics which indeed shows an improvement in all vital fronts, namely a 4.6% reduction in fuel consumption, a 12.4% reduction in battery charge-throughput, and a 3.96% reduction in the fuel cell load-cycle metric.

Figure 6.7 plots the results on the time axis. It shows that the free method indeed selects different running times than the timetable. In some cases it chooses higher speed to finish a segment quicker, and in others it goes slower and thus longer.

Figure 6.8 plots the simulation results against the space axis with x-axis being annotated by the names of the stations. Note that the results now align due to them being plotted against space.

To conclude, jointly optimising speed-EMS-timetable uncovers further dynamic interaction between station running time and the existing speed-EMS dynamics. This enables the joint method to find a more optimal solution by optimising the additional timetable variables. This proves the hypothesis HO3.

Table 6.3: Simulation metrics for joint formulation with and without intermediate timetable.

	ΣH_2 (kg)	ΣW^+_{trc} (MJ)	ΣW^-_{trc} (MJ)	ΣW_{brk} (MJ)	ΣQ_{bat} (MC)	ΣD_{fc} (mV)
timetabled	17.3	783.3	321.3	18.8	1.78	0.40
free	16.5	715.2	285.3	3.9	1.56	0.38
Difference to timetabled (%)	-4.6	-8.6	-11.1	-79.2	-12.4	-3.96

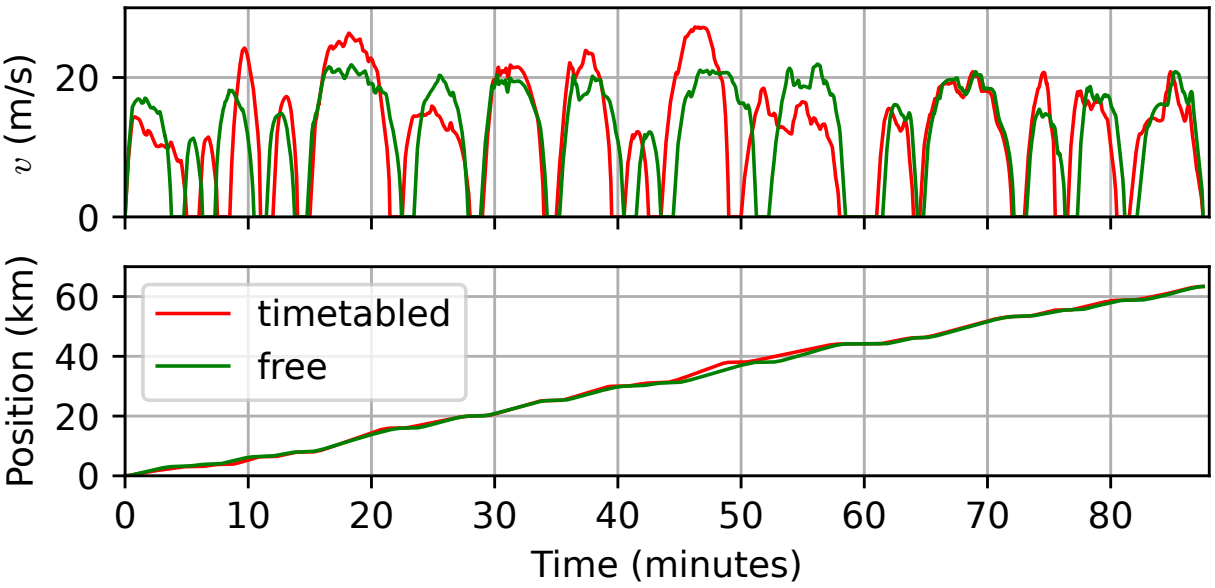

Figure 6.7: Simulation result for timetable optimisation plotted against time.

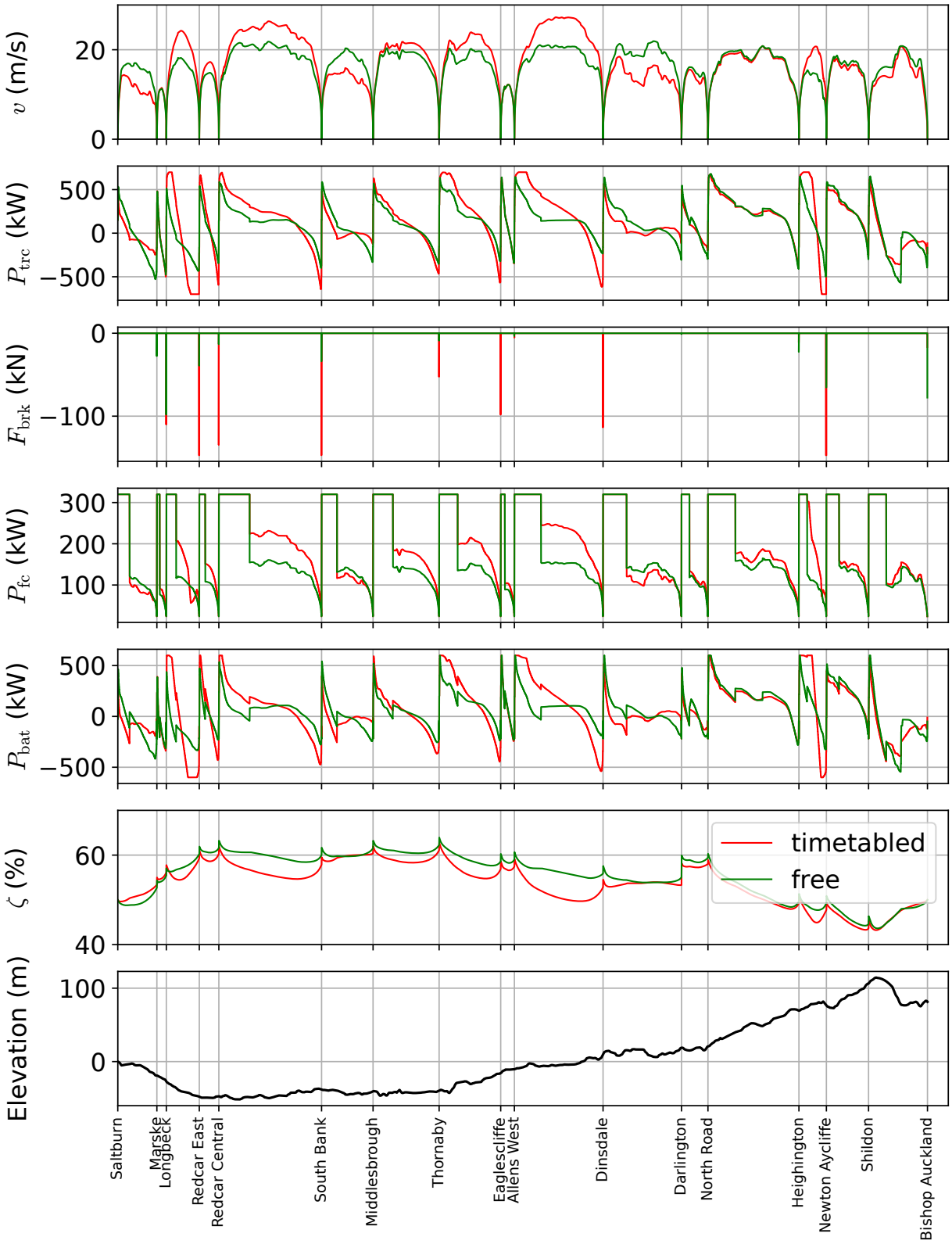

Figure 6.8: Simulation result for timetable optimisation plotted against station name (space).

6.6 Timetable Pareto Curve

Figure 6.9 depicts the Pareto curve for fuel consumption against total journey time. This was generated by optimising (CTT) with various values of the duration constraint (CTT.31) to simulate various trip times. The red star marks the optimal for speed-EMS-running time under the journey time given in the working timetable (87.5 minutes as in Appendix B). The green star marks the optimal solution when the journey time is freely optimised as well.

As journey time increases between the red and green star, fuel is saved because less traction effort is needed. However, fuel consumption climbs again past the green star. This is because traction savings are outweighed by running the train's auxiliary load for longer.

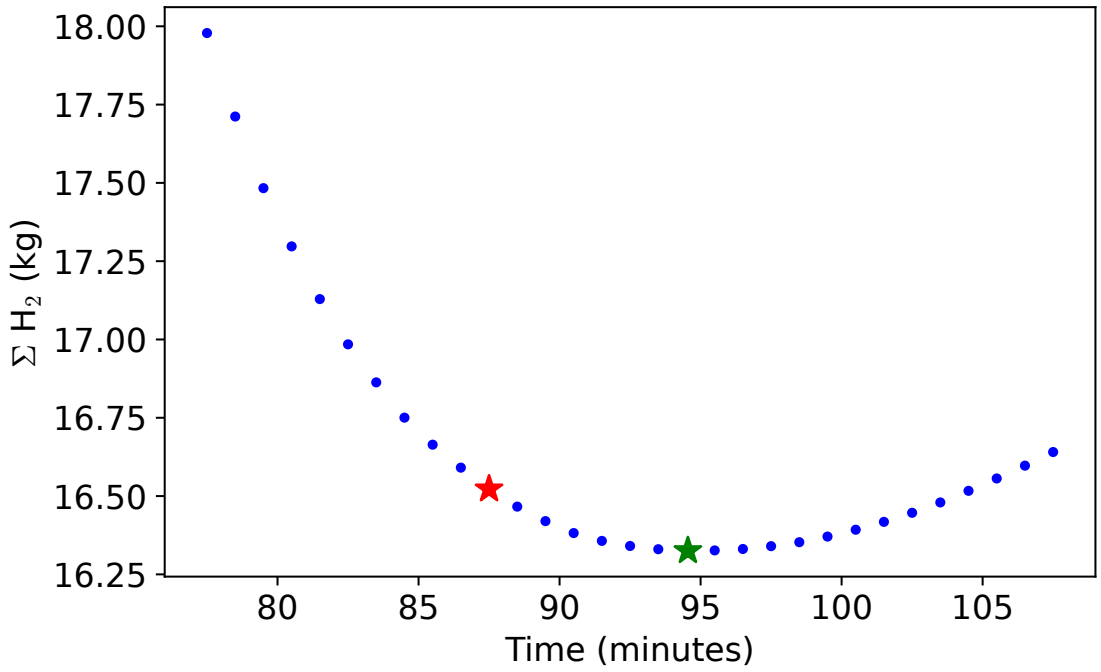

Figure 6.9: Pareto curve for hydrogen consumption vs total trip time.

6.7 Numerical Validation

This section presents various numerical results related to algorithm accuracy and performance.

6.7.1 Polynomial Exactness

It was explained in Section 5.3.3 that the real-world optimality of the solution is dependent on the approximation accuracy of the motor polynomial (5.31) and both fuel cell polynomials (5.13) and (5.38). Figures 6.10 and 6.11 plots an excerpt of the actual against polynomial approximation under the simulated conditions and indeed confirms a high approximation rate.

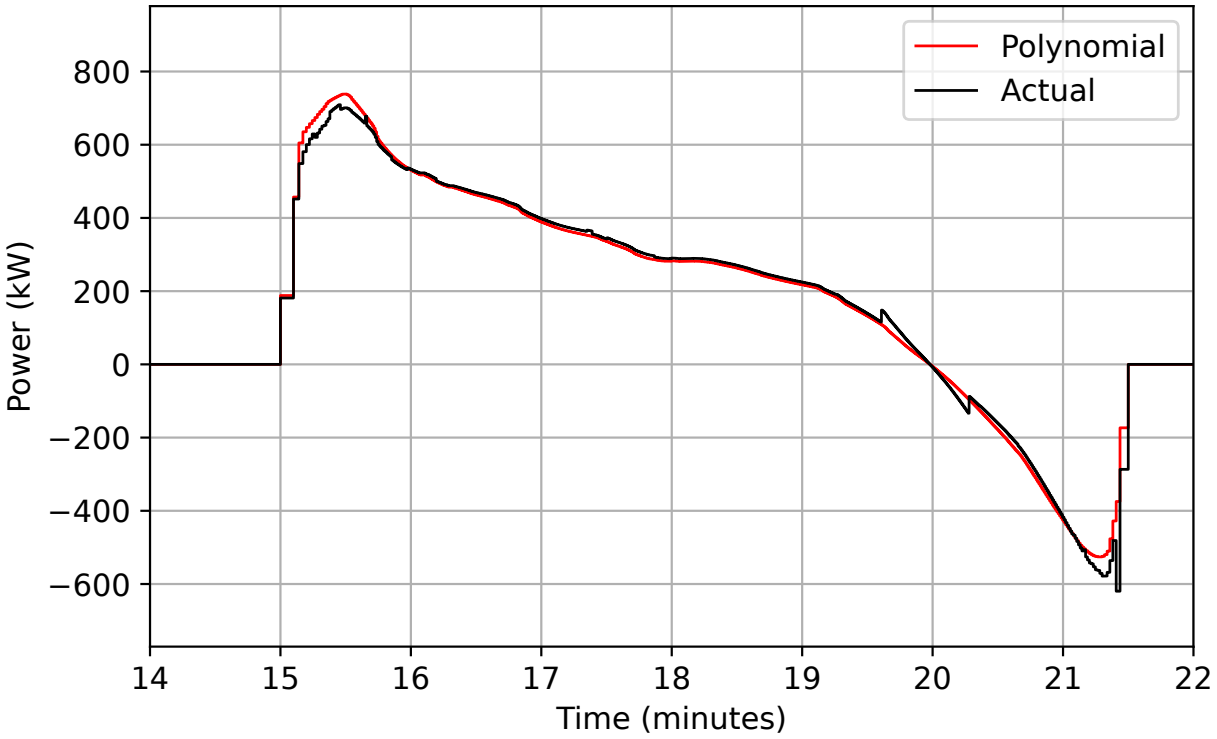

Figure 6.10: Depiction of motor polynomial accuracy.

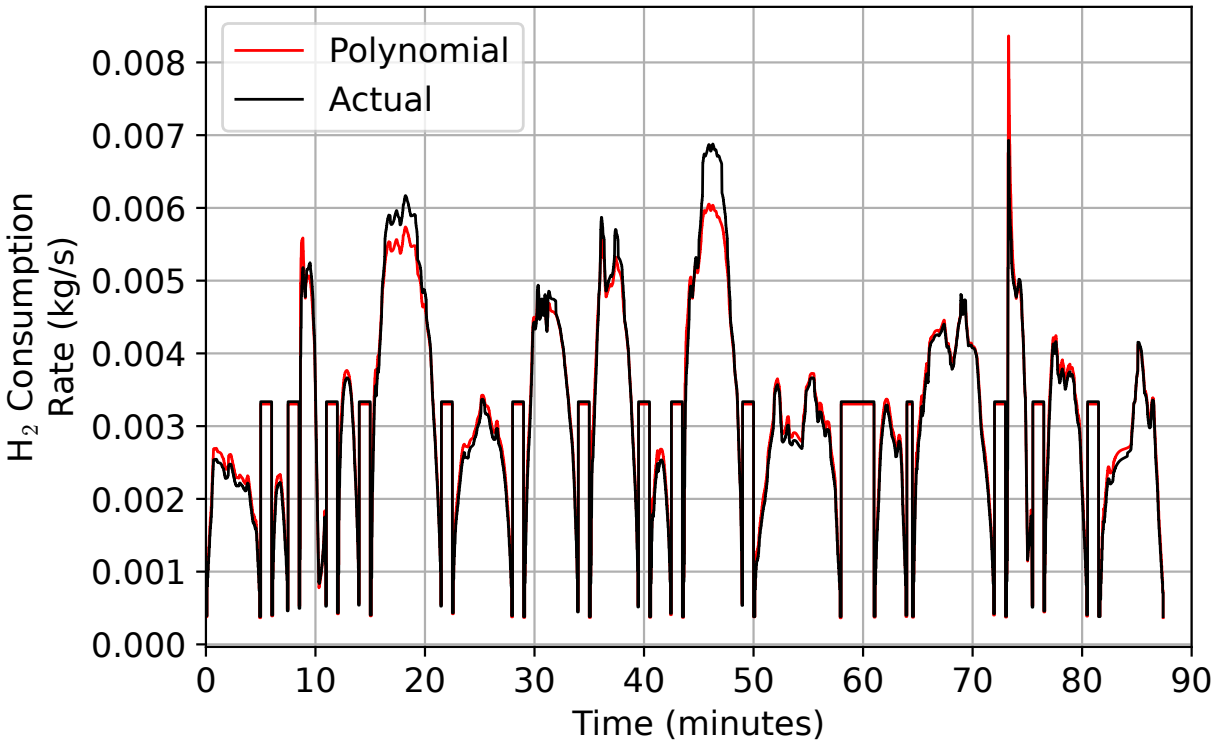

Figure 6.11: Depiction of fuel cell polynomial accuracy.

6.7.2 Constraint Tightness

The optimality of the solution also depends on the relaxed constraints being tightened at equality. Figure 6.12 plots the tightness tolerance of the relaxed constraints in (CTT) which proves solution optimality. The figure is generated by subtracting both sides of the relaxed constraints from each other; therefore, a result closer to zero indicates a tighter constraint. These are scaled according to constraint numerical magnitude.

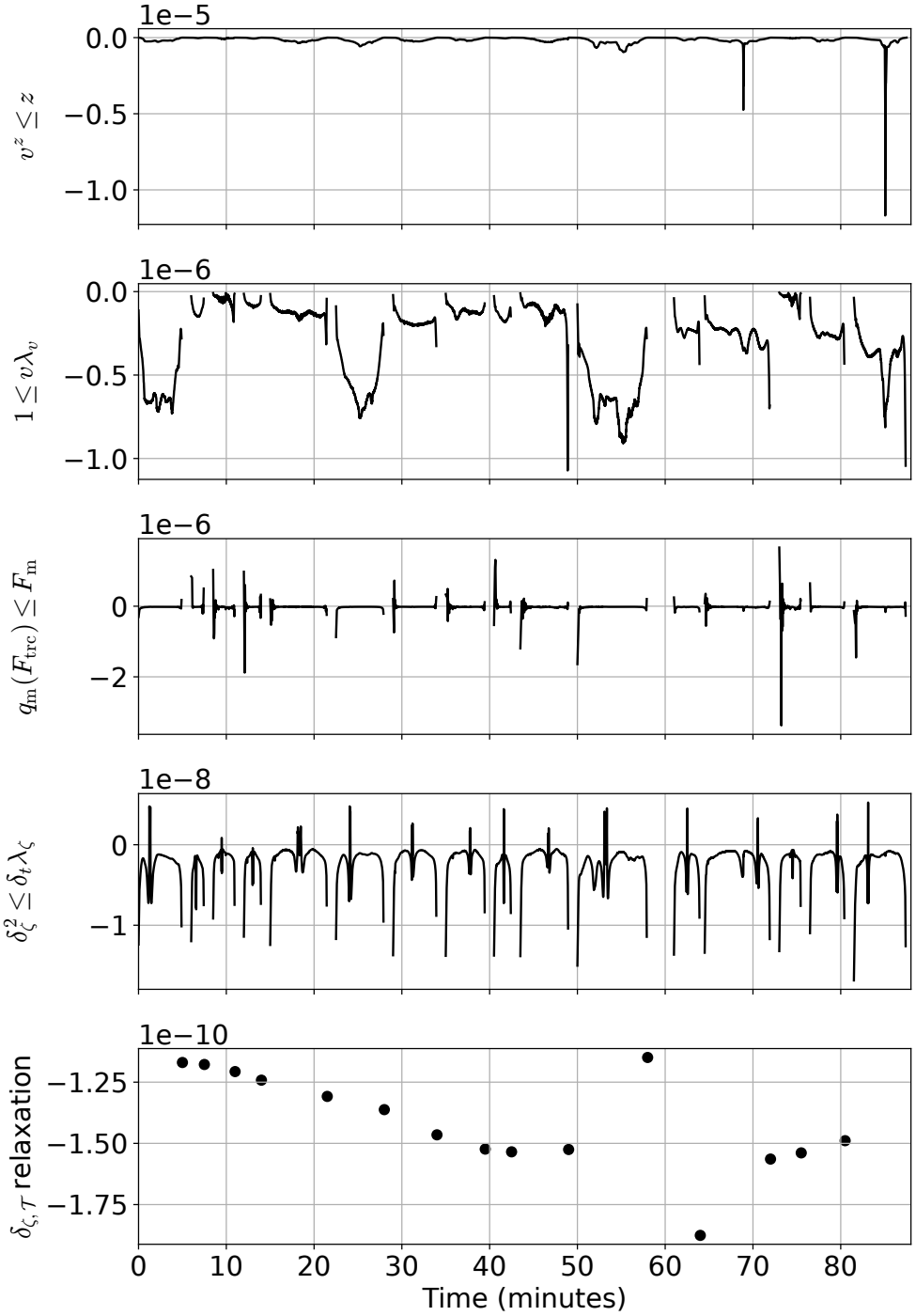

Figure 6.12: The tightness of the relaxed constraints of (CTT).

6.7.3 Computation Time

Table 6.4 lists compute time of (CTT) for various Δ_{s} resolutions. The required compute time grows polynomially with problem size. The results are on the order of seconds,

whereas a relevant example from literature using Dynamic Programming is on the order of hours [154].

Table 6.4: Compute statistics of (CTT) for various problem resolutions.

Δ_s (m)	100 m	50 m	20 m	10 m	5 m
Number Variables	9201	18049	44621	88931	177649
Number Constraints	11415	22349	55184	109937	219566
Algorithm Iterations	31	33	39	44	63
Compute Time (s)	1	3	10	25	74

6.8 Concluding Remarks on Joint Optimisation

This work has proven specific hypotheses regarding optimal train operation and how to compute them. A central theme throughout this work is that jointly optimising more variables and constraints is likely to deliver more optimal results.

A key enabler to the success of the joint method is its ability to fully leverage the dynamic interaction between optimised variables by optimising them all simultaneously. Non-joint optimisation of multiple variables, e.g., sequential optimisation, would fail to effectively uncover this dynamic interaction thereby affecting solution optimality. This was indeed the case for the non-joint results in Sections 6.3 and 6.5. For the former, the EMS optimisation step was given a speed profile and thus could not fully leverage regenerative braking without changing the speed profile. For the latter, the speed-EMS step was given a timetable to follow and thus could not suggest a more optimal timetable for the given powertrain.

Nonetheless, as demonstrated in (BJN) in Section 5.3.1, when speed and EMS formulations were joined, incorporating dynamic interactions jointly can lead to computationally complex formulations. This work took the approach of convexifying the resulting formulation to improve computational efficiency.

7 CONCLUSION

7.1 Summary of Work

This thesis is concerned with optimising the operation of fuel cell hybrid trains with the primary goal of reducing fuel consumption, thereby reducing operational costs and improving the financial viability of such trains. This work builds on the premise that conventional operating strategies might be suboptimal for fuel cell hybrid trains, thus a more optimal operational pattern could be found to save fuel.

Three hypotheses concerning optimal operation were presented, called Operational Hypotheses:

1. The first hypothesises that jointly optimising driving style and EMS is more optimal (fuel efficient) than conventional ecodriving which emphasises coasting. This was pursued because coasting is a popular means of reducing fuel consumption amongst train operators.

2. The second hypothesises that adding measures to reduce powertrain degradation could worsen fuel economy. This was pursued due to the high capital cost of the fuel cell hybrid powertrain thereby motivating operators to explore means of conserving its lifetime.

3. The third hypothesises that jointly optimising the timetable along driving style and EMS is more optimal (fuel efficient) than following a given timetable. This was pursued to assess whether fuel cell hybrid trains can be efficiently used on existing timetables or redesigning the timetable is necessary for optimal operation

To prove the Operational hypotheses, a series of optimisation problems had to be formulated to find the optimal solution of the various objectives. Nonetheless, the coupled dynamics of a hybrid powertrain necessitates a complex joint formulation of several vari-

ables, which could easily grow into an intractable computational problem. This was indeed found to be the case in Section 2.3.1 of the literature review, where existing literature decouples the optimised variables to simplify computational complexity. To tackle this computational challenge, it was hypothesised that convex optimisation could be used for joint optimisation without overly simplifying the powertrain's dynamics, called Algorithmic Hypotheses. The benefits of proving the Algorithmic Hypotheses is owed to the global optimality and computational complexity guarantees afforded by convex optimisation.

The literature review in Chapter 2 firstly covers lithium-ion battery and PEM fuel cell degradation to better understand what measures can be applied to conserve powertrain lifetime. For batteries, it was found that LTO batteries are more durable and posses a higher power rating than incumbent battery chemistries used for electric vehicles. Although this comes at the expense of a lower energy density, it is an acceptable compromise for the fuel cell hybrid powertrain because the battery would only play a supporting role along the fuel cell. It was also found that charge-throughput is the main degradation driver which was later used in Chapter 6 to assess the degradation of simulated operational patterns. For PEM fuel cells, it was found that it is best to hold output power constant at an intermediate level away from idle or maximum power. The variation of fuel cell power output was used in Chapter 6 to assess fuel cell degradation.

Chapter 2 also reviewed rail literature for speed, EMS and timetabling practices and optimisation techniques. It firstly explores publications that exclusively address one of these objectives at a time, after which it explores publications that address multiple of these objectives. This was done to assess the potential benefits of joint optimisation. Some evidence to the superiority of the latter was found. That being said, existing literature made simplifying assumptions to mitigate computational complexity which unfortunately came at the expense of solution optimality.

The last section in Chapter 2 covered automotive EMS literature. This was done due to

the bigger prominence of hybrid vehicles in the automotive domain. In comparison to rail literature, a bigger variety of algorithms was found spanning rule-based, optimisation-based and learning-based. This variety of algorithms was also accompanied by a big variety of powertrain degradation models spanning physics-based and empirical-based models. Crucially, evidence was found to prove the utility of convex methods for joint optimisation [36].

Chapter 3 presented a primer on convex optimisation with a focus on what is directly relevant to this thesis. To this end, the convexity of functions and constraints used in this thesis are proven therein.

Chapter 4 delves into train modelling details. It firstly proposes a hybrid domain approach involving both space and time domains to reap the benefits of both. The spatial domain affords a higher modelling accuracy when the train is moving, whereas the temporal domain is required for when the train is stationary. This hybrid domain approach is novel in comparison to the reviewed rail and automotive literature. A chief enabler of this approach was using mathematical sets to assign each sampling instance to either domains. The remaining of the chapter derives models for the train's longitudinal dynamics and powertrain.

Chapter 5 formulates a series of optimisation problems with increasing levels of fidelity that ultimately proves the Algorithmic Hypotheses. It starts by formulating a speed optimisation formulation in Section 5.1 that is convexified by substituting v^2 (speed squared) by the variable z and introducing the surrogate variable λ_{v} to circumvent the non-linear reciprocal operation for instance duration. Section 5.2 builds an EMS formulation that is convexified by approximating the discrete fuel cell consumption model with a convex polynomial and relaxing the battery state-of-charge equality into an inequality. The convex polynomial approximation was shown to accurately model the discrete consumption model because the latter forms a convex shape by the virtue of being the reciprocal of a concave efficiency curve. This implies that such approximation can be generalised to

other fuel cells. Moreover, it is shown why the optimal solution sits at the boundary of the relaxed battery constraint, which proves that the relaxation done to convexify the formulation does not affect the optimal solution.

Section 5.3 merges the convex speed and EMS formulations into a joint one, though this direct merger results in a non-convex formulation despite both building constituents being convex on their own. This occurs because the speed and EMS dynamics are non-linearly coupled; therefore, by coupling them, one naturally introduces a non-linearity that leads to a non-convex formulation. This coupling was convexified by expressing the coupling through linear work-based terms instead of bi-linear power-based terms which was enabled by the novel hybrid domain approach. Section 5.4 relaxes the duration constraint imposed on intermediate stations which effectively optimises the running time between intermediate stations jointly with speed and EMS.

Based on the reviewed rail literature, this is the first successful attempt at jointly optimising speed-EMS as well as speed-EMS-timetable. Moreover, this was achieved using convex optimisation, adding to that milestone guarantees on solution optimality and computational complexity.

Chapter 6 ran a series of simulations to prove the Operational Hypotheses. To perform an objective comparison, the following metrics were defined: fuel consumption, traction work, mechanical braking work, regenerative braking work, charge-throughput to assess battery degradation, load-cycling to assess fuel cell degradation.

Section 6.3 proved that jointly optimising speed-EMS is more fuel efficient than conventional ecodriving that emphasises coasting. This was found to be the case because coasting delays braking and fails to recover kinetic energy as the train comes to a stop, whereas joint optimisation efficiently uses regenerative braking early on to slow the train. Moreover, coasting patterns require a longer acceleration phase which was found to be more degrading on the fuel cell and battery.

Section 6.4 proved that measures to counter fuel cell degradation comes at the expense

of additional fuel consumption. This was tested by fixing fuel cell power to reduce load cycling. Nonetheless, it was encouraging to find that the increase in fuel consumption was found to be significantly less in magnitude than the reduction in degradation. This suggests that such a measure might be financially viable and even favourable to implement.

Sections 6.5 and 6.6 proved that jointly optimising speed-EMS-timetable is more fuel efficient than following a given timetable. The former achieved this by optimising running time between intermediate stations while maintaining the total trip time, whereas the latter achieved this by optimising both running time and total trip time. This is a novel contribution to rail literature, as existing hybrid train publications only attempt sequential optimisation to reduce computational complexity, where they optimise the driving style based on a given timetable that is optimised separately.

Lastly, Section 6.7 uses numerical examples from the simulations to: i) prove the approximation accuracy of the polynomials, ii) prove the tightness of the relaxed constraints, iii) demonstrate joint optimisation compute time that is on the order of seconds in comparison to sequential examples from literature that are on the order of hours.

7.2 Further Work

Network-wide Scheduling This work focused on a single train, whereas, in reality, a train's operation must be compatible with other traffic sharing the network. Therefore, it remains to be explored how the timetable optimisation techniques proposed here can be integrated into larger scheduling algorithms that optimise network-wide traffic flow, such as those reviewed in Section 2.3.1. Nevertheless, the quick computation time of convex methods would likely facilitate such integration.

Real-World Degradation Testing Degradation is a complex phenomenon that is highly dependent on the accumulative state and conditions experienced by the asset. The

fuel cell degradation metric used in this work is only adequate as a qualitative measure for initial analysis, rather than an accurate measure to quantify the expected degradation from a specified operational pattern. Therefore, detailed degradation modelling is required along real-world testing to assess the financial balance between countering degradation and the increase in fuel consumption. Establishing a Pareto Curve for these contradicting objectives would provide operators with an effective tool for making such a decision.

Optimising Further Systems In light of this work's conclusion that joint optimisation delivers better results, further optimality could be achieved by jointly optimising other systems and variables. One noteworthy example is the HVAC system which is a leading auxiliary load [328]. Existing work from the automotive sector supports the view that HVAC consumption could be reduced by optimising it with the traction load [315]. This evidence encourages pursuing a similar idea in rail.

Human Factors The economic returns of optimising operational patterns is largely dependent on the operator's ability to apply these patterns in practice. This is one of the reasons coasting is popular among operators [29]; coasting is a relatively simple pattern to implement by the driver. An important question to answer is whether the optimised results of this thesis could be implemented repeatedly and reliably by drivers. This research question could be answered through trials on a driver-simulator and trials on a real train.

Bibliography

[1] "Let's raise our ambitions for a cleaner, greener railway," [Online]. Available: https://www.gov.uk/government/speeches/lets-raise-our-ambitions-for-a-cleaner-greener-railway, GOV.UK, February 2018.

[2] "Rail emissions 2020-21," Office of Rail and Road, Report, 2021. [Online]. Available: https://dataportal.orr.gov.uk/media/1993/rail-emissions-2020-21.pdf

[3] L. Benbrahim-Tallaa, R. A. Baan, Y. Grosse, B. Lauby-Secretan, F. El Ghissassi, V. Bouvard, N. Guha, D. Loomis, and K. Straif, "Carcinogenicity of diesel-engine and gasoline-engine exhausts and some nitroarenes," *The lancet oncology*, vol. 13, no. 7, pp. 663–664, 2012.

[4] F. Laden, J. E. Hart, A. Eschenroeder, T. Smith, and E. Garschick, "Historical estimation of diesel exhaust exposure in a cohort study of u.s. railroad workers and lung cancer," *Cancer Causes and Control*, vol. 17, pp. 911–919, 2006.

[5] "Research into air quality in enclosed railway stations (t1122)," RSSB, Tech. Rep., 2019. [Online]. Available: https://www.rssb.co.uk/research-catalogue/CatalogueItem/T1122

[6] "Analysis of air quality on board trains (t1188)," RSSB, Tech. Rep., 2021. [Online]. Available: https://www.rssb.co.uk/research-catalogue/CatalogueItem/T1188

[7] "Main results: Test with hydrogen train in groningen," provine groningen, Report. [Online]. Available: https://www.alstom.com/sites/alstom.com/files/2020/09/30/Rapport%20Waterstoftrein%20Groningen_EN.pdf

[8] Y. Kwon, S. Kim, H. Kim, and J. Byun, "What attributes do passengers value in electrified buses?" *Energies*, vol. 13, no. 10, 2020.

[9] R. Steinberger-Wilckens, J. Radcliffe, N. Al-Mufachi, P. Dodds, A. Abad, O. Jones, and Z. Kurban, "The role of hydrogen and fuel cells in delivering energy security for the uk," H2FCSUPERGEN, Tech. Rep., 2017.

[10] "Rail industry decarbonisation taskforce final report to the minister for rail," 2019, accessed: 2023-24-05. [Online]. Available: https://www.rssb.co.uk/sustainability/decarbonisation

[11] "Traction decarbonisation network strategy: Interim programme business case," Network Rail, Report, July 2020.

[12] B. Horgan, "£30bn rail electrification plan blocked by treasury," 2021, accessed: 2023-24-05. [Online]. Available: https://www.newcivilengineer.com/latest/30bn-rail-electrification-plan-blocked-by-treasury-13-12-2021/

[13] "Great western route modernisation first post-opening evaluation – final report,"

SYSTRA, Report, 2022. [Online]. Available: https://www.gov.uk/government/publications/evaluation-of-the-great-western-route-modernisation

[14] J. G. Allen and G. L. Newmark, "Commuter rail electrifications that never were and what they teach us," *Transportation Research Record: Journal of the Transportation Research Board*, vol. 2677, no. 1, pp. 639–652, 2022.

[15] "Study on the use of fuel cells & hydrogen in the railway environment: Overcoming technological and non-technological barriers to widespread use of fch in rail applications," Roland Berger, Report, 2019.

[16] "Successful year and a half of trial operation of the world's first two hydrogen trains, next project phase begins," May 2020. [Online]. Available: https://www.alstom.com/press-releases-news/2020/5/successful-year-and-half-trial-operation-worlds-first-two-hydrogen

[17] "Green-tech for the us: Stadler signs first ever contract for hydrogen-powered train," December 2019. [Online]. Available: https://www.stadlerrail.com/en/media/article/green-tech-for-the-us-stadler-signs-first-ever-contractfor-hydrogen-powered-train/649/

[18] "Emission-free train solutions to deliver railway decarbonisation," November 2021. [Online]. Available: https://www.alstom.com/press-releases-news/2021/11/emission-free-train-solutions-deliver-railway-decarbonisation

[19] "Siemens mobility develops hydrogen train for climate-neutral rail transport in bavaria," July 2021. [Online]. Available: https://press.siemens.com/global/en/feature/siemens-mobility-develops-hydrogen-train-climate-neutral-rail-transport-bavaria

[20] "Premiere: Deutsche bahn and siemens mobility present new hydrogen train and hydrogen storage tank trailer," May 2022. [Online]. Available: https://press.siemens.com/global/en/pressrelease/premiere-deutsche-bahn-and-siemens-mobility-present-new-hydrogen-train-and-hydrogen

[21] "First hydrogen-powered trains for the berlin-brandenburg metropolitan region," June 2022. [Online]. Available: https://press.siemens.com/global/en/pressrelease/first-hydrogen-powered-trains-berlin-brandenburg-metropolitan-region

[22] "Alstom and eversholt rail sign an agreement for the uk's first ever brand-new hydrogen train fleet," November 2021. [Online]. Available: https://www.alstom.com/press-releases-news/2021/11/alstom-and-eversholt-rail-sign-agreement-uks-first-ever-brand-new

[23] "Path to hydrogen competitiveness: cost perspective," Hydrogen Council, Report, 2020.

[24] J. Olmos, A. Saez-de Ibarra, H. Gaztañaga, D. Lopez, T. Nieva, and I. Aizpuru, "In-depth life cycle cost analysis of a hydrogen electric multiple unit," in *2021 IEEE Vehicle Power and Propulsion Conference (VPPC)*. IEEE, 2021, pp. 1–6.

[25] L. Guzzella and A. Sciarretta, *Vehicle Propulsion Systems: Introduction to Modeling and Optimization*, 3rd ed. Springer-Verlag Berlin Heidelberg, 2013.

[26] M. L. Wright and A. C. Lewis, "Decarbonisation of heavy-duty diesel engines using hydrogen fuel: a review of the potential impact on nox emissions," *Environmental Science: Atmospheres*, vol. 2, no. 5, pp. 852–866, 2022.

[27] F. Hofer, B. Raser, M. Schmidt, and A. Kabza, "H2 engine and fuel cell in heavy commercial vehicles," *MTZ worldwide*, vol. 83, pp. 28–35, February 2022.

[28] H. Douglas, C. Roberts, S. Hillmansen, and F. Schmid, "An assessment of available measures to reduce traction energy use in railway networks," *Energy Conversion and Management*, vol. 106, pp. 1149–1165, 2015.

[29] R. S. Luijt, M. P. F. van den Berge, H. Y. Willeboordse, and J. H. Hoogenraad, "5 years of dutch eco-driving: Managing behavioural change," *Transportation Research Part A: Policy and Practice*, vol. 98, pp. 46–63, 2017.

[30] D. Coleman, P. Howlett, P. Pudney, X. Vu, and R. Yee, "Coasting boards vs optimal control," in *IET Conference on Railway Traction Systems (RTS 2010)*. IET, 2010, Conference Proceedings.

[31] N. Zhao, Z. Tian, L. Chen, C. Roberts, and S. Hillmansen, "Driving strategy optimization and field test on an urban rail transit system," *IEEE Intelligent Transportation Systems Magazine*, vol. 13, no. 3, pp. 34–44, 2021.

[32] S. J. Moura, J. L. Stein, and H. K. Fathy, "Battery-health conscious power management in plug-in hybrid electric vehicles via electrochemical modeling and stochastic control," *IEEE Transactions on Control Systems Technology*, vol. 21, no. 3, pp. 679–694, 2013.

[33] T. Fletcher, R. Thring, and M. Watkinson, "An energy management strategy to concurrently optimise fuel consumption & pem fuel cell lifetime in a hybrid vehicle," *International Journal of Hydrogen Energy*, vol. 41, no. 46, pp. 21 503–21 515, 2016.

[34] X. Yang, X. Li, B. Ning, and T. Tang, "A survey on energy-efficient train operation for urban rail transit," *IEEE Transactions on Intelligent Transportation Systems*, vol. 17, no. 1, pp. 2–13, 2016.

[35] S. Boyd and L. Vandenberghe, *Convex optimization*. Cambridge university press, 2004.

[36] N. Murgovski, L. Johannesson, X. Hu, B. Egardt, and J. Sjoberg, "Convex relaxations in the optimal control of electrified vehicles," in *2015 American Control Conference*. IEEE, 2015.

[37] Y. Jia, R. Jibrin, and D. Gorges, "Energy-optimal adaptive cruise control for electric vehicles based on linear and nonlinear model predictive control," *IEEE Transactions on Vehicular Technology*, vol. 69, no. 12, pp. 14 173–14 187, 2020.

[38] X. Han, L. Lu, Y. Zheng, X. Feng, Z. Li, J. Li, and M. Ouyang, "A review on the key issues of the lithium ion battery degradation among the whole life cycle," *eTransportation*, vol. 1, 2019.

[39] M. Lucu, E. Martinez-Laserna, I. Gandiaga, K. Liu, H. Camblong, W. D. Widanage, and J. Marco, "Data-driven nonparametric li-ion battery ageing model aiming at learning from real operation data - part b: Cycling operation," *Journal of Energy Storage*, vol. 30, 2020.

[40] X.-G. Yang, Y. Leng, G. Zhang, S. Ge, and C.-Y. Wang, "Modeling of lithium plating induced aging of lithium-ion batteries: Transition from linear to nonlinear aging," *Journal of Power Sources*, vol. 360, pp. 28–40, 2017.

[41] S. F. Schuster, T. Bach, E. Fleder, J. Müller, M. Brand, G. Sextl, and A. Jossen, "Nonlinear aging characteristics of lithium-ion cells under different operational conditions," *Journal of Energy Storage*, vol. 1, pp. 44–53, 2015.

[42] M. Klett, R. Eriksson, J. Groot, P. Svens, K. Ciosek Högström, R. W. Lindström, H. Berg, T. Gustafson, G. Lindbergh, and K. Edström, "Non-uniform aging of cycled commercial lifepo4//graphite cylindrical cells revealed by post-mortem analysis," *Journal of Power Sources*, vol. 257, pp. 126–137, 2014.

[43] T. R. Tanim, M. G. Shirk, R. L. Bewley, E. J. Dufek, and B. Y. Liaw, "Fast charge implications: Pack and cell analysis and comparison," *Journal of Power Sources*, vol. 381, pp. 56–65, 2018.

[44] X. Han, M. Ouyang, L. Lu, J. Li, Y. Zheng, and Z. Li, "A comparative study of commercial lithium ion battery cycle life in electrical vehicle: Aging mechanism identification," *Journal of Power Sources*, vol. 251, pp. 38–54, 2014.

[45] J. Vetter, P. Novák, M. R. Wagner, C. Veit, K. C. Möller, J. O. Besenhard, M. Winter, M. Wohlfahrt-Mehrens, C. Vogler, and A. Hammouche, "Ageing mechanisms in lithium-ion batteries," *Journal of Power Sources*, vol. 147, no. 1-2, pp. 269–281, 2005.

[46] J. T. Warner, *Lithium-Ion Battery Chemistries: A Primer*. Elsevier, 2019.

[47] M. Dubarry, N. Qin, and P. Brooker, "Calendar aging of commercial li-ion cells of different chemistries – a review," *Current Opinion in Electrochemistry*, vol. 9, pp. 106–113, 2018.

[48] A. Barré, B. Deguilhem, S. Grolleau, M. Gérard, F. Suard, and D. Riu, "A review on lithium-ion battery ageing mechanisms and estimations for automotive applications," *Journal of Power Sources*, vol. 241, pp. 680–689, 2013.

[49] M. Woody, M. Arbabzadeh, G. M. Lewis, G. A. Keoleian, and A. Stefanopoulou, "Strategies to limit degradation and maximize li-ion battery service lifetime - critical review and guidance for stakeholders," *Journal of Energy Storage*, vol. 28, 2020.

[50] M. Kassem, J. Bernard, R. Revel, S. Pélissier, F. Duclaud, and C. Delacourt, "Calendar aging of a graphite/lifepo4 cell," *Journal of Power Sources*, vol. 208, pp. 296–305, 2012.

[51] J. Groot, "State-of-health estimation of li-ion batteries: Cycle life test methods," Thesis, Chalmers University of Technology, 2012.

[52] Y. Zhang, C.-Y. Wang, and X. Tang, "Cycling degradation of an automotive lifepo4 lithium-ion battery," *Journal of Power Sources*, vol. 196, no. 3, pp. 1513–1520, 2011.

[53] J. Jiang, W. Shi, J. Zheng, P. Zuo, J. Xiao, X. Chen, W. Xu, and J.-G. Zhang, "Optimized operating range for large-format lifepo4/graphite batteries," *Journal of The Electrochemical Society*, vol. 161, no. 3, pp. A336–A341, 2013.

[54] Y. Li, X. Feng, D. Ren, M. Ouyang, L. Lu, and X. Han, "Thermal runaway triggered by plated lithium on the anode after fast charging," *ACS Appl Mater Interfaces*, vol. 11, no. 50, pp. 46 839–46 850, 2019. [Online]. Available: https://www.ncbi.nlm.nih.gov/pubmed/31742989

[55] N. Omar, M. A. Monem, Y. Firouz, J. Salminen, J. Smekens, O. Hegazy, H. Gaulous, G. Mulder, P. Van den Bossche, T. Coosemans, and J. Van Mierlo, "Lithium iron phosphate based battery – assessment of the aging parameters and development of cycle life model," *Applied Energy*, vol. 113, pp. 1575–1585, 2014.

[56] M. Dubarry, C. Truchot, and B. Y. Liaw, "Cell degradation in commercial lifepo4 cells with high-power and high-energy designs," *Journal of Power Sources*, vol. 258, pp. 408–419, 2014.

[57] A. Tomaszewska, Z. Chu, X. Feng, S. O'Kane, X. Liu, J. Chen, C. Ji, E. Endler, R. Li, L. Liu, Y. Li, S. Zheng, S. Vetterlein, M. Gao, J. Du, M. Parkes, M. Ouyang, M. Marinescu, G. Offer, and B. Wu, "Lithium-ion battery fast charging: A review," *eTransportation*, vol. 1, 2019.

[58] S. Gantenbein, M. Schönleber, M. Weiss, and E. Ivers-Tiffée, "Capacity fade in lithium-ion batteries and cyclic aging over various state-of-charge ranges," *Sustainability*, vol. 11, no. 23, 2019.

[59] A. Mukhopadhyay and B. W. Sheldon, "Deformation and stress in electrode materials for li-ion batteries," *Progress in Materials Science*, vol. 63, pp. 58–116, 2014.

[60] D. Anseán, J. Viera, M. González, V. García, J. Álvarez, and J. Antuña, "High power lifepo4 cell evaluation: fast charge, depth of discharge and fast discharge dependency," *World Electric Vehicle Journal*, vol. 6, 2013.

[61] J. Wang, P. Liu, J. Hicks-Garner, E. Sherman, S. Soukiazian, M. Verbrugge, H. Tataria, J. Musser, and P. Finamore, "Cycle-life model for graphite-lifepo4 cells," *Journal of Power Sources*, vol. 196, no. 8, pp. 3942–3948, 2011.

[62] M. Dubarry, C. Truchot, B. Y. Liaw, K. Gering, S. Sazhin, D. Jamison, and C. Michelbacher, "Evaluation of commercial lithium-ion cells based on composite positive electrode for plug-in hybrid electric vehicle applications. part ii. degradation mechanism under 2c cycle aging," *Journal of Power Sources*, vol. 196, no. 23, pp. 10 336–10 343, 2011.

[63] I. Belharouak, G. M. Koenig, and K. Amine, "Electrochemistry and safety of li4ti5o12 and graphite anodes paired with limn2o4 for hybrid electric vehicle li-ion battery applications," *Journal of Power Sources*, vol. 196, no. 23, pp. 10 344–10 350, 2011.

[64] A. Burke and M. Miller, "Life cycle testing of lithium batteries for fast charging and second-use applications," in *EVS27 International Battery, Hybrid and Fuel Cell Electric Vehicle Symposium*, 2013.

[65] A.-I. Stroe, "Analysis of performance and degradation for lithium titanate oxide batteries," Thesis, Aalborg University, 2018.

[66] X. Han, M. Ouyang, L. Lu, and J. Li, "Cycle life of commercial lithium-ion batteries with lithium titanium oxide anodes in electric vehicles," *Energies*, vol. 7, no. 8, pp. 4895–4909, 2014.

[67] T. Hang, D. Mukoyama, H. Nara, N. Takami, T. Momma, and T. Osaka, "Electrochemical impedance spectroscopy analysis for lithium-ion battery using li4ti5o12 anode," *Journal of Power Sources*, vol. 222, pp. 442–447, 2013.

[68] F. Hall, J. Touzri, S. Wußler, H. Buqa, and W. G. Bessler, "Experimental investigation of the thermal and cycling behavior of a lithium titanate-based lithium-ion pouch cell," *Journal of Energy Storage*, vol. 17, pp. 109–117, 2018.

[69] M. Saeed, F. Briz, J. M. Guerrero, I. Larrazabal, D. Ortega, V. Lopez, and J. J. Valera, "Onboard energy storage systems for railway: Present and trends," *IEEE Open Journal of Industry Applications*, vol. 4, pp. 238–259, 2023.

[70] T. Nemeth, P. Schröer, M. Kuipers, and D. U. Sauer, "Lithium titanate oxide battery cells for high-power automotive applications – electro-thermal properties, aging behavior and cost considerations," *Journal of Energy Storage*, vol. 31, 2020.

[71] "Sria key performance indicators (kpis): Kpis for trains," accessed: 2022-24-08. [Online]. Available: https://www.clean-hydrogen.europa.eu/knowledge-management/sria-key-performance-indicators-kpis_en

[72] L. E. Post and Matthew, "Fuel cell buses in u.s. transit fleets: Current status 2017," National Renewable Energy Laboratory, Report, 2017.

[73] "Ballard fcmove specification sheet," accessed: 2022-24-08. [Online]. Available: https://www.ballard.com/about-ballard/publication_library/product-specification-sheets/fcmovetm-spec-sheet

[74] P. Rama, R. Chen, and J. Andrews, "A review of performance degradation and failure modes for hydrogen-fuelled polymer electrolyte fuel cells," *Proceedings of the Institution of Mechanical Engineers, Part A: Journal of Power and Energy*, vol. 222, no. 5, pp. 421–441, 2008.

[75] R. Lin, B. Li, Y. P. Hou, and J. M. Ma, "Investigation of dynamic driving cycle effect on performance degradation and micro-structure change of pem fuel cell," *International Journal of Hydrogen Energy*, vol. 34, no. 5, pp. 2369–2376, 2009.

[76] H. Chen, Z. Zhan, P. Jiang, Y. Sun, L. Liao, X. Wan, Q. Du, X. Chen, H. Song, R. Zhu, Z. Shu, S. Li, and M. Pan, "Whole life cycle performance degradation test and rul prediction research of fuel cell mea," *Applied Energy*, vol. 310, 2022.

[77] M. Ji and Z. Wei, "A review of water management in polymer electrolyte membrane fuel cells," *Energies*, vol. 2, no. 4, pp. 1057–1106, 2009.

[78] S. J. C. Cleghorn, D. K. Mayfield, D. A. Moore, J. C. Moore, G. Rusch, T. W. Sherman, N. T. Sisofo, and U. Beuscher, "A polymer electrolyte fuel cell life test: 3 years of continuous operation," *Journal of Power Sources*, vol. 158, no. 1, pp. 446–454, 2006.

[79] X. Huang, R. Solasi, Y. Zou, M. Feshler, K. Reifsnider, D. Condit, S. Burlatsky, and T. Madden, "Mechanical endurance of polymer electrolyte membrane and pem fuel cell durability," *Journal of Polymer Science Part B: Polymer Physics*, vol. 44, no. 16, pp. 2346–2357, 2006.

[80] M. P. Rodgers, L. J. Bonville, H. R. Kunz, D. K. Slattery, and J. M. Fenton, "Fuel cell perfluorinated sulfonic acid membrane degradation correlating accelerated stress testing and lifetime," *Chem Rev*, vol. 112, no. 11, pp. 6075–103, 2012. [Online]. Available: https://www.ncbi.nlm.nih.gov/pubmed/23061417

[81] G. Wang, F. Huang, Y. Yu, S. Wen, and Z. Tu, "Degradation behavior of a proton exchange membrane fuel cell stack under dynamic cycles between idling and rated condition," *International Journal of Hydrogen Energy*, vol. 43, no. 9, pp. 4471–4481, 2018.

[82] C. Wang, Q. Zhao, X. Zhou, J. Wang, and Y. Tang, "Degradation characteristics of membrane electrode assembly under drive cycle test protocol," *International Journal of Green Energy*, vol. 16, no. 10, pp. 789–795, 2019.

[83] L. Placca and R. Kouta, "Fault tree analysis for pem fuel cell degradation process modelling," *International Journal of Hydrogen Energy*, vol. 36, no. 19, pp. 12 393–12 405, 2011.

[84] C. Robin, M. Gérard, M. Quinaud, J. d'Arbigny, and Y. Bultel, "Proton exchange membrane fuel cell model for aging predictions: Simulated equivalent active surface area loss and comparisons with durability tests," *Journal of Power Sources*, vol. 326, pp. 417–427, 2016.

[85] M. Jouin, R. Gouriveau, D. Hissel, M.-C. Péra, and N. Zerhouni, "Degradations analysis and aging modeling for health assessment and prognostics of pemfc," *Reliability Engineering & System Safety*, vol. 148, pp. 78–95, 2016.

[86] L. Dubau, L. Castanheira, M. Chatenet, F. Maillard, J. Dillet, G. Maranzana, S. Abbou, O. Lottin, G. De Moor, A. El Kaddouri, C. Bas, L. Flandin, E. Rossinot, and N. Caqué, "Carbon corrosion induced by membrane failure: The weak link of pemfc long-term performance," *International Journal of Hydrogen Energy*, vol. 39, no. 36, pp. 21 902–21 914, 2014.

[87] T. Chu, Q. Tang, Q. Wang, Y. Wang, H. Du, Y. Guo, B. Li, D. Yang, P. Ming, and C. Zhang, "Experimental study on the effect of flow channel parameters on the durability of pemfc stack and analysis of hydrogen crossover mechanism," *Energy*, vol. 264, 2023.

[88] M. M. Mench, E. C. Kumbur, and T. N. Veziroglu, *Polymer Electrolyte Fuel Cell Degradation*. Academic Press, 2012.

[89] Y.-H. Lai, C. K. Mittelsteadt, C. S. Gittleman, and D. A. Dillard, "Viscoelastic stress analysis of constrained proton exchange membranes under humidity cycling," *Journal of Fuel Cell Science and Technology*, vol. 6, no. 2, 2009.

[90] Y.-H. Lai, K. M. Rahmoeller, J. H. Hurst, R. S. Kukreja, M. Atwan, A. J. Maslyn, and C. S. Gittleman, "Accelerated stress testing of fuel cell membranes subjected to combined mechanical/chemical stressors and cerium migration," *Journal of The Electrochemical Society*, vol. 165, no. 6, pp. F3217–F3229, 2018.

[91] M. Mayur, M. Gerard, P. Schott, and W. Bessler, "Lifetime prediction of a polymer electrolyte membrane fuel cell under automotive load cycling using a physically-based catalyst degradation model," *Energies*, vol. 11, no. 8, 2018.

[92] R. L. Borup, J. R. Davey, F. H. Garzon, D. L. Wood, and M. A. Inbody, "Pem fuel cell electrocatalyst durability measurements," *Journal of Power Sources*, vol. 163, no. 1, pp. 76–81, 2006.

[93] S. Yamamoto, S. Sugawara, and K. Shinohara, *Fuel Cell Stack Durability for Vehicle Application.* Springer, 2009, pp. 467–482.

[94] M. L. Perry, R. M. Darling, S. Kandoi, T. W. Patterson, and C. Reiser, *Operating Requirements for Durable Polymer-Electrolyte Fuel Cell Stacks.* Springer, 2009, pp. 399–417.

[95] R. B. e. al, "Scientific aspects of polymer electrolyte fuel cell durability and degradation," *American Chemical Society*, vol. 107, no. 10, p. 3904–3951, 2007.

[96] M. Uchimura and S. S. Kocha, "The impact of cycle profile on pemfc durability," *ECS Transactions*, vol. 11, pp. 1215–1226, 2007.

[97] H. Chen, X. Zhao, T. Zhang, and P. Pei, "The reactant starvation of the proton exchange membrane fuel cells for vehicular applications: A review," *Energy Conversion and Management*, vol. 182, pp. 282–298, 2019.

[98] J. Park, H. Oh, T. Ha, Y. I. Lee, and K. Min, "A review of the gas diffusion layer in proton exchange membrane fuel cells: Durability and degradation," *Applied Energy*, vol. 155, pp. 866–880, 2015.

[99] J. Zhang, *PEM fuel cell testing and diagnosis.* Amsterdam ; Boston: Elsevier, 2013. [Online]. Available: Publisherdescriptionhttp://www.loc.gov/catdir/enhancements/fy1606/2013444692-d.html

[100] T. Zhang, P. Wang, H. Chen, and P. Pei, "A review of automotive proton exchange membrane fuel cell degradation under start-stop operating condition," *Applied Energy*, vol. 223, pp. 249–262, 2018.

[101] M. Seddiq, H. Khaleghi, and M. Mirzaei, "Numerical analysis of gas cross-over through the membrane in a proton exchange membrane fuel cell," *Journal of Power Sources*, vol. 161, no. 1, pp. 371–379, 2006.

[102] S. Kundu, M. Fowler, L. C. Simon, and R. Abouatallah, "Reversible and irreversible degradation in fuel cells during open circuit voltage durability testing," *Journal of Power Sources*, vol. 182, no. 1, pp. 254–258, 2008.

[103] P. Pei, Q. Chang, and T. Tang, "A quick evaluating method for automotive fuel cell lifetime," *International Journal of Hydrogen Energy*, vol. 33, no. 14, pp. 3829–3836, 2008.

[104] R. Shimoi, T. Aoyama, and A. Iiyama, "Development of fuel cell stack durability based on actual vehicle test data: Current status and future work," *SAE International Journal of Engines*, vol. 2, no. 1, pp. 960–970, 2009.

[105] F. C. Barbosa, "Hybrid rail technology review: An intermediate pathway for electrifying the freight and commuter rail sector - a technical and operational assessment," in *2021 Joint Rail Conference*, 2021, Conference Proceedings.

[106] M. Schenker, T. Schirmer, and H. Dittus, "Application and improvement of a direct method optimization approach for battery electric railway vehicle operation," *Proceedings of the Institution of Mechanical Engineers, Part F: Journal of Rail and Rapid Transit*, 2020.

[107] M. Miyatake and K. Matsuda, "Optimal speed and charge/discharge control of a train with onboard energy storage devices for minimum energy operation," in *International Symposium on Power Electronics, Electrical Drives, Automation and Motion*, 2008.

[108] Y. Sun, M. Anwar, N. M. S. Hassan, M. Spiryagin, and C. Cole, "A review of hydrogen technologies and engineering solutions for railway vehicle design and operations," *Railway Engineering Science*, vol. 29, no. 3, pp. 212–232, 2021.

[109] G. M. Scheepmaker, R. M. P. Goverde, and L. G. Kroon, "Review of energy-efficient train control and timetabling," *European Journal of Operational Research*, vol. 257, no. 2, pp. 355–376, 2017.

[110] P. G. Howlett, I. P. Milroy, and P. J. Pudney, "Energy-efficient train control," *Control Engineering Practice*, vol. 2, no. 2, pp. 193–200, 1994.

[111] R. R. Liu and I. M. Golovitcher, "Energy-efficient operation of rail vehicles," *Transportation Research Part A: Policy and Practice*, vol. 37, no. 10, pp. 917–932, 2003.

[112] G. M. Scheepmaker and R. M. P. Goverde, "Energy-efficient train control using nonlinear bounded regenerative braking," *Transportation Research Part C: Emerging Technologies*, vol. 121, 2020.

[113] Z. Huang, C. Wu, S. Lu, and F. Xue, *Hydrogen Consumption Minimization for Fuel Cell Trains Based on Speed Trajectory Optimization*, ser. Lecture Notes in Electrical Engineering, 2020, book section Chapter 32, pp. 335–345.

[114] S. Lu, S. Hillmansen, T. K. Ho, and C. Roberts, "Single-train trajectory optimization," *IEEE Transactions on Intelligent Transportation Systems*, vol. 14, no. 2, pp. 743–750, 2013.

[115] K. Yedavalli, L. Guo, and D. S. Zinger, "Simple control system for a switcher locomotive hybrid fuel cell power system," *IEEE Transactions on Industry Applications*, vol. 47, no. 6, pp. 2384–2390, 2011.

[116] I. Krastevm, N. Mukherjee, P. Tricoli, and S. Hillmansen, "New modular hybrid energy storage system and its control strategy for a fuel cell locomotive," in *2015 17th European Conference on Power Electronics and Applications (EPE'15 ECCE-Europe)*. IEEE, 2015.

[117] J. P. Torreglosa, P. Garcia, L. M. Fernandez, and F. Jurado, "Predictive control for the energy management of a fuel-cell–battery–supercapacitor tramway," *IEEE Transactions on Industrial Informatics*, vol. 10, no. 1, pp. 276–285, 2014.

[118] M. Cipek, D. Pavković, Z. Kljaić, and T. J. Mlinarić, "Assessment of battery-hybrid diesel-electric locomotive fuel savings and emission reduction potentials based on a realistic mountainous rail route," *Energy*, vol. 173, pp. 1154–1171, 2019.

[119] P. Garcia, L. M. Fernandez, C. A. Garcia, and F. Jurado, "Energy management system of fuel-cell-battery hybrid tramway," *IEEE Transactions on Industrial Electronics*, vol. 57, no. 12, pp. 4013–4023, 2010.

[120] H. Peng, J. Li, A. Thul, K. Deng, C. Ünlübayir, L. Löwenstein, and K. Hameyer, "A scalable, causal, adaptive rule-based energy management for fuel cell hybrid railway vehicles learned from results of dynamic programming," *eTransportation*, vol. 4, 2020.

[121] M. Saadat, M. Esfahanian, and M. H. Saket, "Reducing fuel consumption of diesel-electric locomotives using hybrid powertrain and fuzzy look-ahead control," *Proceedings of the Institution of Mechanical Engineers, Part F: Journal of Rail and Rapid Transit*, vol. 231, no. 4, pp. 406–418, 2016.

[122] P. Fragiacomo and P. Francesco, "Energy performance of a fuel cell hybrid system for rail vehicle propulsion," in *72nd Conference of the Italian Thermal Machines Engineering Association*. Elsevier, 2017.

[123] G. Zhang, W. Chen, and Q. Li, "Modeling, optimization and control of a fc/battery hybrid locomotive based on advisor," *International Journal of Hydrogen Energy*, vol. 42, no. 29, pp. 18 568–18 583, 2017.

[124] G. D'Ovidio, A. Ometto, and O. Valentini, "A novel predictive power flow control strategy for hydrogen city rail train," *International Journal of Hydrogen Energy*, vol. 45, no. 7, pp. 4922–4931, 2020.

[125] D. Meegahawatte, S. Hillmansen, C. Roberts, M. Falco, A. McGordon, and P. Jennings, "Analysis of a fuel cell hybrid commuter railway vehicle," *Journal of Power Sources*, vol. 195, no. 23, pp. 7829–7837, 2010.

[126] V. Herrera, A. Milo, H. Gaztañaga, I. Etxeberria-Otadui, I. Villarreal, and H. Camblong, "Adaptive energy management strategy and optimal sizing applied on a battery-supercapacitor based tramway," *Applied Energy*, vol. 169, pp. 831–845, 2016.

[127] W. Lhomme, T. Letrouvé, L. Boulon, S. Jemeï, A. Bouscayrol, F. Chauvet, and F. Tournez, "Ieee vts motor vehicles challenge 2019 – energy management of a dual-mode locomotive," in *2018 IEEE Vehicle Power and Propulsion Conference (VPPC)*. IEEE, 2018.

[128] D. Sofía Mendoza, J. Solano, and L. Boulon, "Energy management strategy to optimise regenerative braking in a hybrid dual-mode locomotive," *IET Electrical Systems in Transportation*, vol. 10, no. 4, pp. 391–400, 2020.

[129] C. Jia, W. Qiao, and L. Qu, "A cost-oriented control strategy for energy management of a dual-mode locomotive," in *2019 IEEE Vehicle Power and Propulsion Conference (VPPC)*. IEEE, 2019.

[130] A. Aroua, A. Ball, S. Messal, W. Lhomme, and C. Depature, "Fuel cell dual-mode train: Impact of charge depleting strategy on hydrogen consumption," in *2020 IEEE Vehicle Power and Propulsion Conference (VPPC)*, 2020, pp. 1–6.

[131] P. García, J. P. Torreglosa, L. M. Fernández, and F. Jurado, "Control strategies for high-power electric vehicles powered by hydrogen fuel cell, battery and supercapacitor," *Expert Systems with Applications*, vol. 40, no. 12, pp. 4791–4804, 2013.

[132] W. Zhang, J. Li, L. Xu, and M. Ouyang, "Optimization for a fuel cell/battery/capacity tram with equivalent consumption minimization strategy," *Energy Conversion and Management*, vol. 134, pp. 59–69, 2017.

[133] P. García, J. P. Torreglosa, L. M. Fernández, and F. Jurado, "Viability study of a fc-battery-sc tramway controlled by equivalent consumption minimization strategy," *International Journal of Hydrogen Energy*, vol. 37, no. 11, pp. 9368–9382, 2012.

[134] J. P. Torreglosa, F. Jurado, P. García, and L. M. Fernández, "Hybrid fuel cell and battery tramway control based on an equivalent consumption minimization strategy," *Control Engineering Practice*, vol. 19, no. 10, pp. 1182–1194, 2011.

[135] Z. Hong, Q. Li, Y. Han, W. Shang, Y. Zhu, and W. Chen, "An energy management strategy based on dynamic power factor for fuel cell/battery hybrid locomotive," *International Journal of Hydrogen Energy*, vol. 43, no. 6, pp. 3261–3272, 2018.

[136] U. Sarma and S. Ganguly, "An energy management optimization approach for proton exchange membrane fuel cell-battery hybrid energy system for railway applications," *Electrical Engineering*, 2022.

[137] K. Deng, Y. Liu, D. Hai, H. Peng, L. Löwenstein, S. Pischinger, and K. Hameyer, "Deep reinforcement learning based energy management strategy of fuel cell hybrid railway vehicles considering fuel cell aging," *Energy Conversion and Management*, vol. 251, 2022.

[138] N. Bešinović, R. Goverde, G. Nicholson, and H. Steele, "Review of railway timetabling developments: planning phases, goals and future directions," Preprint available at https://www.researchgate.net/publication/353378414_Review_of_railway_timetabling_developments_planning_phases_goals_and_future_directions, July 2021.

[139] M. Hampaeyan Miandoab, V. Ghezavati, and D. Mohammaditabar, "Developing a simultaneous scheduling of passenger and freight trains for an inter-city railway considering optimization of carbon emissions and waiting times," *Journal of Cleaner Production*, vol. 248, p. 119303, 2020. [Online]. Available: https://www.sciencedirect.com/science/article/pii/S0959652619341733

[140] N. Zhao, C. Roberts, S. Hillmansen, and G. Nicholson, "A multiple train trajectory optimization to minimize energy consumption and delay," *IEEE Transactions on Intelligent Transportation Systems*, vol. 16, no. 5, pp. 2363–2372, 2015.

[141] X. Li and H. K. Lo, "An energy-efficient scheduling and speed control approach for metro rail operations," *Transportation Research Part B: Methodological*, vol. 64, pp. 73–89, 2014. [Online]. Available: https://www.sciencedirect.com/science/article/pii/S0191261514000484

[142] V. D. Martinis, U. Weidmann, and M. Gallo, "Towards a simulation-based framework for evaluating energy-efficient solutions in train operation," *WIT Transactions on the Built Environment*, 2014.

[143] J. Yang, X. Xu, Y. Peng, P. Deng, X. Wu, and J. Zhang, "Hierarchical energy management of a hybrid propulsion system considering speed profile optimization," *Energy*, vol. 244, 2022.

[144] K. Deng, T. Fang, H. Feng, H. Peng, L. Löwenstein, and K. Hameyer, "Hierarchical eco-driving and energy management control for hydrogen powered hybrid trains," *Energy Conversion and Management*, vol. 264, 2022.

[145] L. Zhou, L. Tong, J. Chen, J. Tang, and X. Zhou, "Joint optimization of high-speed train timetables and speed profiles: A unified modeling approach using space-time-speed grid networks," *Transportation Research Part B: Methodological*, vol. 97, pp. 157–181, 2017.

[146] P. Wang, N. Besinovic, R. M. P. Goverde, and F. Corman, "Improving the utilization of regenerative energy and shaving power peaks by railway timetable adjustment," *IEEE Transactions on Intelligent Transportation Systems*, vol. 23, no. 9, pp. 15 742–15 754, 2022.

[147] M. Miyatake and H. Ko, "Optimization of train speed profile for minimum energy consumption," *IEEJ Transactions on Electrical and Electronic Engineering*, vol. 5, no. 3, pp. 263–269, 2010. [Online]. Available: https://onlinelibrary.wiley.com/doi/abs/10.1002/tee.20528

[148] Y. Huang, L. Yang, T. Tang, Z. Gao, F. Cao, and K. Li, "Train speed profile optimization with on-board energy storage devices: A dynamic programming based approach," *Computers & Industrial Engineering*, vol. 126, pp. 149–164, 2018. [Online]. Available: https://www.sciencedirect.com/science/article/pii/S0360835218304406

[149] Z. Xiao, H. Chen, J. Guo, Q. Wang, P. Sun, and X. Feng, "Joint optimization of speed and voltage trajectories for hybrid electric trams," *IEEE Transactions on Industry Applications*, pp. 1–1, 2021.

[150] C. Wu, W. Zhang, S. Lu, Z. Tan, F. Xue, and J. Yang, "Train speed trajectory optimization with on-board energy storage device," *IEEE Transactions on Intelligent Transportation Systems*, vol. 20, no. 11, pp. 4092–4102, 2019.

[151] C. Wu, B. Xu, S. Lu, F. Xue, L. Jiang, and M. Chen, "Adaptive eco-driving strategy

and feasibility analysis for electric trains with on-board energy storage devices," *IEEE Transactions on Transportation Electrification*, pp. 1–1, 2021.

[152] C. Wu, S. Lu, F. Xue, L. Jiang, M. Chen, and J. Yang, "A two-step method for energy-efficient train operation, timetabling and on-board energy storage device management," *IEEE Transactions on Transportation Electrification*, pp. 1–1, 2021.

[153] G. Meng, C. Wu, B. Zhang, F. Xue, and S. Lu, "Net hydrogen consumption minimization of fuel cell hybrid trains using a time-based co-optimization model," *Energies*, vol. 15, no. 8, 2022.

[154] H. Peng, Y. Chen, Z. Chen, J. Li, K. Deng, A. Thul, L. Löwenstein, and K. Hameyer, "Co-optimization of total running time, timetables, driving strategies and energy management strategies for fuel cell hybrid trains," *eTransportation*, vol. 9, 2021.

[155] E. Tazelaar, B. Veenhuizen, J. Jagerman, and T. Faassen, "Energy management strategies for fuel cell hybrid vehicles; an overview," in *EVS27 International Battery, Hybrid and Fuel Cell Electric Vehicle Symposium*, 2013.

[156] O. Erdinc and M. Uzunoglu, "Recent trends in pem fuel cell-powered hybrid systems: Investigation of application areas, design architectures and energy management approaches," *Renewable and Sustainable Energy Reviews*, vol. 14, no. 9, pp. 2874–2884, 2010.

[157] N. Sulaiman, M. A. Hannan, A. Mohamed, P. J. Ker, E. H. Majlan, and W. R. Wan Daud, "Optimization of energy management system for fuel-cell hybrid electric vehicles: Issues and recommendations," *Applied Energy*, vol. 228, pp. 2061–2079, 2018.

[158] M. Yue, S. Jemei, R. Gouriveau, and N. Zerhouni, "Review on health-conscious energy management strategies for fuel cell hybrid electric vehicles: Degradation models and strategies," *International Journal of Hydrogen Energy*, vol. 44, no. 13, pp. 6844–6861, 2019.

[159] K. Song, F. Li, X. Hu, L. He, W. Niu, S. Lu, and T. Zhang, "Multi-mode energy management strategy for fuel cell electric vehicles based on driving pattern identification using learning vector quantization neural network algorithm," *Journal of Power Sources*, vol. 389, pp. 230–239, 2018.

[160] M. Sorrentino, V. Cirillo, and L. Nappi, "Development of flexible procedures for co-optimizing design and control of fuel cell hybrid vehicles," *Energy Conversion and Management*, vol. 185, pp. 537–551, 2019.

[161] M. Kandidayeni, A. Macias Fernandez, L. Boulon, and S. Kelouwani, "Efficiency upgrade of hybrid fuel cell vehicles' energy management strategies by online systemic management of fuel cell," *IEEE Transactions on Industrial Electronics*, pp. 1–1, 2020.

[162] H. Zhang, X. Li, X. Liu, and J. Yan, "Enhancing fuel cell durability for fuel cell plug-in hybrid electric vehicles through strategic power management," *Applied Energy*, vol. 241, pp. 483–490, 2019.

[163] V. Paladini, T. Donateo, A. de Risi, and D. Laforgia, "Super-capacitors fuel-cell hybrid electric vehicle optimization and control strategy development," *Energy Conversion and Management*, vol. 48, no. 11, pp. 3001–3008, 2007.

[164] L. Xu, F. Yang, J. Li, M. Ouyang, and J. Hua, "Real time optimal energy management strategy targeting at minimizing daily operation cost for a plug-in fuel cell city bus," *International Journal of Hydrogen Energy*, vol. 37, no. 20, pp. 15 380–15 392, 2012.

[165] J. Samir, C. Adnen, B. S. Sami, and V. E. Balas, "An efficient design of fuel cell electric vehicle with ultra-battery separated by an energy management system," in *2016 7th International Conference on Sciences of Electronics, Technologies of Information and Telecommunications (SETIT)*. IEEE, 2016.

[166] J.-J. Hwang, Y.-J. Chen, and J.-K. Kuo, "The study on the power management system in a fuel cell hybrid vehicle," *International Journal of Hydrogen Energy*, vol. 37, no. 5, pp. 4476–4489, 2012.

[167] H. Hemi, J. Ghouili, and A. Cheriti, "A real time energy management for electrical vehicle using combination of rule-based and ecms," in *2013 IEEE Electrical Power & Energy Conference*. IEEE, 2013.

[168] S. Changizian, P. Ahmadi, M. Raeesi, and N. Javani, "Performance optimization of hybrid hydrogen fuel cell-electric vehicles in real driving cycles," *International Journal of Hydrogen Energy*, 2020.

[169] D. Jannuzzi, "Use of supercapacitors, fuel cells and electrochemical batteries for electric road vehicles: A control strategy," in *33rd Annual Conference of the IEEE Industrial Electronics Society (IECON)*, 2007.

[170] K. Davis and J. G. Hayes, "Fuel cell vehicle energy management strategy based on the cost of ownership," *IET Electrical Systems in Transportation*, vol. 9, no. 4, pp. 226–236, 2019.

[171] A. Macias Fernandez, M. Kandidayeni, L. Boulon, and H. Chaoui, "An adaptive state machine based energy management strategy for a multi-stack fuel cell hybrid electric vehicle," *IEEE Transactions on Vehicular Technology*, vol. 69, no. 1, pp. 220–234, 2020.

[172] H. Hemi, J. Ghouili, and A. Cheriti, "A real time fuzzy logic power management strategy for a fuel cell vehicle," *Energy Conversion and Management*, vol. 80, pp. 63–70, 2014.

[173] A. Fadel and B. Zhou, "Power management methodologies for fuel cell-battery hybrid vehicles," *SAE International*, 2010.

[174] B. Tifour, B. Moussa, H. Ahmed, and T. Camel, "Monitoring and energy management approach for a fuel cell hybrid electric vehicle," *Diagnostyka*, pp. 15–29, 2020.

[175] Q. Li, W. Chen, Y. Li, S. Liu, and J. Huang, "Energy management strategy for

fuel cell/battery/ultracapacitor hybrid vehicle based on fuzzy logic," *International Journal of Electrical Power & Energy Systems*, vol. 43, no. 1, pp. 514–525, 2012.

[176] J. Solano Martínez, R. I. John, D. Hissel, and M.-C. Péra, "A survey-based type-2 fuzzy logic system for energy management in hybrid electrical vehicles," *Information Sciences*, vol. 190, pp. 192–207, 2012.

[177] J. Solano Martínez, J. Mulot, F. Harel, D. Hissel, M.-C. Péra, R. I. John, and M. Amiet, "Experimental validation of a type-2 fuzzy logic controller for energy management in hybrid electrical vehicles," *Engineering Applications of Artificial Intelligence*, vol. 26, no. 7, pp. 1772–1779, 2013.

[178] A. Ravey, B. Blunier, and A. Miraoui, "Control strategies for fuel-cell-based hybrid electric vehicles: From offline to online and experimental results," *IEEE Transactions on Vehicular Technology*, vol. 61, no. 6, pp. 2452–2457, 2012.

[179] S. Ahmadi, S. M. T. Bathaee, and A. H. Hosseinpour, "Improving fuel economy and performance of a fuel-cell hybrid electric vehicle (fuel-cell, battery, and ultracapacitor) using optimized energy management strategy," *Energy Conversion and Management*, vol. 160, pp. 74–84, 2018.

[180] S. Ahmadi and S. M. T. Bathaee, "Multi-objective genetic optimization of the fuel cell hybrid vehicle supervisory system: Fuzzy logic and operating mode control strategies," *International Journal of Hydrogen Energy*, vol. 40, no. 36, pp. 12 512–12 521, 2015.

[181] A. Ravey, A. Mohammadi, and D. Bouquain, "Control strategy of fuel cell electric vehicle including degradation process," in *IECON2015-Yokohama*, 2015.

[182] M. Zandi, A. Payman, J.-P. Martin, S. Pierfederici, B. Davat, and F. Meibody-Tabar, "Energy management of a fuel cell/supercapacitor/battery power source for electric vehicular applications," *IEEE Transactions on Vehicular Technology*, vol. 60, no. 2, pp. 433–443, 2011.

[183] R. Zhang and J. Tao, "Ga-based fuzzy energy management system for fc/sc-powered hev considering h2 consumption and load variation," *IEEE Transactions on Fuzzy Systems*, vol. 26, no. 4, pp. 1833–1843, 2018.

[184] R. Zhang, J. Tao, and H. Zhou, "Fuzzy optimal energy management for fuel cell and supercapacitor systems using neural network based driving pattern recognition," *IEEE Transactions on Fuzzy Systems*, vol. 27, no. 1, pp. 45–57, 2019.

[185] D. Zhou, A. Al-Durra, F. Gao, A. Ravey, I. Matraji, and M. Godoy Simões, "Online energy management strategy of fuel cell hybrid electric vehicles based on data fusion approach," *Journal of Power Sources*, vol. 366, pp. 278–291, 2017.

[186] M. Kandidayeni, A. O. Macias Fernandez, A. Khalatbarisoltani, L. Boulon, S. Kelouwani, and H. Chaoui, "An online energy management strategy for a fuel cell/battery vehicle considering the driving pattern and performance drift impacts," *IEEE Transactions on Vehicular Technology*, vol. 68, no. 12, pp. 11 427–11 438, 2019.

[187] M. Yue, S. Jemei, and N. Zerhouni, "Health-conscious energy management for fuel

cell hybrid electric vehicles based on prognostics-enabled decision-making," *IEEE Transactions on Vehicular Technology*, vol. 68, no. 12, pp. 11 483–11 491, 2019.

[188] X. Zhang, C. C. Mi, A. Masrur, and D. Daniszewski, "Wavelet-transform-based power management of hybrid vehicles with multiple on-board energy sources including fuel cell, battery and ultracapacitor," *Journal of Power Sources*, vol. 185, no. 2, pp. 1533–1543, 2008.

[189] M. Ibrahim, G. Wimmer, S. Jemei, and D. Hissel, "Energy management for a fuel cell hybrid electrical vehicle," in *IECON 2014 - 40th Annual Conference of the IEEE Industrial Electronics Society*. IEEE, 2014.

[190] K. Simmons, Y. Guezennec, and S. Onori, "Modeling and energy management control design for a fuel cell hybrid passenger bus," *Journal of Power Sources*, vol. 246, pp. 736–746, 2014.

[191] M. Ansarey, M. Shariat Panahi, H. Ziarati, and M. Mahjoob, "Optimal energy management in a dual-storage fuel-cell hybrid vehicle using multi-dimensional dynamic programming," *Journal of Power Sources*, vol. 250, pp. 359–371, 2014.

[192] A. M. Ali, A. Ghanbar, and D. Soffker, "Optimal control of multi-source electric vehicles in real time using advisory dynamic programming," *IEEE Transactions on Vehicular Technology*, vol. 68, no. 11, pp. 10 394–10 405, 2019.

[193] Y. Wang, S. J. Moura, S. G. Advani, and A. K. Prasad, "Power management system for a fuel cell/battery hybrid vehicle incorporating fuel cell and battery degradation," *International Journal of Hydrogen Energy*, vol. 44, no. 16, pp. 8479–8492, 2019.

[194] F. Martel, S. Kelouwani, Y. Dubé, and K. Agbossou, "Optimal economy-based battery degradation management dynamics for fuel-cell plug-in hybrid electric vehicles," *Journal of Power Sources*, vol. 274, pp. 367–381, 2015.

[195] F. Martel, Y. Dube, S. Kelouwani, and K. Agbossou, "Economy-focused phev battery lifetime management through optimal fuel cell load sharing," in *2015 IEEE Vehicle Power and Propulsion Conference (VPPC)*. IEEE, 2015.

[196] F. Herb, P. R. Akula, K. Trivedi, L. Jandhyala, A. Narayana, and M. Wöhr, "Theoretical analysis of energy management strategies for fuel cell electric vehicle with respect to fuel cell and battery aging," in *2013 World Electric Vehicle Symposium and Exhibition (EVS27)*. IEEE, 2013.

[197] W. Zhou, L. Yang, Y. Cai, and T. Ying, "Dynamic programming for new energy vehicles based on their work modes part ii: Fuel cell electric vehicles," *Journal of Power Sources*, vol. 407, pp. 92–104, 2018.

[198] S. Kelouwani, N. Henao, K. Agbossou, Y. Dube, and L. Boulon, "Two-layer energy-management architecture for a fuel cell hev using road trip information," *IEEE Transactions on Vehicular Technology*, vol. 61, no. 9, pp. 3851–3864, 2012.

[199] D. Fares, R. Chedid, F. Panik, S. Karaki, and R. Jabr, "Dynamic programming

technique for optimizing fuel cell hybrid vehicles," *International Journal of Hydrogen Energy*, vol. 40, no. 24, pp. 7777–7790, 2015.

[200] A. Schell, H. Peng, D. Tran, E. Stamos, C.-C. Lin, and M. J. Kim, "Modelling and control strategy development for fuel cell electric vehicles," *Annual Reviews in Control*, vol. 29, no. 1, pp. 159–168, 2005.

[201] C.-C. Lin, M.-J. Kim, H. Peng, and J. W. Grizzle, "System-level model and stochastic optimal control for a pem fuel cell hybrid vehicle," *Journal of Dynamic Systems, Measurement, and Control*, vol. 128, no. 4, pp. 878–890, 2006.

[202] M.-J. Kim and H. Peng, "Power management and design optimization of fuel cell/battery hybrid vehicles," *Journal of Power Sources*, vol. 165, no. 2, pp. 819–832, 2007.

[203] L. Serrao, A. Sciarretta, O. Grondin, A. Chasse, Y. Creff, D. Di Domenico, P. Pognant-Gros, C. Querel, and L. Thibault, "Open issues in supervisory control of hybrid electric vehicles: A unified approach using optimal control methods," *Oil & Gas Science and Technology – Revue d'IFP Energies nouvelles*, vol. 68, no. 1, pp. 23–33, 2013.

[204] C. H. Zheng, N. W. Kim, and S. W. Cha, "Optimal control in the power management of fuel cell hybrid vehicles," *International Journal of Hydrogen Energy*, vol. 37, no. 1, pp. 655–663, 2012.

[205] C. H. Zheng, G. Q. Xu, Y. I. Park, W. S. Lim, and S. W. Cha, "Prolonging fuel cell stack lifetime based on pontryagin's minimum principle in fuel cell hybrid vehicles and its economic influence evaluation," *Journal of Power Sources*, vol. 248, pp. 533–544, 2014.

[206] B. Geng, J. K. Mills, and D. Sun, "Two-stage energy management control of fuel cell plug-in hybrid electric vehicles considering fuel cell longevity," *IEEE Transactions on Vehicular Technology*, vol. 61, no. 2, pp. 498–508, 2012.

[207] K. Ettihir, L. Boulon, and K. Agbossou, "Optimization-based energy management strategy for a fuel cell/battery hybrid power system," *Applied Energy*, vol. 163, pp. 142–153, 2016.

[208] K. Ettihir, M. Higuita Cano, L. Boulon, and K. Agbossou, "Design of an adaptive ems for fuel cell vehicles," *International Journal of Hydrogen Energy*, vol. 42, no. 2, pp. 1481–1489, 2017.

[209] B. J., D. S., B. F., and G. T.M., "Global optimisation in the power management of a fuel cell hybrid vehicle (fchv)," in *2006 IEEE Vehicle Power and Propulsion Conference*. IEEE, 2006.

[210] F. Odeim, J. Roes, L. Wülbeck, and A. Heinzel, "Power management optimization of fuel cell/battery hybrid vehicles with experimental validation," *Journal of Power Sources*, vol. 252, pp. 333–343, 2014.

[211] C. Liu and L. Liu, "Optimal power source sizing of fuel cell hybrid vehicles based

on pontryagin's minimum principle," *International Journal of Hydrogen Energy*, vol. 40, no. 26, pp. 8454–8464, 2015.

[212] C.-Y. Li and G.-P. Liu, "Optimal fuzzy power control and management of fuel cell/battery hybrid vehicles," *Journal of Power Sources*, vol. 192, no. 2, pp. 525–533, 2009.

[213] R. Dinnawi, D. Fares, R. Chedid, S. Karaki, and R. A. Jabr, "Optimized energy management system for fuel cell hybrid vehicles," in *17th IEEE Mediterranean Electrotechnical Conference*. IEEE, 2014.

[214] D. Fares, R. Chedid, S. Karaki, R. Jabr, F. Panik, H. Gabele, and Y. Huang, "Optimal power allocation for a fchv based on linear programming and pid controller," *International Journal of Hydrogen Energy*, vol. 39, no. 36, pp. 21 724–21 738, 2014.

[215] V. Paladini, T. Donateo, A. de Risi, and D. Laforgia, "Control strategy optimization of a fuel-cell electric vehicle," *Journal of Fuel Cell Science and Technology*, vol. 5, no. 2, 2008.

[216] R. Álvarez Fernández, S. Corbera Caraballo, F. Beltrán Cilleruelo, and J. A. Lozano, "Fuel optimization strategy for hydrogen fuel cell range extender vehicles applying genetic algorithms," *Renewable and Sustainable Energy Reviews*, vol. 81, pp. 655–668, 2018.

[217] M. J. Gielniak and Z. J. Shen, "Power management strategy based on game theory for fuel cell hybrid electric vehicles," *IEEE 60th Vehicular Technology Conference*, 2004.

[218] L. Xu, J. Li, J. Hua, X. Li, and M. Ouyang, "Optimal vehicle control strategy of a fuel cell/battery hybrid city bus," *International Journal of Hydrogen Energy*, vol. 34, no. 17, pp. 7323–7333, 2009.

[219] P. Rodatz, G. Paganelli, A. Sciarretta, and L. Guzzella, "Optimal power management of an experimental fuel cell/supercapacitor-powered hybrid vehicle," *Control Engineering Practice*, vol. 13, no. 1, pp. 41–53, 2005.

[220] L. Xu, J. Li, J. Hua, X. Li, and M. Ouyang, "Adaptive supervisory control strategy of a fuel cell/battery-powered city bus," *Journal of Power Sources*, vol. 194, no. 1, pp. 360–368, 2009.

[221] J. Bernard, S. Delprat, T. M. Guerra, and F. N. Büchi, "Fuel efficient power management strategy for fuel cell hybrid powertrains," *Control Engineering Practice*, vol. 18, no. 4, pp. 408–417, 2010.

[222] M. G. Carignano, R. Costa-Castelló, V. Roda, N. M. Nigro, S. Junco, and D. Feroldi, "Energy management strategy for fuel cell-supercapacitor hybrid vehicles based on prediction of energy demand," *Journal of Power Sources*, vol. 360, pp. 419–433, 2017.

[223] H. Li, A. Ravey, A. N'Diaye, and A. Djerdir, "A novel equivalent consumption minimization strategy for hybrid electric vehicle powered by fuel cell, battery and supercapacitor," *Journal of Power Sources*, vol. 395, pp. 262–270, 2018.

[224] G. Paganelli, T. M. Guerra, S. Delprat, Y. Guezennec, and G. Rizzoni, "Optimal control theory applied to hybrid fuel cell powered vehicle," *IFAC Proceedings Volumes*, vol. 35, no. 1, pp. 253–258, 2002.

[225] Y. Liu, J. Li, Z. Chen, D. Qin, and Y. Zhang, "Research on a multi-objective hierarchical prediction energy management strategy for range extended fuel cell vehicles," *Journal of Power Sources*, vol. 429, pp. 55–66, 2019.

[226] Y. Guezennec, T.-y. Choi, G. Paganelli, and G. Rizzoni, "Supervisory control of fuel cell vehicles and its link to overall system efficiency and low-level control requirements," in *Proceedings of the 2003 American Control Conference.* IEEE, 2003.

[227] H. Li, A. Ravey, A. N'Diaye, and A. Djerdir, "Online adaptive equivalent consumption minimization strategy for fuel cell hybrid electric vehicle considering power sources degradation," *Energy Conversion and Management*, vol. 192, pp. 133–149, 2019.

[228] Q. Chen, L. Gao, R. A. Dougal, and S. Quan, "Multiple model predictive control for a hybrid proton exchange membrane fuel cell system," *Journal of Power Sources*, vol. 191, no. 2, pp. 473–482, 2009.

[229] X. Hu, C. Zou, X. Tang, T. Liu, and L. Hu, "Cost-optimal energy management of hybrid electric vehicles using fuel cell/battery health-aware predictive control," *IEEE Transactions on Power Electronics*, vol. 35, no. 1, pp. 382–392, 2020.

[230] A. Serpi and M. Porru, "Modelling and design of real-time energy management systems for fuel cell/battery electric vehicles," *Energies*, vol. 12, no. 22, 2019.

[231] V. Puig, R. Costa-Castello, and J. L. Sampietro3, "Economic mpc for the energy management of hybrid vehicles including fuel cells and supercapacitors," in *2016 UKACC 11th International Conference on Control (CONTROL)*, 2016.

[232] Y. Zhou, A. Ravey, and M.-C. Péra, "Multi-mode predictive energy management for fuel cell hybrid electric vehicles using markov driving pattern recognizer," *Applied Energy*, vol. 258, 2020.

[233] A. Arce, A. J. del Real, and C. Bordons, "Mpc for battery/fuel cell hybrid vehicles including fuel cell dynamics and battery performance improvement," *Journal of Process Control*, vol. 19, no. 8, pp. 1289–1304, 2009.

[234] Q. Guo, Z. Zhao, P. Shen, and P. Zhou, "Optimization management of hybrid energy source of fuel cell truck based on model predictive control using traffic light information," *Control Theory and Technology*, vol. 17, no. 4, pp. 309–324, 2019.

[235] A. Dalvi and M. Guay, "Control and real-time optimization of an automotive hybrid fuel cell power system," *Control Engineering Practice*, vol. 17, no. 8, pp. 924–938, 2009.

[236] D. Zhou, A. Ravey, A. Al-Durra, and F. Gao, "A comparative study of extremum seeking methods applied to online energy management strategy of fuel cell hybrid electric vehicles," *Energy Conversion and Management*, vol. 151, pp. 778–790, 2017.

[237] D. Zhou, A. Al-Durra, I. Matraji, A. Ravey, and F. Gao, "Online energy management strategy of fuel cell hybrid electric vehicles: A fractional-order extremum seeking method," *IEEE Transactions on Industrial Electronics*, vol. 65, no. 8, pp. 6787–6799, 2018.

[238] C. Majed, S. H. Karaki, and R. Jabr, "Neural network technique for hybrid electric vehicle optimization," in *2016 18th Mediterranean Electrotechnical Conference (MELECON)*. IEEE, 2016.

[239] Y. Ates, O. Erdinc, M. Uzunoglu, and B. Vural, "Energy management of an fc/uc hybrid vehicular power system using a combined neural network-wavelet transform based strategy," *International Journal of Hydrogen Energy*, vol. 35, no. 2, pp. 774–783, 2010.

[240] P. M. Muñoz, G. Correa, M. E. Gaudiano, and D. Fernández, "Energy management control design for fuel cell hybrid electric vehicles using neural networks," *International Journal of Hydrogen Energy*, vol. 42, no. 48, pp. 28 932–28 944, 2017.

[241] W.-S. Lin and C.-H. Zheng, "Energy management of a fuel cell/ultracapacitor hybrid power system using an adaptive optimal-control method," *Journal of Power Sources*, vol. 196, no. 6, pp. 3280–3289, 2011.

[242] N. P. Reddy, D. Pasdeloup, M. K. Zadeh, and R. Skjetne, "An intelligent power and energy management system for fuel cell/battery hybrid electric vehicle using reinforcement learning," in *2019 IEEE Transportation Electrification Conference and Expo (ITEC)*. IEEE, 2019.

[243] R. C. Hsu, S.-M. Chen, W.-Y. Chen, and C.-T. Liu, "A reinforcement learning based dynamic power management for fuel cell hybrid electric vehicle," in *2016 Joint 8th International Conference on Soft Computing and Intelligent Systems (SCIS) and 17th International Symposium on Advanced Intelligent Systems (ISIS)*. IEEE, 2016.

[244] J. Yuan, L. Yang, and Q. Chen, "Intelligent energy management strategy based on hierarchical approximate global optimization for plug-in fuel cell hybrid electric vehicles," *International Journal of Hydrogen Energy*, vol. 43, no. 16, pp. 8063–8078, 2018.

[245] H. Sun, Z. Fu, F. Tao, L. Zhu, and P. Si, "Data-driven reinforcement-learning-based hierarchical energy management strategy for fuel cell/battery/ultracapacitor hybrid electric vehicles," *Journal of Power Sources*, vol. 455, 2020.

[246] T. Gole, A. Hange, R. Dhar, A. Bhurke, and F. Kazi, "Reinforcement learning based energy management in hybrid electric vehicle," in *2019 International Conference on Power Electronics, Control and Automation (ICPECA)*. IEEE, 2019.

[247] M. Kandidayeni, A. Macias, L. Boulon, and S. Kelouwani, "Investigating the impact of ageing and thermal management of a fuel cell system on energy management strategies," *Applied Energy*, vol. 274, 2020.

[248] M. Carignano, V. Roda, R. Costa-Castello, L. Valino, A. Lozano, and F. Barreras,

"Assessment of energy management in a fuel cell/battery hybrid vehicle," *IEEE Access*, vol. 7, pp. 16 110–16 122, 2019.

[249] A. Santucci, A. Sorniotti, and C. Lekakou, "Power split strategies for hybrid energy storage systems for vehicular applications," *Journal of Power Sources*, vol. 258, pp. 395–407, 2014.

[250] H. Lim and W. Su, "Hierarchical energy management for power-split plug-in hevs using distance-based optimized speed and soc profiles," *IEEE Transactions on Vehicular Technology*, vol. 67, no. 10, pp. 9312–9323, 2018.

[251] Z. Li, L. Chen, C. Roberts, and N. Zhao, "Dynamic trajectory optimization design for railway driver advisory system," *IEEE Intelligent Transportation Systems Magazine*, vol. 10, no. 1, pp. 121–132, 2018.

[252] L. Serrao, S. Onori, and G. Rizzoni, "Ecms as a realization of pontryagin's minimum principle for hev control," in *2009 American Control Conference*. IEEE, 2009.

[253] A. H. Ganesh and B. Xu, "A review of reinforcement learning based energy management systems for electrified powertrains: Progress, challenge, and potential solution," *Renewable and Sustainable Energy Reviews*, vol. 154, p. 111833, 2022.

[254] L. Hewing, K. P. Wabersich, M. Menner, and M. N. Zeilinger, "Learning-based model predictive control: Toward safe learning in control," *Annual Review of Control, Robotics, and Autonomous Systems*, vol. 3, pp. 269–296, 2020.

[255] G. Li, W. Zhuang, G. Yin, Y. Ren, and Y. Ding, "Energy management strategy and size optimization of a lfp/lto hybrid battery system for electric vehicle," *SAE Technical Paper Series*, 2019.

[256] M. Dubarry and B. Y. Liaw, "Identify capacity fading mechanism in a commercial lifepo4 cell," *Journal of Power Sources*, vol. 194, no. 1, pp. 541–549, 2009.

[257] I. Carrilero, D. Anseán, J. C. Viera, Y. Fernández, and M. González, "Impact of fast-charging and regenerative braking in lifepo4 batteries for electric bus applications," in *2017 IEEE Vehicle Power and Propulsion Conference (VPPC)*, 2017.

[258] S. B. Peterson, J. Apt, and J. F. Whitacre, "Lithium-ion battery cell degradation resulting from realistic vehicle and vehicle-to-grid utilization," *Journal of Power Sources*, vol. 195, no. 8, pp. 2385–2392, 2010.

[259] M. Koller, T. Borsche, A. Ulbig, and G. Andersson, "Defining a degradation cost function for optimal control of a battery energy storage system," in *2013 IEEE Grenoble Conference*. IEEE.

[260] T. M. Padovani, M. Debert, G. Colin, and Y. Chamaillard, "Optimal energy management strategy including battery health through thermal management for hybrid vehicles," in *7th IFAC Symposium on Advances in Automotive Control*. Elsevier, 2013.

[261] L. De Pascali, F. Biral, and S. Onori, "Aging-aware optimal energy management control for a parallel hybrid vehicle based on electrochemical-degradation dynamics," *IEEE Transactions on Vehicular Technology*, pp. 1–1, 2020.

[262] X. Jin, A. P. Vora, V. Hoshing, T. Saha, G. M. Shaver, O. Wasynczuk, and S. Varigonda, "Comparison of li-ion battery degradation models for system design and control algorithm development," in *2017 American Control Conference*, 2017.

[263] B. Gao, L. Guo, Q. Zheng, B. Huang, and H. Chen, "Acceleration speed optimization of intelligent evs in consideration of battery aging," *IEEE Transactions on Vehicular Technology*, vol. 67, no. 9, pp. 8009–8018, 2018.

[264] X. Jin, A. Vora, V. Hoshing, T. Saha, G. Shaver, R. E. García, O. Wasynczuk, and S. Varigonda, "Physically-based reduced-order capacity loss model for graphite anodes in li-ion battery cells," *Journal of Power Sources*, vol. 342, pp. 750–761, 2017.

[265] S. Mohajer, J. Sabatier, P. Lanusse, and o. Cois, "A fractional-order electro-thermal aging model for lifetime enhancement of lithium-ion batteries," in *9th Vienna International Conference on Mathematical Modelling*, ser. IFAC-PapersOnLine, vol. 51. Elsevier, 2018, Conference Proceedings, pp. 220–225.

[266] S. Ebbesen, P. Elbert, and L. Guzzella, "Battery state-of-health perceptive energy management for hybrid electric vehicles," *IEEE Transactions on Vehicular Technology*, vol. 61, no. 7, pp. 2893–2900, 2012.

[267] T. H. Pham, J. T. B. A. Kessels, P. P. J. van den Bosch, and R. G. M. Huisman, "Analytical solution to energy management guaranteeing battery life for hybrid trucks," *IEEE Transactions on Vehicular Technology*, vol. 65, no. 10, pp. 7956–7971, 2016.

[268] X. Wang, S. Ma, and J. Wang, "Predictive energy management for hybrid electric vehicles considering extension of the battery life," *Proceedings of the Institution of Mechanical Engineers, Part D: Journal of Automobile Engineering*, vol. 232, no. 4, pp. 499–510, 2017.

[269] L. Xu, C. D. Mueller, J. Li, M. Ouyang, and Z. Hu, "Multi-objective component sizing based on optimal energy management strategy of fuel cell electric vehicles," *Applied Energy*, vol. 157, pp. 664–674, 2015.

[270] Z. Hu, J. Li, L. Xu, Z. Song, C. Fang, M. Ouyang, G. Dou, and G. Kou, "Multi-objective energy management optimization and parameter sizing for proton exchange membrane hybrid fuel cell vehicles," *Energy Conversion and Management*, vol. 129, pp. 108–121, 2016.

[271] H. Jiang, L. Xu, J. Li, Z. Hu, and M. Ouyang, "Energy management and component sizing for a fuel cell/battery/supercapacitor hybrid powertrain based on two-dimensional optimization algorithms," *Energy*, vol. 177, pp. 386–396, 2019.

[272] F. Martel, Y. Dubé, S. Kelouwani, J. Jaguemont, and K. Agbossou, "Long-term assessment of economic plug-in hybrid electric vehicle battery lifetime degradation management through near optimal fuel cell load sharing," *Journal of Power Sources*, vol. 318, pp. 270–282, 2016.

[273] E. Martinez-Laserna, V. Herrera, I. Gandiaga, A. Milo, E. Sarasketa-Zabala, and H. Gaztañaga, "Li-ion battery lifetime model's influence on the economic assessment

of a hybrid electric bus's operation," *World Electric Vehicle Journal*, vol. 9, no. 2, 2018.

[274] E. Sarasketa-Zabala, I. Gandiaga, E. Martinez-Laserna, L. M. Rodriguez-Martinez, and I. Villarreal, "Cycle ageing analysis of a lifepo4/graphite cell with dynamic model validations: Towards realistic lifetime predictions," *Journal of Power Sources*, vol. 275, pp. 573–587, 2015.

[275] F. Jin, M. Wang, and C. Hu, "A fuzzy logic based power management strategy for hybrid energy storage system in hybrid electric vehicles considering battery degradation," in *2016 IEEE Transportation Electrification Conference and Expo (ITEC)*. IEEE, 2016.

[276] A. Hoke, A. Brissette, D. Maksimović, A. Pratt, and K. Smith, "Electric vehicle charge optimization including effects of lithium-ion battery degradation," in *2011 IEEE Vehicle Power and Propulsion Conference*. IEEE, 2011.

[277] L. Serrao, S. Onori, A. Sciarretta, Y. Guezennec, and G. Rizzoni, "Optimal energy management of hybrid electric vehicles including battery aging," in *Proceedings of the 2011 American Control Conference*. IEEE, 2011.

[278] V. Marano, S. Onori, Y. Guezennec, G. Rizzoni, and N. Madella, "Lithium-ion batteries life estimation for plug-in hybrid electric vehicles," in *2009 IEEE Vehicle Power and Propulsion Conference*. IEEE, 2009.

[279] S. Sabatini and M. Corno, "Battery aging management for fully electric vehicles," in *2018 European Control Conference (ECC)*. IEEE, 2018.

[280] L. Tang, "Optimal energy management strategy for hybrid electric vehicles with consideration of battery life," Thesis, The Ohio State University, 2017.

[281] G. Suri and S. Onori, "A control-oriented cycle-life model for hybrid electric vehicle lithium-ion batteries," *Energy*, vol. 96, pp. 644–653, 2016.

[282] O. Arslan, B. Yıldız, and O. E. Karaşan, "Minimum cost path problem for plug-in hybrid electric vehicles," *Transportation Research Part E: Logistics and Transportation Review*, vol. 80, pp. 123–141, 2015.

[283] P. Ramadass, B. Haran, P. M. Gomadam, R. White, and B. N. Popov, "Development of first principles capacity fade model for li-ion cells," *Journal of The Electrochemical Society*, vol. 151, no. 2, 2004.

[284] X. Ma, Y. Zhang, C. Yin, and S. Yuan, "Multi-objective optimization considering battery degradation for a multi-mode power-split electric vehicle," *Energies*, vol. 10, no. 7, 2017.

[285] R. D. Perkins, A. V. Randall, X. Zhang, and G. L. Plett, "Controls oriented reduced order modeling of lithium deposition on overcharge," *Journal of Power Sources*, vol. 209, pp. 318–325, 2012.

[286] F. Xu, X. Jiao, M. Sasaki, and Y. Wang, "Energy management optimization in consideration of battery deterioration for commuter plug-in hybrid electric vehicle,"

in *2016 55th Annual Conference of the Society of Instrument and Control Engineers of Japan (SICE)*. IEEE, 2016.

[287] F. Xu, X. Jiao, Y. Wang, and Y. Jing, "Battery-lifetime-conscious energy management strategy based on sp-sdp for commuter plug-in hybrid electric vehicles," *IEEJ Transactions on Electrical and Electronic Engineering*, vol. 13, no. 3, pp. 472–479, 2018.

[288] H. Wenzl, A. Haubrock, and H.-P. Beck, "Degradation of lithium ion batteries under complex conditions of use," *Zeitschrift für Physikalische Chemie*, vol. 227, no. 1, pp. 57–72, 2013.

[289] J. Schmalstieg, S. Käbitz, M. Ecker, and D. U. Sauer, "A holistic aging model for li(nimnco)o2 based 18650 lithium-ion batteries," *Journal of Power Sources*, vol. 257, pp. 325–334, 2014.

[290] I. Baghdadi, O. Briat, J.-Y. Delétage, P. Gyan, and J.-M. Vinassa, "Lithium battery aging model based on dakin's degradation approach," *Journal of Power Sources*, vol. 325, pp. 273–285, 2016.

[291] J. de Hoog, J.-M. Timmermans, D. Ioan-Stroe, M. Swierczynski, J. Jaguemont, S. Goutam, N. Omar, J. Van Mierlo, and P. Van Den Bossche, "Combined cycling and calendar capacity fade modeling of a nickel-manganese-cobalt oxide cell with real-life profile validation," *Applied Energy*, vol. 200, pp. 47–61, 2017.

[292] I. Bloom, B. Colea, J. Sohna, S. Jonesa, E. Polzina, V. Battagliaa, G. Henriksena, C. Motlochb, R. Richardsonb, T. Unkelhaeuserc, D. Ingersollc, and H. Casec, "An accelerated calendar and cycle life study of li-ion cells," *Journal of Power Sources*, vol. 101, no. 2, pp. 238–247, 2001.

[293] K. Miettinen, *Nonlinear multiobjective optimization*, ser. International series in operations research & management science. Boston: Kluwer Academic Publishers, 1999. [Online]. Available: Publisherdescriptionhttp://www.loc.gov/catdir/enhancements/fy0819/98037888-d.htmlTableofcontentsonlyhttp://www.loc.gov/catdir/enhancements/fy0819/98037888-t.html

[294] Z. Khalik, T. Romijn, M. Donkers, and S. Weiland, "Effects of battery charge acceptance and battery aging in complete vehicle energy management," in *20th IFAC World Congress*. Elsevier, 2017.

[295] A. D. Filippi, S. Stockar, S. Onori, M. Canova, and Y. Guezennec, "Model-based life estimation of li-ion batteries in phevs using large scale vehicle simulations: An introductory study," in *2010 IEEE Vehicle Power and Propulsion Conference*. IEEE, 2010.

[296] J. Kim, Y. Park, J. D. Fox, S. Boyd, and W. Dally, "Optimal operation of a plug-in hybrid vehicle with battery thermal and degradation model," in *2020 American Control Conference*, 2020.

[297] S. Bauer, A. Suchaneck, and F. Puente León, "Thermal and energy battery management optimization in electric vehicles using pontryagin's maximum principle," *Journal of Power Sources*, vol. 246, pp. 808–818, 2014.

[298] C. Wei, T. Hofman, E. I. Caarls, and R. v. Iperen, "Zone model predictive control for battery thermal management including battery aging and brake energy recovery in electrified powertrains," in *9th IFAC Symposium on Advances in Automotive Control AAC 2019*, 2019.

[299] P. Pei and H. Chen, "Main factors affecting the lifetime of proton exchange membrane fuel cells in vehicle applications: A review," *Applied Energy*, vol. 125, pp. 60–75, 2014.

[300] X. Hu, J. Jiang, B. Egardt, and D. Cao, "Advanced power-source integration in hybrid electric vehicles: Multicriteria optimization approach," *IEEE Transactions on Industrial Electronics*, vol. 62, no. 12, pp. 7847–7858, 2015.

[301] X. Hu, N. Murgovski, L. M. Johannesson, and B. Egardt, "Optimal dimensioning and power management of a fuel cell/battery hybrid bus via convex programming," *IEEE/ASME Transactions on Mechatronics*, vol. 20, no. 1, pp. 457–468, 2015.

[302] Y. Yan, Q. Li, W. Chen, W. Huang, and J. Liu, "Hierarchical management control based on equivalent fitting circle and equivalent energy consumption method for multiple fuel cells hybrid power system," *IEEE Transactions on Industrial Electronics*, vol. 67, no. 4, pp. 2786–2797, 2020.

[303] S. G. Rinaldo, J. Stumper, and M. Eikerling, "Physical theory of platinum nanoparticle dissolution in polymer electrolyte fuel cells," *The Journal of Physical Chemistry C*, vol. 114, pp. 5773–5785, 2010.

[304] R. M. Darling and J. P. Meyers, "Kinetic model of platinum dissolution in pemfcs," *Journal of The Electrochemical Society*, vol. 150, no. 11, 2003.

[305] R. Chandrasekaran, W. Bi, and T. F. Fuller, "Robust design of battery/fuel cell hybrid systems—methodology for surrogate models of pt stability and mitigation through system controls," *Journal of Power Sources*, vol. 182, no. 2, pp. 546–557, 2008.

[306] W. Bi and T. F. Fuller, "Modeling of pem fuel cell pt/c catalyst degradation," *Journal of Power Sources*, vol. 178, no. 1, pp. 188–196, 2008.

[307] D. V. Ngo, T. Hofman, M. Steinbuch, and A. F. A. Serrarens, "An optimal control-based algorithm for hybrid electric vehicle using preview route information," in *Proceedings of the 2010 American Control Conference*. IEEE, 2010.

[308] L. Johannesson, N. Murgovski, E. Jonasson, J. Hellgren, and B. Egardt, "Predictive energy management of hybrid long-haul trucks," *Control Engineering Practice*, vol. 41, pp. 83–97, 2015.

[309] S. Uebel, N. Murgovski, B. Baker, and J. Sjoberg, "A two-level mpc for energy management including velocity control of hybrid electric vehicles," *IEEE Transactions on Vehicular Technology*, vol. 68, no. 6, pp. 5494–5505, 2019.

[310] D. Maamria, K. Gillet, G. Colin, Y. Chamaillard, and C. Nouillant, "Computation of eco-driving cycles for hybrid electric vehicles: Comparative analysis," *Control Engineering Practice*, vol. 71, pp. 44–52, 2018.

[311] T. v. Keulen, B. d. Jager, and M. Steinbuch, "Optimal trajectories for vehicles with energy recovery options," in *18th IFAC World Congress*, vol. 44, 2011.

[312] B. Chen, S. A. Evangelou, and R. Lot, "Series hybrid electric vehicle simultaneous energy management and driving speed optimization," *IEEE/ASME Transactions on Mechatronics*, vol. 24, no. 6, pp. 2756–2767, 2019.

[313] Z. Khalik, G. Padilla, T. Romijn, and M. Donkers, "Vehicle energy management with ecodriving: A sequential quadratic programming approach with dual decomposition," in *2018 Annual American Control Conference (ACC)*. IEEE, 2018.

[314] Y. Kim, M. Figueroa-Santos, N. Prakash, S. Baek, J. B. Siegel, and D. M. Rizzo, "Co-optimization of speed trajectory and power management for a fuel-cell/battery electric vehicle," *Applied Energy*, vol. 260, 2020.

[315] Z. Shuofeng, M. R. Amini, J. Sun, and C. Mi, "A two-layer real-time optimization control strategy for integrated battery thermal management and hvac system in connected and automated hevs," *IEEE Transactions on Vehicular Technology*, vol. 70, no. 7, pp. 6567–6576, 2021.

[316] B. Chen, X. Li, S. A. Evangelou, and R. Lot, "Joint propulsion and cooling energy management of hybrid electric vehicles by optimal control," *IEEE Transactions on Vehicular Technology*, vol. 69, no. 5, pp. 4894–4906, 2020.

[317] Gurobi Optimization, "Quadratic constraints," 2024. [Online]. Available: https://www.gurobi.com/documentation/current/refman/quadratic_constraints.html

[318] H. Douglas, P. Weston, D. Kirkwood, S. Hillmansen, and C. Roberts, "Method for validating the train motion equations used for passenger rail vehicle simulation," *Proceedings of the Institution of Mechanical Engineers, Part F: Journal of Rail and Rapid Transit*, vol. 231, no. 4, pp. 455–469, 2016.

[319] K. B. Wipke, M. R. Cuddy, and S. D. Burch, "Advisor 2.1: A user-friendly advanced powertrain simulation using a combined backward/forward approach," *IEEE Transactions on Vehicular Technology*, vol. 48, no. 6, 1999.

[320] B. Thorstensen, "A parametric study of fuel cell system efficiency under full and part load operation," *Journal of Power Sources*, vol. 92, pp. 9–16, 2000.

[321] S. Pelletier, O. Jabali, G. Laporte, and M. Veneroni, "Battery degradation and behaviour for electric vehicles: Review and numerical analyses of several models," *Transportation Research Part B: Methodological*, vol. 103, pp. 158–187, 2017.

[322] N. Ghaviha, M. Bohlin, C. Holmberg, and E. Dahlquist, "Speed profile optimization of catenary-free electric trains with lithium-ion batteries," *Journal of Modern Transportation*, vol. 27, no. 3, pp. 153–168, 2019.

[323] L. Liberti and N. Maculan, *Global optimization: from theory to implementation*. Springer Science & Business Media, 2006, vol. 84.

[324] M. Lipscomb, "Tees valley hydrogen trains," in *Digital Stakeholders Workshop HyTunnel-CS Project*, 2020, Conference Proceedings.

[325] D. Westcough and M. Lipscomb, "Development of a passenger rail traction decarbonisation strategy," Railway Industry Association, Report, 2020. [Online]. Available: https://smarttransportpub.blob.core.windows.net/web/1/root/nril-development-of-a-passenger-rail-traction-decarbonisation-strategy.pdf

[326] C. Calvert, J. Allan, P. Amor, S. Hillmansen, C. Roberts, and P. Weston, "Concept development and testing of the uk's first hydrogen-hybrid train (hydroflex)," *Railway Engineering Science*, vol. 29, no. 3, pp. 248–257, 2021. [Online]. Available: https://doi.org/10.1007/s40534-021-00256-9

[327] Gurobi Optimization, LLC, "Gurobi Optimizer Reference Manual," 2023. [Online]. Available: https://www.gurobi.com

[328] T. Letrouve, A. Pam, P. Aubin, A. Verdicchio, L. Planchette, S. Bayoudh, and F. Lheriau, "Stabilization of electric supply network with the electric flexibility of on-board hvac system," in *World Congress on Railway Research*, 2022, Conference Proceedings.

[329] Y. Guan, Z. Q. Zhu, I. Afinowi, J. Mipo, and P.Farah, "Difference in maximum torque-speed characteristics of induction machine between motor and generator operation modes for electric vehicle application," in *2014 International Conference on Electrical Machines (ICEM)*. IEEE, 2014, Conference Proceedings.

[330] Ballard, "Fcvelocity-hd100," https://www.ballard.com/about-ballard/publication_library/product-specification-sheets/fcvelocity-hd-spec-sheet.

[331] A. Farmann, W. Waag, and D. U. Sauer, "Application-specific electrical characterization of high power batteries with lithium titanate anodes for electric vehicles," *Energy*, vol. 112, pp. 294–306, 2016.

[332] "Summer school success: rail decarbonisation," University of Birmingham, August 2023, accessed: 2023-09-10. [Online]. Available: https://www.birmingham.ac.uk/news/2023/summer-school-success-rail-decarbonisation

[333] "Cilt freight electrification map," Chartered Institute of Logistics and Transport, Report, 2023.

A SIMULATED TRAIN

A.1 Physical Parameters

Table A.1: Physical parameters of simulated train.

Vehicle		Motor		Fuel Cell		Battery	
m	150 t	$\overline{F_\mathrm{m}}$	87 kN	$\overline{P_\mathrm{fc}}$	400 kW	U_oc	600 V
λ	0.0625	$\underline{F_\mathrm{m}}$	−87 kN	$\underline{P_\mathrm{fc}}$	24 kW	Q	375 Ah
a	1.743 kN	$\overline{P_\mathrm{m}}$	700 kW	LHV	120 MJ · kg^{-1}	R_bat	14.4 mΩ
b	76.4 kg · s^{-1}	$\underline{P_\mathrm{m}}$	−770 kW			$\underline{\zeta}$	20%
c	6.2 kg · m^{-1}					$\overline{\zeta}$	80%
P_aux	100 kW					$\overline{P_\mathrm{batt}}$	650 kW
$\underline{F_\mathrm{brk}}$	−147 kN					$\underline{P_\mathrm{batt}}$	−600 kW

Explanation of Motor Parameters Electric machines posses an asymmetric torque-speed curve between motoring and generation modes, more specifically the magnitude of the curve is higher in generation than motoring. Therefore, the magnitude of the negative power limit was set 10% higher than nominal positive. The positive and negative traction forces were set equal. This is plotted in Fig. 4.3, aligning with the induction motor trends demonstrated in [329, Fig. 15].

Explanation of Fuel Cell Parameters The fuel cell power limits were computed by assuming four units of the Ballard FVveloCity HD100 [330]. Each has a lower power limit of 6 kW and upper power limit of 100 kW which leads to total limits $\overline{P_\mathrm{fc}}$ 24 kW and $\overline{P_\mathrm{fc}}$ 400 kW.

Explanation of Battery Parameters The battery pack has a capacity of at least 220 kWh at an open-circuit voltage of 600 V. This is a capacity of at least 366 Ah. An LTO cell was assumed to have an open-circuit voltage of 2.5 V, internal resistance of 14.4 mΩ and capacity of 15Ah [331]. Therefore, 240 cells in series are required to achieve the open-circuit voltage (240*2.5V=600V), and 25 modules in parallel are required to achieve the required capacity (25*15Ah = 375Ah). The battery's equivalent internal resistance is $240 * 14.4\,\mathrm{m\Omega}/25 = 138.24\,\mathrm{m\Omega}$.

The battery's power is limited by (4.32). This computes to $600\,\mathrm{V}^2/(4 * 138.24\,\mathrm{m\Omega}) = 651\,\mathrm{kW}$. Therefore, 650 kW was chosen for the discharge limit, whereas −600 kW was used for the charging limit to reduce battery degradation. The discharge limit is adequate along the fuel cell's power limit of 400 kW in providing for $\overline{P_\mathrm{m}}$ and P_aux.

A.2 Polynomial Parameters

Table A.2: Polynomial parameters of simulated train.

$q_\mathrm{m}(F_\mathrm{trc})$ (5.31)		$q_\mathrm{fc}(P_\mathrm{fc})$ (5.13)		$q_\mathrm{fc}(F_\mathrm{fc})$ (5.38)	
p_{02}	$3.114\mathrm{e}-6$	p_2	$6.929\mathrm{e}-6$	p_{02}	$8.323\mathrm{e}-5$
p_{01}	1.026	p_1	1.321	p_{01}	1.528
		p_0	3283.97	p_{00}	$5.818\mathrm{e}-7$

B SIMULATED LINE

Table B.1: Timetable of simulated rail journey.

Station	Time since origin incl. dwell (s)	Dwell Time (s)	Distance (km)
Saltburn	0	-	0
Marske	300	60	3.06
Longbeck	450	60	3.8
Redcar East	660	60	6.38
Redcar Central	840	60	7.91
South Bank	1290	60	15.95
Middlesbrough	1680	60	19.98
Thornaby	2040	60	25.15
Eaglescliffe	2370	60	29.97
Allens West	2550	60	31.04
Dinsdale	2940	60	37.98
Darlington	3480	180	44.12
North Road	3840	30	46.19
Heighington	4320	60	53.31
Newton Aycliffe	4530	60	55.46
Shildon	4830	60	58.76
Bishop Auckland	5250	-	63.37

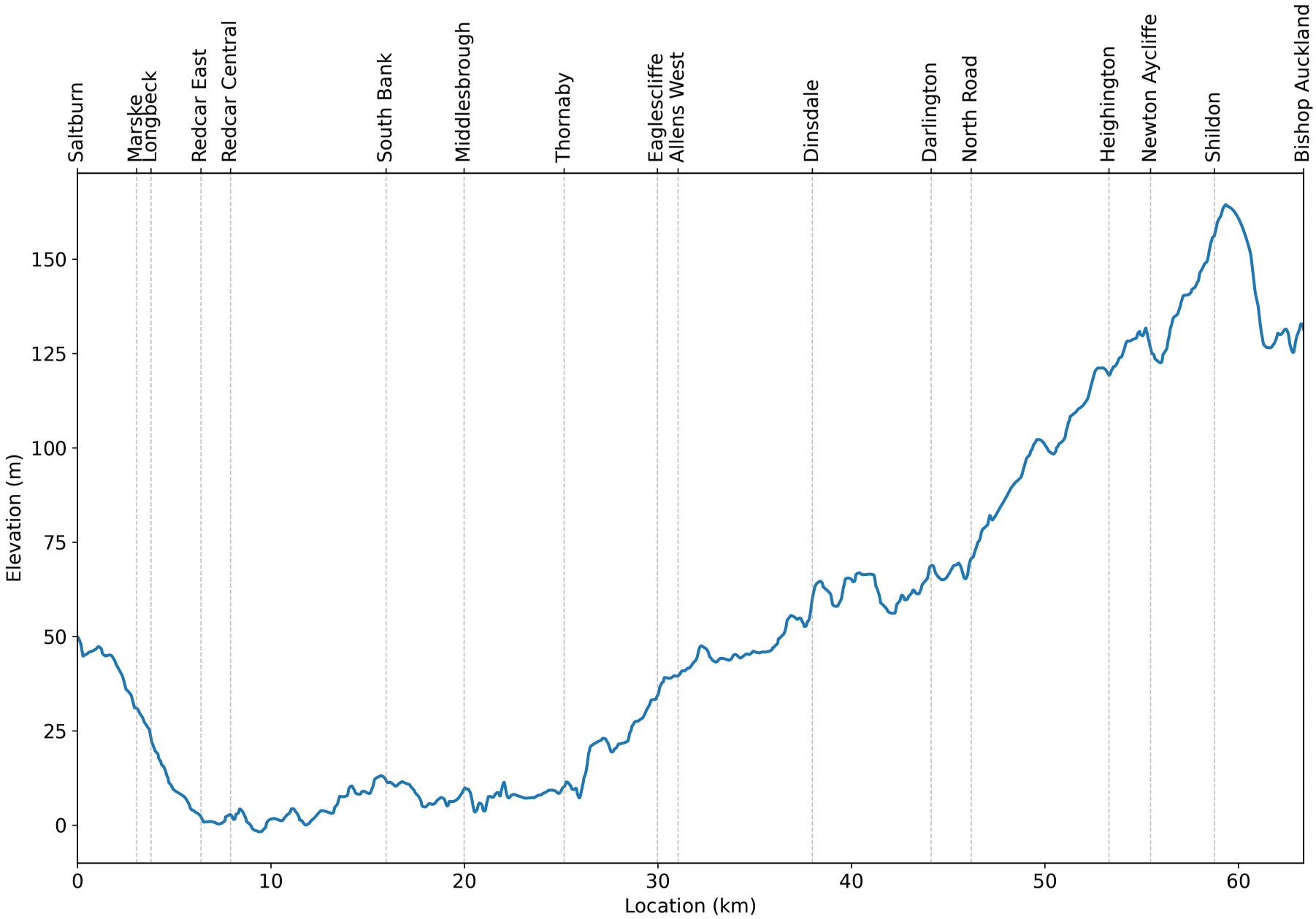

Figure B.1: Elevation of simulated rail journey.

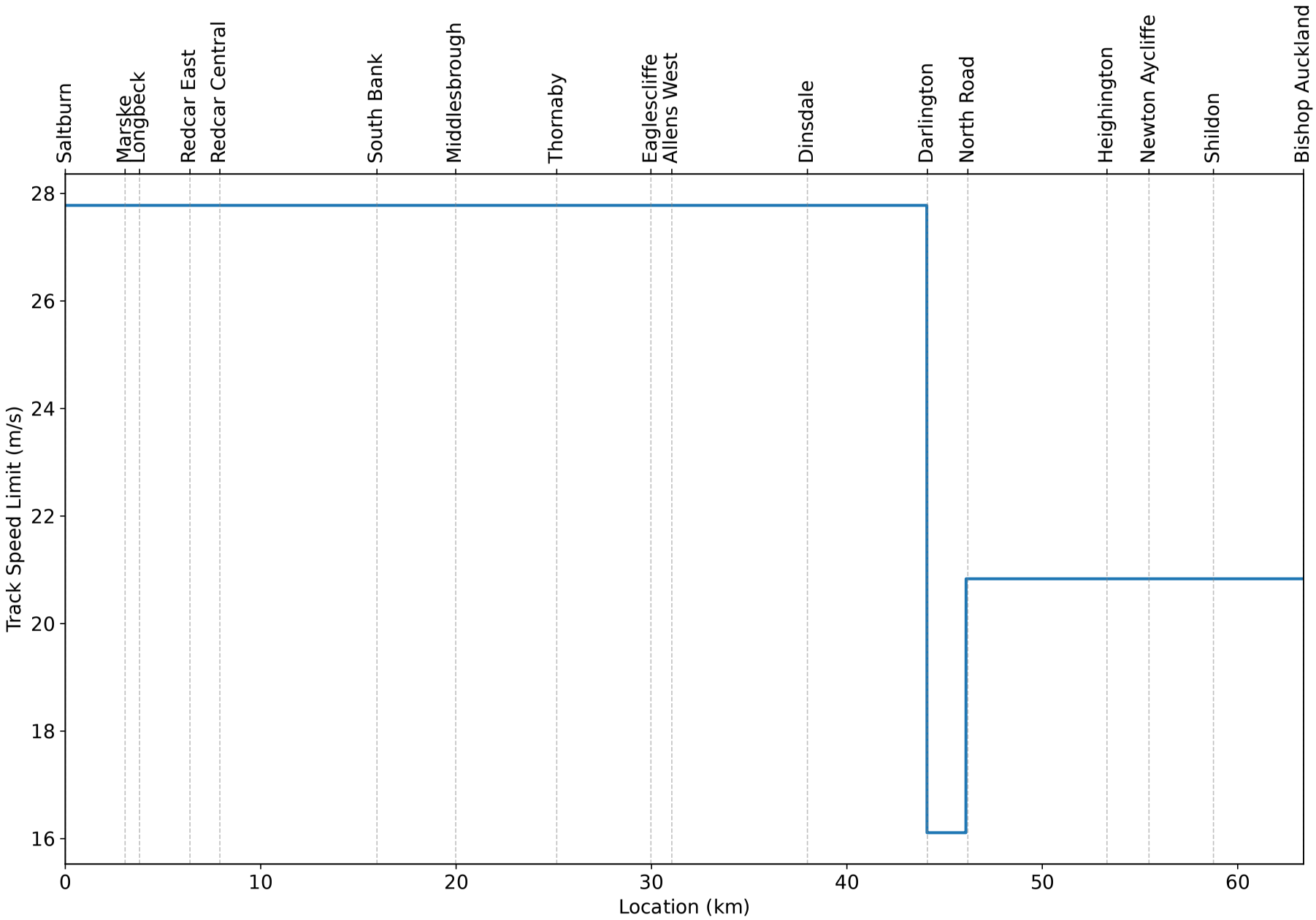

Figure B.2: Track speed limit of simulated rail journey.

C CONTRIBUTIONS

C.1 Publications

During this PhD programme, I submitted the following peer-reviewed papers about fuel cell hybrid trains:

1. *R. Jibrin*, S. Hillmansen, C. Roberts, N. Zhao, Z. Tian, "Convex optimization of speed and energy management system for fuel cell hybrid trains," in 2021 IEEE Vehicle Power and Propulsion Conference (VPPC), 25-28 October, 2021, Gijon, Spain. DOI: 10.1109/VPPC53923.2021.9699165.

2. *R. Jibrin*, S. Hillmansen, C. Roberts, "Impact of conventional driving strategies on fuel cell hybrid trains," in 2022 World Congress on Railway Research (WCRR), 6-10 June, 2022, Birmingham, United Kingdom.

3. *R. Jibrin*, S. Hillmansen, C. Roberts, "Convex optimization for fuel cell hybrid trains: speed, energy management system, and battery thermals," in 2022 European Control Conference (ECC), 12-15 July, 2022, London, United Kingdom. DOI: 10.23919/ECC55457.2022.9838209.

The first paper was presented at the IEEE Vehicle Power and Propulsion Conference. This paper focused on powertrain modelling and optimisation.

The second paper was presented at the World Congress on Railway Research which is the world's largest rail research conference and is attended by both rail industry and academia. It highlighted the disparities between conventional driving strategies and emerging optimal driving strategies for fuel cell hybrid trains.

The third paper was submitted to the European Control Conference which is hosted by the International Federation of Automatic Control. This paper presented how auxiliary

Figure C.1: Photo of the summer school attendees in the UKRRIN CEDS building.

vehicle systems could be integrated into traction optimisation.

C.2 2023 Birmingham Decarbonisation Summer School

The multidisciplinary challenges facing rail decarbonisation inspired me to organise the 2023 Birmingham Decarbonisation Summer School [332]. This was a postgraduate summer school about rail decarbonisation. Its aim was engaging researchers with the challenges facing rail decarbonisation. It was attended by 24 PhD students and postdoctoral researchers from 11 UK universities. It was held in-person in the UKRRIN CEDS building at the University of Birmingham from the 24th till the 28th of July 2023.

The summer school delivered its objective through two sets of activities that spanned the week:

1. a series of seminars to familiarise attendees with rail, along,
2. a team competition for proposing a rail decarbonisation plan for the Birmingham-Peterborough rail line.

Seminars

The following technical seminars were given by experts from academia and industry:

- *Introduction to Summer School and Ricardo Rail* by Jake Cartmell.

- *The RSSB Sustainable Rail Blueprint* by George Davies.
- *About Freightliner Operations* by Mark Riley.
- *Appraisal of Green Projects* by Trevor Bradbury.
- *Introduction to Electrification* by Kevin Blacktop.
- *Railway Decarbonisation* by Prof. Stuart Hillmansen.
- *Railway Operation and Timetabling* by Dr Jin Liu.
- *Air Quality Appraisal* by Ferdinand Turral.

Moreover, the technical seminars were complemented by the following seminars:

- *Embedding equality, diversity and inclusion in your research and research proposals* by Sarah MacMillan.
- *Successfully presenting you and your ideas* by Nicola Gittins.

Team Competition

The competition challenged teams to propose a solution to decarbonise the Birmingham - Peterborough rail line, shown in Fig. C.2. This line is only partially electrified where it meets the East Coast Mainline at Peterborough. The line operates mixed traffic, including cross-country passenger services and freight traffic from Felixstowe.

The proposals were evaluated by a panel of rail experts. The winning team proposed to fully electrify the line, going beyond Peterborough all the way to Felixstowe. This is due to the strategic importance of Felixstowe for rail freight. Similar recommendations were published in a recent report by the Chartered Institute of Logistics and Transport (CILT) [333].

The summer school was a successful collaboration between industry and academia. It left attendees with a very positive experience, 70% of whom agreed that their participation encouraged them to consider a career in rail and net zero.

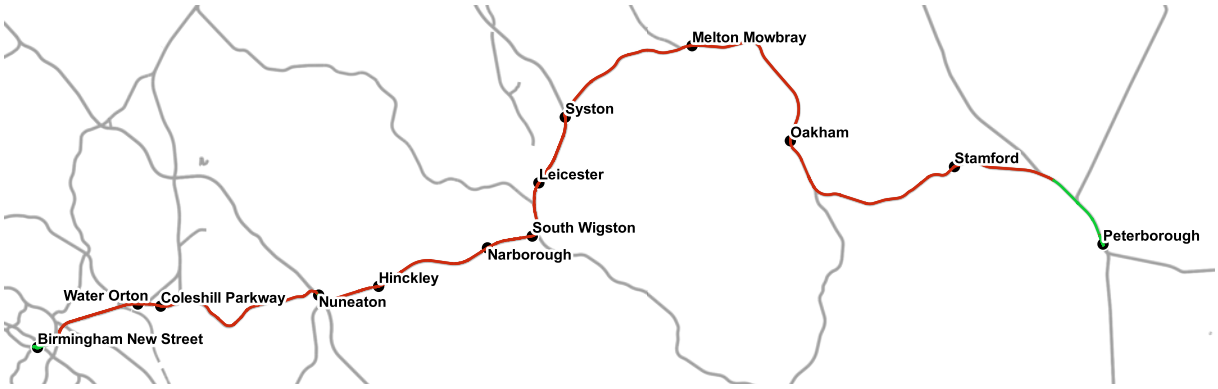

Figure C.2: The Birmingham to Peterborough line.